**Title**

Physical cues regulate the localization and activation of TGFβ receptors to control the quantity and quality of signaling pathway activity

**Permalink**

https://escholarship.org/uc/item/29p4k5dh

**Author**

Monteiro, David Antonio

**Publication Date**

2020

Peer reviewed|Thesis/dissertation

Physical cues regulate the localization and activation of TGFβ receptors to control the quantity and quality of signaling pathway activity

by
David Monteiro

DISSERTATION
Submitted in partial satisfaction of the requirements for degree of
DOCTOR OF PHILOSOPHY

in

Bioengineering

in the

GRADUATE DIVISION

of the

UNIVERSITY OF CALIFORNIA, SAN FRANCISCO
AND
UNIVERSITY OF CALIFORNIA, BERKELEY
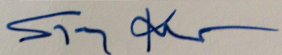
Approved:

DocuSigned by:

*Tamara Alliston*                                           Tamara Alliston
E233CABEF261499...                                                      Chair

DocuSigned by:

*[signature]*                                           Sanjay Kumar
DocuSigned by: 42B...
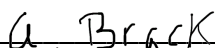*A. Brack*                                           Andrew Brack
8019548714A4420...

_____

_____
                                                Committee Members

# Acknowledgements

This work and the completion of my PhD would not have been possible without the amazing support provided by my mentors, colleagues, family, and friends. I truly appreciate all of you.

Firstly, thank you to my family for all your support, for pushing me to finish in the face of forest fires, earthquakes, and a pandemic. Thank you, Dad, for coming to visit me a few times, thank you, Mom, for all of our chats on the phone, and thank you Claudia for pursuing a "real" career and getting married (thanks Kjell!) to take the pressure off of your older brother for a few years. Thank you also to Jo, Elizabeth, Nicholas, Catherine, and Patrick for your local support – thanks to you I was never too far away from family.

Secondly, thank you to my friends – Nick, Jon, Roberto, Courtney, Allison, Karen, Rami, Torrey, and countless others who have kept me excited about my work and who I have had the opportunity to work with, travel with, eat with, and who have taught me a lot about life. Thank you to Nick who helped me navigate immense challenges on both coasts; to Jon and Roberto for helping me grow up and get acclimated to the Bay Area; to Courtney for joining Tamara's lab with me and for being an amazing friend, colleague, and scientist; to Karen and Allison for motivating me with your incredible work ethic; to Rami for making a lot of great moments even greater; and to Torrey for late nights discussing literature. It would not have been the same without you there.

Thirdly, thank you to my colleagues and mentors who have – at different times – nurtured, inspired, critiqued, and praised. Thank you to my advisor, Tamara Alliston, for your constant inspiration and support, for teaching me and listening to me, and for providing an incredible environment and assembling an incredible team to work alongside. Thank you to Woo Lee who started everything off over 10 years ago. Thank you to Ortho Lab PI's Jeff Lotz, Rich Schneider, and Aaron Fields for advice and feedback during lab meetings and otherwise. Thank you to my thesis committee members Andrew Brack and Sanjay Kumar for thoughtful discussions about my research and career. Thank you to Joanna and Chris who welcomed me into the Alliston lab and

got me excited about TGFβ. Thank you to Neha, Spenser, Tristan, Serra, Gaby, and Cristal for your guidance and advice. Thank you to Courtney, Karsyn, Charlie, Luke, Jihee, JJ, Minali, Darnell, and everybody else who I was fortunate enough to share time in the lab with. You all truly made my time at Parnassus memorable.

Fourthly, thank you to Mary Ann for your encouragement and advice, for laughing and crying with me on Skype/Zoom before videocalls were cool, and for being an amazing scientist and partner. I do not think anyone could have done the long-distance double-PhD as successfully as you and I have.

Osteoblastly, if you are reading this, thank you too.

# Abstract

Physical cues regulate the localization and activation of TGFβ receptors to control

the quantity and quality of signaling pathway activity

by

David Monteiro

In addition to biological cues, the cellular microenvironment is rife with physical cues that coordinate cellular behavior through regulation of signaling pathways such as the transforming growth factor beta (TGFβ) pathway. These cues – substrate stiffness or topography, mechanical compression, tension, or fluid shear stress, among others – exert their effects in controlling major cellular decisions such as proliferation, migration, or differentiation through direct and indirect processes. In the skeleton, accurate cellular detection of physical changes in the microenvironment is necessary to preserve homeostasis, and disruption of this can drive disease progression. For example, in bone, mechanoregulation of the TGFβ pathway in response to mechanical compression is required for bone anabolism. Likewise, in cartilage, dysregulation of TGFβ signaling can promote an osteoarthritic phenotype. However, the set of mechanisms that enable mechanoregulation of TGFβ signaling remain to be fully elucidated. This work uses molecular biology, engineering, and computational approaches to investigate the molecular mechanisms underlying regulation of the TGFβ signaling pathway by substrate stiffness/cytoskeletal tension and fluid shear stress, two major physical cues within the context of the skeleton. These findings reveal new roles for TGFβ receptors in defining the cellular TGFβ response to changes in physical cues in the microenvironment.

# Table of Contents

# List of Figures

# List of Tables

# Chapter 1

# TGFβ signaling in the skeleton

**Introduction**

In humans, the skeleton plays several important roles: it provides support for the body and protects the internal organs, it facilitates movement, and it serves as a reservoir of minerals such as calcium and phosphate. To do this, the three major bone cell types – the bone-surface dwelling osteoblasts and osteoclasts and the embedded osteocytes – maintain skeletal structure and function through precise and coordinated actions. The competing processes of bone formation by osteoblasts and bone resorption by osteoclasts preserve bone homeostasis by contributing to a state of dynamic equilibrium. The activities of these cells are known to be controlled at least in part by osteocytes, which are considered the main mechanosensitive cells in bone [1,2]. Despite making up over 90% of the cells in bone, only more recently have osteocytes been closely studied, due in part to the difficulty in isolating them. As former osteoblasts that have become buried within bone, osteocytes are connected to each other and to the vasculature through the lacunocanalicular network – a series of cavities (lacunae) within which osteocytes reside that are linked by canaliculi, which facilitate inter-osteocyte communication as well as nutrient and waste exchange. While much has been uncovered about the specific roles that osteocytes play both in

1

maintaining bone homeostasis and in enabling bone adaptation to loading, many essential questions remain unanswered, such as 1) how are mechanical loads transduced by osteocytes into changes in the activities of biological signaling pathways? and 2) how do cells integrate concurrent physical and biological cues to generate unique downstream responses?
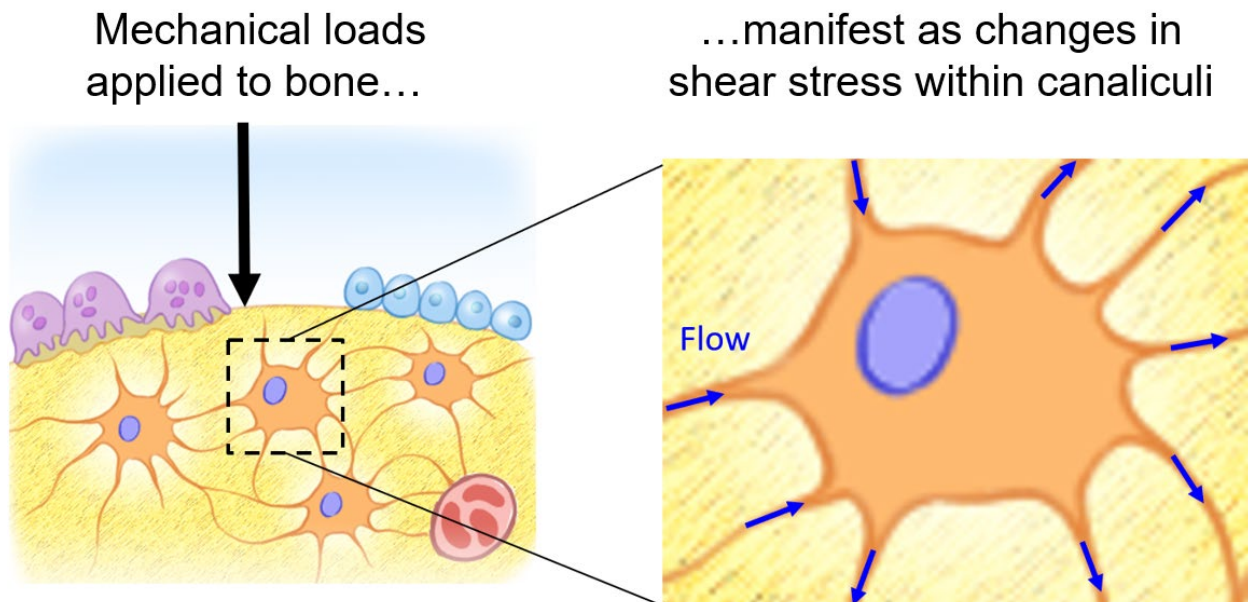


**Figure 1.1:** Schematic of fluid flow in the osteocyte canalicular network. Illustration by M. Ouchida, adapted from Dole et al. 2017 [3].

**Osteocyte mechanotransduction**

In the 19th century, surgeon Julius Wolff formulated Wolff's Law, the notion that bone adapts – for example, by changing its size or shape – to the mechanical loads it experiences so as to resist that type of loading. In humans, this phenomenon is evident in the increased bone mass in the dominant arm of tennis players or baseball pitchers due to localized strains [4]. Likewise, bone unloading such as that experienced by astronauts in microgravity can lead to 1-2% reduction in bone mineral density per month [5]. At the cellular level, these compressive loads applied to bone manifest as changes in fluid shear stress (FSS) within the lacunocanalicular

network [6] that are sensed by osteocytes via cell surface mechanosensors such as integrins [7], the primary cilium [8], Connexin gap junctions [9], or ion channels such as Piezo1 [10] or TRPV4 [11]. Interestingly, the relationship between bone strain, magnitudes of fluid shear stress experienced by osteocytes near the loading site, and locations of new bone formation following mechanical load is complex [12].

The osteocyte response to FSS stimulation involves the concurrent regulation of many critical signaling pathways – such as the transforming growth factor beta (TGFβ) and Wnt/β-catenin pathways. FSS regulation of Wnt signaling within the context of bone mechanotransduction has been extensively studied, due in part to the well-known role of Sclerostin/*Sost*, a mechanosensitive inhibitor of Wnt signaling that plays a critical role in osteoblast bone formation [6]. On the other hand, while FSS regulation of TGFβ signaling has been studied extensively in other cellular contexts – for example in kidney epithelial cells or vascular endothelial cells [13–15] – the mechanisms through which it is targeted by mechanical load in osteocytes remain to be fully elucidated, despite the critical roles that it plays in bone homeostasis and mechanoadaptation [3,16]. Work by Nguyen, et al. showed that mechanoregulation of Sclerostin expression requires functional TGFβ signaling; however, the mechanism that links FSS and TGFβ signaling in osteocytes is not yet fully understood. Interestingly, the deubiquitinase *Cyld* was recently found to be required for load-mediated regulation of Smad2/3 phosphorylation in mouse osteocytes following hindlimb loading [17].

Over the past decade, advances in computational modeling, high-resolution imaging, and microfluidics/bioreactors have been applied to address fundamental questions in osteocyte mechanobiology. In part, these tools have enabled more physiologically relevant *in vitro* studies that closely replicate the *in vivo* osteocyte microenvironment, for example, by allowing a higher degree of control over fundamental parameters such as cell-cell spacing in 2- and 3-D, or by more easily enabling co-culture of multiple distinct cell types. These platforms have also been used to recreate the mechanical environment that osteocytes experience during compressive loading and

unloading of bone by providing a dynamic environment where cells can be stimulated with FSS or experience prolonged microgravity.

With the goal of creating a cell line that better recapitulates the biology of *bone-a fide* osteocytes, Spatz, et al. developed the OCY454 osteocyte-like cell line, and subjected these cells both to FSS in 2-D and 3-D using a Flexcell Streamer device and to an unloading environment achieved by a NASA rotating wall vessel system [18]. They found that both short- (2 hour) and long-term (1-3 day) stimulation with FSS reduced *Sost* mRNA expression whereas cellular unloading led to an increase in *Sost*, sclerostin protein, and *Rankl*/*Opg* ratio. Work by Gu et al. and Sun et al. used PDMS microfluidic chambers to study the differentiation of the early osteocytic cell line MLO-A5 and primary murine osteoblasts, respectively, cocultured with 20-25 μm diameter biphasic calcium phosphate (BCP) microbeads within a 3D perfusion culture platform [19,20]. The microbeads enabled cell-cell spacing of ~20 μm and the formation of cell-cell processes through openings in the beads, which in the longer-term allowed the entrapped cells to exhibit gene expression (*Sost* and *Fgf23*) and nonproliferative behavior characteristic of mature osteocytes. On the contrary, cells grown in 2-D maintained their original phenotype. While these studies evaluated cell phenotype and characterized the osteocytic response to short-term FSS stimulation or long-term perfusion culture, they did not evaluate protein-level changes in signaling pathway activity as a result of FSS stimulation.

**Mechanoregulation of TGFβ signaling in bone**

In the skeleton, the TGFβ pathway plays several critical, yet distinct, roles in the three bone cell types to regulate both bone mass and bone quality [21,22]. Osteoblasts produce and export inactive TGFβ that remains bound to the extracellular matrix (ECM) in a latent form [23]. Activation of latent TGFβ can be achieved through several mechanisms, including by integrins, or following secretion of acid or proteases by resorbing osteoclasts [24]. In osteocytes, TGFβ plays important roles both in the control of perilacunar/canalicular remodeling and in coordinating

4

the mechanoregulation of sclerostin expression through its canonical effector Smad3, where it acts alongside the Wnt pathway [3,16]. While interactions between the Wnt and TGFβ signaling pathways are known to include effector crosstalk and regulation of shared target genes, their independent roles in regulating bone mechanoadaptation remain to be fully elucidated [25].

A more thorough understanding of mechanoregulation of TGFβ signaling in bone has the potential to uncover new cellular mechanisms involved in bone anabolism or identify new targets for therapies to skeletal pathologies such as arthritis or osteoporosis. Indeed, dysregulation of TGFβ signaling plays a causal role in many skeletal pathologies such as Camurati-Engelmann disease [26] and some forms of osteogenesis imperfecta [27]. These conditions highlight the close relationship between the TGFβ signaling pathway and the material properties of bone matrix, which are linked via a feedback loop [28]: TGFβ regulates the composition of bone matrix [21], which both controls the activation of latent TGFβ ligand [29] and calibrates cytoskeletal tension to prime the cellular response to TGFβ [30,31].

**TGFβ signaling in cartilage and cartilage/bone TGFβ crosstalk**

The mechanical forces that induce changes in FSS within osteocyte canaliculi also produce compression and tension in cartilage. Compression of cartilage results in the depletion of water from its proteoglycan-rich ECM, which induces changes in hydrostatic and osmotic pressure that can be damaging depending on the intensity of the applied loads [32–34]. Chondrocytes respond to these mechanical cues through mechanisms that overlap with those used by other skeletal cells such as osteocytes and subsequently regulate the activities of signaling pathways such as the TGFβ pathway, including ion channels, focal adhesions, and the primary cilium [35–37]. While TGFβ signaling typically promotes chondrocyte homeostasis, dysregulation of TGFβ signaling through Smad3 is casually implicated in human osteoarthritis, due at least in part to a shift in the balance between cartilage matrix synthesis and degradation [38–40]. Further, in osteoarthritis, chondrocytes undergo an undesired shift from canonical TGFβ

signaling through ALK5 and Smad2/3 to that through ALK1 and Smad1/5/8 [41]. More recent results have highlighted the close relationship between TGFβ signaling in coordinating bone and cartilage homeostasis as osteocytic TGFβ signaling was shown to be play a critical role in maintaining cartilage health and in coordinating the cartilage response to injury [42]

**Summary**

This work uses a combination of molecular biology, computational, and engineering approaches to evaluate mechanoregulation of the TGFβ signaling pathway by substrate stiffness and FSS stimulation in skeletal cells, with a focus on TGFβ receptors. First, TIRF and sptPALM high-resolution imaging of ATDC5 chondroprogenitor cells grown on polyacrylamide and PDMS gels revealed the existence of a focal adhesion-localized TGFβ receptor subpopulation whose heteromerization could be induced by disrupting cytoskeletal tension. With the goal of exploring the extent to which other physical cues regulate the TGFβ pathway through similar mechanisms, I designed a PDMS microfluidic cell culture system as a platform within which cells could be cultured and stimulated with precise levels of FSS. Using this system for protein-, RNA-, and imaging readouts, I tested the hypothesis that FSS is a potent agonist of the TGFβ pathway in OCY454 osteocyte-like cells. My results show that FSS rapidly induces TβRI/TβRII heteromerization, Smad1 and Smad2/3 phosphorylation, Smad2/3 nuclear translocation, and the expression of established TGFβ-regulated genes. This mechanism, which requires the presence of functional TGFβ superfamily ligands, concurrently activates several distinct TGFβ receptor subsets in a manner that differs quantitatively and qualitatively from that which could be achieved with treatment with TGFβ or BMP4 alone. Together, this work is one of the first to highlight TGFβ receptor-level mechanoregulation as a critical mechanism by which cells can prime their response to TGFβ superfamily ligands to calibrate the intensity and quality of downstream signaling.

**References**

1       Klein-Nulend, J. *et al.* (1995) Sensitivity of osteocytes to biomechanical stress in vitro. *FASEB J.  Off. Publ. Fed. Am. Soc.  Exp. Biol.* 9, 441–445

2       Burger, E.H. *et al.* (1995) Function of osteocytes in bone--their role in mechanotransduction. *J. Nutr.* 125, 2020S-2023S

3       Dole, N.S. *et al.* (2017) Osteocyte-Intrinsic TGF-beta Signaling Regulates Bone Quality through Perilacunar/Canalicular Remodeling. *Cell Rep.* 21, 2585–2596

4       McClanahan, B.S. *et al.* (2002) Side-to-side comparisons of bone mineral density in upper and lower limbs of  collegiate athletes. *J. strength Cond. Res.* 16, 586–590

5       Orwoll, E.S. *et al.* (2013) Skeletal health in long-duration astronauts: nature, assessment, and management  recommendations from the NASA Bone Summit. *J. bone Miner. Res. Off. J. Am. Soc.  Bone Miner. Res.* 28, 1243–1255

6       Kamel, M.A. *et al.* (2010) Activation of β-catenin signaling in MLO-Y4 osteocytic cells versus 2T3 osteoblastic  cells by fluid flow shear stress and PGE2: Implications for the study of mechanosensation in bone. *Bone* 47, 872–881

7       Litzenberger, J.B. *et al.* (2010) Beta1 integrins mediate mechanosensitive signaling pathways in osteocytes. *Calcif. Tissue Int.* 86, 325–332

8       Temiyasathit, S. and Jacobs, C.R. (2010) Osteocyte primary cilium and its role in bone mechanotransduction. *Ann. N. Y. Acad. Sci.* 1192, 422–428

9       Li, X. *et al.* (2013) Connexin 43 is a potential regulator in fluid shear stress-induced signal transduction in osteocytes. *J. Orthop. Res.  Off. Publ. Orthop. Res.  Soc.* 31, 1959–1965

10      Li, X. *et al.* (2019) Stimulation of Piezo1 by mechanical signals promotes bone anabolism. *Elife* 8,

11      Lyons, J.S. *et al.* (2017) Microtubules tune mechanotransduction through NOX2 and TRPV4 to decrease sclerostin  abundance in osteocytes. *Sci. Signal.* 10,

12      Carrieroa, A. *et al.* (2018) Spatial relationship between bone formation and mechanical

stimulus within cortical bone: Combining 3D fluorochrome mapping and poroelastic finite element modelling. *Bone reports* 8, 72–80

13    Walshe, T.E. *et al.* (2013) The role of shear-induced transforming growth factor-beta signaling in the endothelium. *Arterioscler. Thromb. Vasc. Biol.* 33, 2608–2617

14    Zhou, J. *et al.* (2012) Force-specific activation of Smad1/5 regulates vascular endothelial cell cycle progression in response to disturbed flow. *Proc. Natl. Acad. Sci. U. S. A.* 109, 7770–7775

15    Kunnen, S.J. *et al.* (2017) Fluid shear stress-induced TGF-beta/ALK5 signaling in renal epithelial cells is modulated by MEK1/2. *Cell. Mol. Life Sci.* 74, 2283–2298

16    Nguyen, J. *et al.* (2013) Load regulates bone formation and Sclerostin expression through a TGFbeta-dependent mechanism. *PLoS One* 8, e53813

17    Nguyen, J. *et al.* (2020) CYLD, a mechanosensitive deubiquitinase, regulates TGFβ signaling in load-induced  bone formation. *Bone* 131, 115148

18    Spatz, J.M. *et al.* (2015) The Wnt Inhibitor Sclerostin Is Up-regulated by Mechanical Unloading in Osteocytes in Vitro. *J. Biol. Chem.* 290, 16744–16758

19    Gu, Y. *et al.* (2015) Microbeads-Guided Reconstruction of 3D Osteocyte Network during Microfluidic  Perfusion Culture. *J. Mater. Chem. B* 3, 3625–3633

20    Sun, Q. *et al.* (2015) Ex vivo 3D osteocyte network construction with primary murine bone cells. *Bone Res.* 3, 15026

21    Balooch, G. *et al.* (2005) TGF-beta regulates the mechanical properties and composition of bone matrix. *Proc. Natl. Acad. Sci. U. S. A.* 102, 18813–18818

22    Edwards, J.R. *et al.* (2010) Inhibition of TGF-β signaling by 1D11 antibody treatment increases bone mass and quality in vivo. *J. Bone Miner. Res.* 25, 2419–26

23    Erlebacher, A. *et al.* (1998) Osteoblastic responses to TGF-beta during bone remodeling. *Mol. Biol. Cell* 9, 1903–1918

24    Oursler, M.J. (1994) Osteoclast synthesis and secretion and activation of latent

transforming growth factor beta. *J. bone Miner. Res. Off. J. Am. Soc. Bone Miner. Res.* 9, 443–452

25    Guo, X. and Wang, X.-F. (2009) Signaling cross-talk between TGF-beta/BMP and other pathways. *Cell Res.* 19, 71–88

26    Kinoshita, A. *et al.* (2000) Domain-specific mutations in TGFB1 result in Camurati-Engelmann disease. *Nat. Genet.* 26, 19–20

27    Grafe, I. *et al.* (2014) Excessive transforming growth factor-β signaling is a common mechanism in osteogenesis imperfecta. *Nat. Med.* 20, 670–675

28    Rys, J.P. *et al.* (2016) Mechanobiology of TGFbeta signaling in the skeleton. *Matrix Biol.* 52–54, 413–425

29    Hinz, B. (2015) The extracellular matrix and transforming growth factor-beta1: Tale of a strained relationship. *Matrix Biol.* 47, 54–65

30    Allen, J.L. *et al.* (2012) ECM stiffness primes the TGFbeta pathway to promote chondrocyte differentiation. *Mol. Biol. Cell* 23, 3731–3742

31    Rys, J.P. *et al.* (2015) Discrete spatial organization of TGFbeta receptors couples receptor multimerization and signaling to cellular tension. *Elife* 4, e09300

32    Smith, R.L. *et al.* (1996) In vitro stimulation of articular chondrocyte mRNA and extracellular matrix synthesis by hydrostatic pressure. *J. Orthop. Res. Off. Publ. Orthop. Res. Soc.* 14, 53–60

33    Smith, R.L. *et al.* (2000) Time-dependent effects of intermittent hydrostatic pressure on articular chondrocyte type II collagen and aggrecan mRNA expression. *J. Rehabil. Res. Dev.* 37, 153–161

34    Guilak, F. *et al.* (2002) The effects of osmotic stress on the viscoelastic and physical properties of articular chondrocytes. *Biophys. J.* 82, 720–727

35    Phan, M.N. *et al.* (2009) Functional characterization of TRPV4 as an osmotically sensitive ion channel in porcine articular chondrocytes. *Arthritis Rheum.* 60, 3028–3037

36 Millward-Sadler, S.J. and Salter, D.M. (2004) Integrin-dependent signal cascades in chondrocyte mechanotransduction. *Ann. Biomed. Eng.* 32, 435–446

37 Wann, A.K.T. *et al.* (2012) Primary cilia mediate mechanotransduction through control of ATP-induced Ca2+ signaling in compressed chondrocytes. *FASEB J. Off. Publ. Fed. Am. Soc. Exp. Biol.* 26, 1663–1671

38 Valdes, A.M. *et al.* (2010) Genetic variation in the SMAD3 gene is associated with hip and knee osteoarthritis. *Arthritis Rheum.* 62, 2347–2352

39 Blaney Davidson, E.N. *et al.* (2007) TGF-beta and osteoarthritis. *Osteoarthr. Cartil.* 15, 597–604

40 Chen, C.G. *et al.* (2012) Chondrocyte-intrinsic Smad3 represses Runx2-inducible matrix metalloproteinase 13 expression to maintain articular cartilage and prevent osteoarthritis. *Arthritis Rheum.* 64, 3278–3289

41 Blaney Davidson, E.N. *et al.* (2009) Increase in ALK1/ALK5 ratio as a cause for elevated MMP-13 expression in osteoarthritis in humans and mice. *J. Immunol.* 182, 7937–7945

42 Bailey, K.N. *et al.* (2020) Mechanosensitive Control of Articular Cartilage and Subchondral Bone Homeostasis Requires Osteocytic TGFβ Signaling. *Arthritis Rheumatol. (Hoboken, N.J.)* DOI: 10.1002/art.41548

# Chapter 2

# TGFβ receptors: generating a signaling fingerprint

**Introduction**

The cellular microenvironment is full of biochemical and mechanical cues that play complex roles in coordinating cellular behavior, in part through regulation of critical signaling pathways such as the TGFβ pathway. Cells sense and respond to these cues, which, in healthy tissues, influence major decisions such as migration or differentiation. Perturbation in these cues or in how they are interpreted can lead to cancer or drive disease progression. The mechanisms through which cells discriminate among concurrent cues, each of which can enhance or repress TGFβ signaling, remain unknown, and accurate cellular detection of these different inputs is imperative because they prompt distinct cellular responses.

Cell surface receptors play essential roles in maintaining cellular homeostasis by controlling the subcellular localization and duration of signaling pathway activation by extracellular stimuli. Significant advances in our understanding of mechanobiology and cellular behavior have been made from the study of TGFβ receptor-level regulation. However, more work is necessary to further understand homeostatic and disease mechanisms and ultimately to develop more

targeted therapies for cancers or other dysfunctions that accompany dysregulated TGFβ signaling. This chapter will discuss established and recently uncovered mechanisms through which TGFβ receptors are primed for or restrained from signaling, including how they are targeted by different physical cues.

The cell surface is covered with unique sensors that transmit information about the biochemical and physical nature of the surrounding microenvironment to the inside of the cell. These range from integrins, which can detect the stiffness and topography of extracellular matrix (ECM); to ion channels such as TRPV4 or Piezo1 that can be activated in part by osmotic cues, such as changes in extracellular $Ca^{2+}$ concentrations; to receptors of the TGFβ, Wnt, and Hedgehog signaling pathways that facilitate autocrine and juxtacrine communication and cell signaling. Signals from these sensors are integrated in a cell type-specific and context-dependent manner to guide migration, proliferation, lineage selection, and differentiation, among other cellular processes.

Signaling pathway activation is classically initiated by ligand binding to a functional, transmembrane receptor complex that relays this signal to intracellular proteins, for example, by facilitating their phosphorylation or dephosphorylation. These effectors, such as Smads in the case of TGFβ or β-catenin for Wnt signaling, motivate cellular responses in part by undergoing nuclear translocation and interacting with transcription factors to regulate gene expression. In particular, the TGFβ signaling pathway is considered the archetype of context-dependent signaling pathways due to its extensive network of receptors, canonical and non-canonical effectors, co-activators, and co-repressors that modulate downstream signaling. To this end, knowledge learned from study of the TGFβ signaling pathway can be extended to gain useful insights about the mechanisms underlying cellular calibration of other signaling pathways.
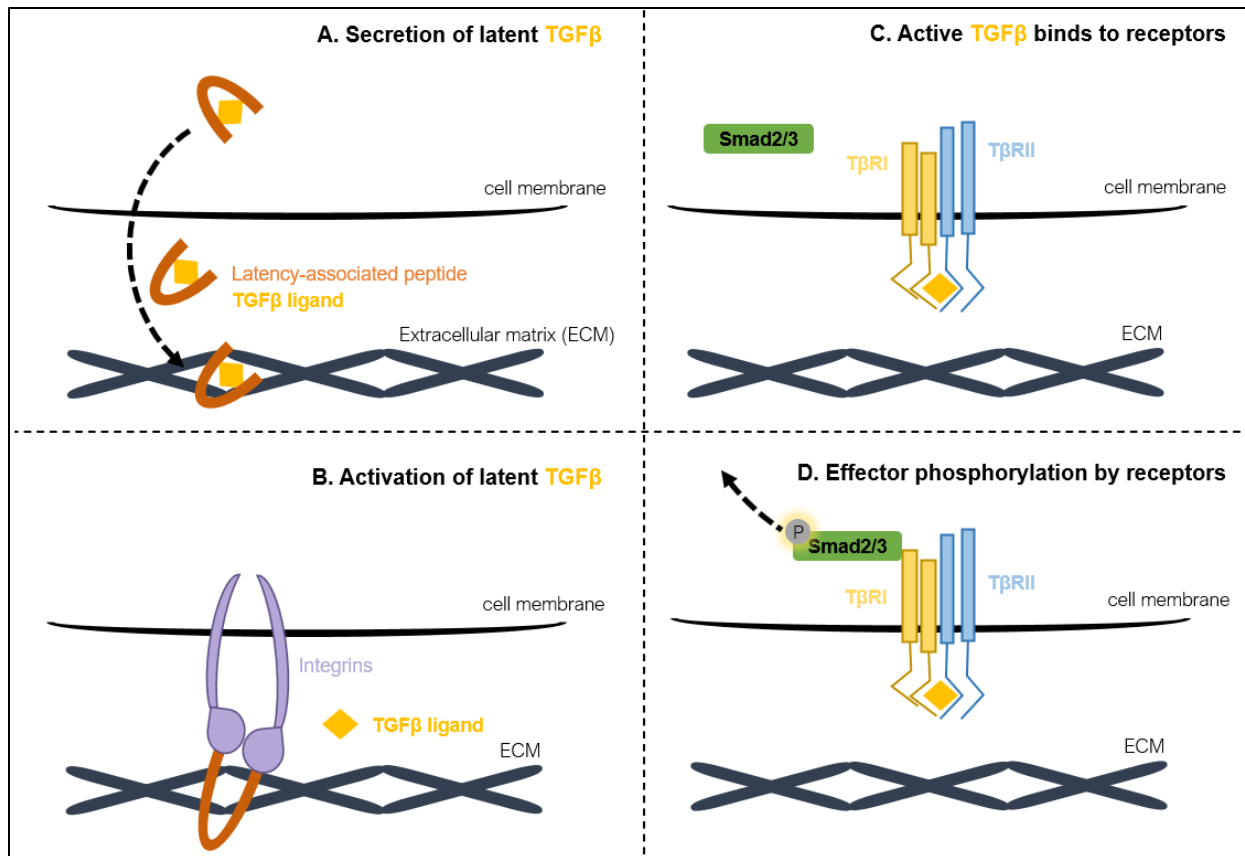
**Figure 2.1: The TGFβ signaling pathway.** (A) TGFβ ligand is produced by the cell in a latent form (complexed with latency-associated peptide (LAP) and latent TGFβ-binding protein (LTBP)) which cannot bind to receptors and is secreted where it binds to the cellular ECM. (B) TGFβ ligand can be released from this complex following the interactions of integrins such as αV with the LAP RGD motif. (C) The active TGFβ ligand binds to a type II receptor dimer, which recruits and phosphorylates a type I receptor dimer. (D) The TGFβ ligand + heterotetrameric receptor complex recruits and phosphorylates an intracellular effector, canonically Smad2 or Smad3.

The hierarchical nature of the TGFβ signaling pathway lends itself to multi-level regulation by other biochemical pathways and mechanical cues. This regulation ranges from ligand synthesis and activation; to receptor organization and multimerization; to effector activation and nuclear translocation, enabling the creation of a unique signaling *fingerprint* in response to a unique combination of concurrent inputs. These inputs, such as substrate stiffness, extracellular glucose concentration, or acute TGFβ stimulation can both increase or decrease cellular responsiveness to TGFβ superfamily ligands or shift signaling from canonical to non-canonical

pathways – controlling both the quantity and quality (type) of signaling that takes place. Given that one role of receptors is to transduce extracellular signals across the plasma membrane, receptor-level regulation is of critical importance in coordinating the location, duration, and intensity of TGFβ pathway activation. Thus, this review will discuss general themes of receptor-level regulation as well as provide examples of mechanisms that confer unique sensitivities to distinct physical and biochemical cues, with a focus on the TGFβ signaling pathway (Fig. 2.1).

**Table 2.1: Mechanisms of TGFβ receptor-level regulation**

| Mechanism | Examples | References |
|---|---|---|
| Non-canonical ligand-receptor interactions | • Distinct ligand-receptor affinities<br>• Ligand heterodimers<br>• Receptor heterodimers | [12,13]<br>[14]<br>[15–17] |
| Localization at mechanosensory sites | • At the primary cilium<br>• At focal adhesions | [38,40]<br>[44] |
| Trafficking to the cell membrane | • Following insulin/glucose treatment<br>• Following TGFβ treatment | [19,68]<br>[22] |
| Internalization from cell-surface microdomains | • Clathrin vs. caveolae<br>• Double-positive endosomes | [24,26]<br>[28] |
| Interactions with type III receptors | • Betaglycan<br>• Endoglin | [30,31]<br>[36,69] |

**Mechanisms of receptor-level regulation**

The TGFβ superfamily consists of over 30 structurally similar ligands that include TGFβs, BMPs, and Activins, among others, which are cell regulatory proteins that play distinct but overlapping roles in coordinating tissue growth and development as well as in the maintenance of homeostasis. Proteins from this family compete for binding to transmembrane receptor serine/threonine kinases, which include seven type I receptors and five type II receptors, in addition to two type III receptors, endoglin and betaglycan, that do not participate directly in

signaling but regulate ligand-receptor binding and receptor turnover [1]. These receptors form multimeric complexes with ligands that facilitate recruitment, binding, and phosphorylation of canonical Smad effectors and non-canonical effectors such as TAK1, Akt, or others [2,3]. Activated Smad effectors then translocate to the nucleus where they participate in the regulation of gene transcription, microRNA expression, and epigenetic remodeling [4–7].

*Ligand-receptor complex formation*

An early, traditional, understanding of canonical TGFβ superfamily signaling begins with active (dimeric) ligand binding to a receptor type II homodimer, which recruits and phosphorylates a receptor type I homodimer [8,9]. The resulting heterotetramer is capable of phosphorylating a Smad2/3 (for TGFβ, Activin, or Nodal ligands) or Smad1/5/8 effector (for BMPs or GDFs), that complexes with Smad4 before translocating to the nucleus. Since the 1990s, many studies have refined this perspective on ligand-receptor interactions by revealing variant signaling mechanisms, including the ability for type I and type II receptors to form multimeric complexes even in the absence of TGFβ ligand [10]. In fact, these multimeric receptor complexes were shown by Huang et al. to consist of two pairs of TβRI-TβRII heterodimers, each of which have the ability to signal independently [11]. More recent work has begun to evaluate the ability of TGFβ superfamily ligands to interact with diverse receptor complexes with distinct affinities, however, the preferred type I receptors for the TGFβ, BMP, and Activin ligand families is shown in Fig 6.5B.

Competition among ligands for specific receptors plays an important role in defining the cellular TGFβ response [12]. The relative local levels of ligands and receptors boosts signaling by higher-affinity ligand-receptor interactions, but also temporarily blocks signaling by lower-affinity interactions, which can become favorable as concentrations of specific ligands or receptors change. Work to characterize these preferences of different ligands for specific receptors is underway, and complements a large body of existing literature. In a more recent

15

study, Khalil et al. quantified the abilities of several TGFβ superfamily ligands to specifically induce dimerization of ActR2b and ALK4, ALK5, or ALK7 [13].

This complexity of TGFβ family signaling is compounded by heterodimerization at ligand- and receptor-levels, which can act to enhance or antagonize signaling. For example, only BMP2/BMP7 heterodimers are able to activate BMP signaling in the early zebrafish embryo, whereas homodimers of either ligand cannot, due to their ability to simultaneously engage two different BMP type I receptors [14]. Similarly, heterodimers of BMP type I receptors, such as those between ALK2 and ALK1 or ALK3 can form under certain conditions, for example in mediating BMP9-induced osteogenic signaling in mesenchymal stem cells [15,16]. While the specific mechanisms that promote receptor homo/heteromerization are not entirely clear, more recent work has shown that the presence of specific ligands can play an important role. One study showed that ALK2-ALK3 heterodimers could form only in the presence of BMP2 or BMP6, but that ALK3 homodimers formed even in their absence [17]. Further downstream, these receptor-receptor interactions participate in control of the balance between canonical and non-canonical signaling: recent work showed that treatment with TGFβ can induce Smad1/5/8 phosphorylation through ALK5 recruitment and activation of ALK2 [18]. Taken together, these results reinforce the notion that TGFβ family/Smad signaling is extremely dynamic, with specific ligand/receptor affinities and interactions providing significant signaling complexity that enables the generation of precise cellular responses.

*Receptor trafficking and internalization*

The abundance of TGFβ receptors present at the cell surface is in constant flux, due to several mechanisms that concurrently and dynamically regulate their transport to and from the plasma membrane in response to biological and mechanical stimuli. A significant fraction of the cell's receptor pool is intracellular, where they do not play active roles in ligand binding. Thus, the ability to rapidly recruit these receptors to the membrane where they can respond to ligand

provides cells with a means to calibrate their individual TGFβ responsiveness. For example, Wu and Derynck used a biotinylation approach to show that treatment with glucose induces a significant increase in cell-surface TGFβ receptors within 15 minutes [19]. Similarly, separate studies by Huang et al. used $I^{125}$-TGFβ crosslinking to assess receptor recruitment following treatment with ethanol and DMSO, reagents used in cell culture experiments in addition to their diverse roles in human health in preventing atherosclerosis and as a drug carrier, respectively [20,21]. They found that TβRI and TβRII were recruited at different rates from intracellular pools to the cell membrane following treatment with either reagent, which significantly enhanced the downstream TGFβ response in Mv1Lu cells.

Treatment of cells with exogenous TGFβ plays a complex, dynamic role in coordinating membrane receptor levels. In HaCaT and A549 cells, TGFβ induces an increase in cell-surface receptors within as soon as 5 minutes via a mechanism that involves activation of Akt and subsequent phosphorylation of the RabGAP AS160 [22]. However, TGFβ is also capable of initiating a negative feedback loop through upregulation of genes such as Smad7 and Smurf1/2 which promote the inactivation and degradation of receptors [23]. Especially interesting are the differences in the depletion rates of ALK5 and TβRII following treatment with TGFβ, with most TβRII depletion from the cell membrane occurring within 10 minutes after treatment with TGFβ whereas ALK5 was only maximally depleted after 4 hours, suggesting that TβRII depletion from the cell membrane is sufficient to attenuate the TGFβ response [23]. Given that TβRII is more selective for complexing with TGFβ ligands than ALK5, this could be a mechanism to specifically shut down TGFβ signaling but maintain cellular sensitivity to other (e.g. Activin) ligands, which can complex with ALK5 but have a separate type II receptors.

Not only is the sheer number of receptors at the cell membrane important in responding to stimuli, so too is their localization to discrete cell-surface microdomains. These microdomains confer unique internalization dynamics to subpopulations of TGFβ receptors, for example through clathrin-mediated or clathrin-independent pathways [24]. Clathrin-mediated endocytosis is

thought to support Smad signaling by providing receptors with access to the Smad anchor SARA within early endosomes, and studies have shown that receptor type I activation is required to promote this internalization [25,26]. On the contrary, endocytosis via lipid rafts/caveolae is thought to promote receptor degradation or non-canonical signaling. Proteins such as syntenin have been shown to increase TGFβ signaling by inhibiting the interactions between caveolin-1 and TβRI and suppressing caveolae-mediated internalization of TβRI [27]. More recent studies have shown that the roles of clathrin and caveolae in controlling TGFβ receptor internalization are more complex than previously thought. Of particular interest was the discovery of caveolin-1 and EEA1 double-positive early endosomes, which revealed a new level of interaction between these internalization mechanisms that were originally thought to independently regulate receptor trafficking [28]. The extent to which specific receptor subtypes have inherent affinities for these microdomains/internalization pathways remains unknown, however, early studies showed that different receptor chimeras – including signaling competent heteromeric and homomeric combinations – were internalized at similar rates [29].

*TGFβ coreceptors: betaglycan and endoglin*

While not required for canonical TGFβ signaling pathway activation, in contrast to type I and type II receptors, betaglycan (TβRIII) and endoglin are accessory transmembrane receptors/coreceptors that play several roles in controlling TGFβ signaling at the cell membrane, by binding other receptors or ligands and facilitating their functional interactions. Betaglycan, as the only canonical type III receptor, is a proteoglycan that binds TGFβ ligand and improves the affinity with which TβRII binds it, which is critical particularly in the case of the TGFβ2 isoform that has the least affinity of the three TGFβ ligand isoforms for type I and type II receptors [30]. In parallel, betaglycan also regulates the interactions of inhibins with their corresponding receptors ActRII and ActRIIB [31,32]. Given that one role of inhibins is to block activin signaling, betaglycan effectively plays dual roles in concurrently enhancing and blocking TGFβ signaling through

different branches of the pathway. While typically within the cell membrane, a soluble form of betaglycan also occurs naturally, which competes with TGFβ ligands for access to membrane-bound type I and type II receptors [33].

Despite having functions that overlap with those of betaglycan, endoglin is not explicitly known as a TGFβ type III receptor. Nonetheless, endoglin is a transmembrane glycoprotein with high sequence similarly to betaglycan that interacts with betaglycan and other TGFβ receptors to regulate signaling. In addition to TGFβs, endoglin also interacts with other TGFβ superfamily such as BMP9 and BMP10 [34,35]. Interestingly, endoglin is unable to bind to several types of ligand in the absence of their corresponding type II receptor, which sets it apart from betaglycan [36]. The extent to which coreceptors such as betaglycan and endoglin regulate effector selection or the outcomes of downstream signaling remains unclear. Lee et al. showed that betaglycan enhances BMP signaling through both ALK3 and ALK6, but concurrently promotes the internalization of ALK6 while maintaining ALK3 at the cell membrane [37].

*A signaling locus: the primary cilium*

The primary cilium is a solitary cell surface organelle that extends from the plasma membrane of almost all cell types that has important roles in coordinating cellular homeostasis (i.e. through mechanisms that remain unclear). Resembling a cellular antenna, the primary cilium plays many roles in a variety of cellular contexts, and serves as both a chemosensor and mechanosensor that can detect changes in ECM properties but also other physical cues such as fluid shear stress. The base of the primary cilium, called the ciliary pocket, is a locus for signaling pathways such as the TGFβ pathway, and work by Clement et al. identified the ciliary pocket as a hotspot for clathrin-mediated endocytosis of TGFβ receptors, showing that ALK5 and TGFβRII are trafficked there – likely from the ciliary tip – following treatment with exogenous TGFβ [38].

The length of the primary cilium is an important variable in controlling its sensitivity to local biological and chemical stimuli: nutrient-poor microenvironments can induce ciliary growth and

longer cilia are more sensitive to mechanical deflections [39]. In this manner, the primary cilium enables crosstalk between mechanical and biological cues through pathways such as TGFβ. The contrary is true as well: disorders that arise from mutations that disrupt ciliary function overlap with those associated with dysregulated TGFβ or BMP signaling. Work by Labour et al. demonstrated the critical role of the primary cilium in coordinating TGFβ-induced hMSC chemotaxis, showing that cilia-deficient hMSCs exhibited no increase in phospho-Smad3 and reduced migration capacity following treatment with TGFβ1 [40]. Their work also showed distinct localization patterns of the non-phosphorylated and phosphorylated forms of ALK5, with the former spread throughout the entire cilia and the latter concentrating at the ciliary base.

The primary cilium is not only essential in regulating TGFβ-Smad2/3 signaling, but also plays a major role in coordinating BMP-Smad1/5/8 signaling, potentially by serving as a locus for BMP receptors. Recent work has shown that endothelial cells possessing primary cilia exhibit a higher sensitivity to BMP9 signaling, in particular with simultaneous application of low fluid shear stress [41]. However, many questions remain about whether or not this primary cilium-localized receptor population is responsive to changes in physical cues such as fluid shear stress.

**Mechanoregulation of TGFβ receptors**

Cells experience several distinct mechanical cues that play important roles in modulating or priming the cellular response to biochemical cues. These cues – such as extracellular matrix stiffness or topography; pressure or fluid shear stress; or stretch – intersect with the TGFβ pathway at multiple hierarchical levels and play critical roles in regulating downstream signaling.

*Substrate stiffness, topography, and mechanical stretch*

An organized mechanotransduction pathway communicates changes in extracellular matrix stiffness to cells and allows them to modify their internal cytoskeletal tension in response. Integrin binding to ECM ligands leads to the formation of focal adhesions, via recruitment of

proteins such as vinculin, talin, focal adhesion kinase, and α-actinin. These proteins interact with GTPases such as Rho to regulate cytoskeletal organization and actomyosin contractility, which ultimately lead to changes in cell shape. The role of ECM stiffness in enabling activation of latent TGFβ has been well described; however, less well known are the mechanisms through which ECM stiffness coordinates the activity of TGFβ receptors to control downstream signaling [42,43].

We recently identified a cytoskeletal tension-sensitive functional subpopulation of TGFβ receptors localized at focal adhesions [44]. In cells grown on stiff substrates such as glass or tissue culture plastic, we observed a peripheral ring of TGFβ receptor type II surrounding ALK5 and ALK1 at these adhesion sites. When cytoskeletal tension was disrupted using a pharmacological Rho/ROCK or myosin II inhibitor, the spatial segregation of the two receptor populations collapsed, resulting in receptor colocalization and functional multimerization, priming them to respond to TGFβ ligand. This work identified a new mechanism of TGFβ signaling regulation, whereby spatial segregation of complimentary receptor types can be disrupted to enable a robust signaling response only in the presence of a specific combination of physical and biological cues.

In addition to stiffness, surface topography has also been shown to influence a variety of cellular decisions, including differentiation, in part through regulation of TGFβ signaling. Characterized by a distribution of peaks and valleys at the microscale or nanoscale, topography plays a major role in regulating cellular morphology and cytoskeletal tension by coordinating the direction and integrity of protrusions such as integrins that directly interact with the surrounding matrix. Zhang et al. have shown that the surface topography of calcium phosphate ceramics plays a major role in coordinating the quantity of TGFβ receptors along the ciliary axoneme [45]. Their results show that cells grown on surfaces with a submicron-scale topography had longer primary cilia and increased levels of TβRII along their lengths than those grown on surfaces with a micron-scale topography.

Work by Allen, et al. showed a similar result in fibroblasts grown on microfibers of varying lengths [46]. Cells grown on long fibers exhibited a reduction in TGFβ ligand, TGFβ receptor, and Smad3 gene expression than cells grown on short fibers or on flat surfaces, which subsequently reduced collagen deposition by the cells around the fibers. They postulated that longer fibers are interpreted by the cells as an increase in substrate compliance (reduction in stiffness) due to a more deformable interface. If this is the case, it would be interesting to see if TGFβ receptor localization at focal adhesions could also be modulated by substrate topography.

Similar to changes in substrate stiffness, mechanical stretch is physical cue that is typically applied to cells growing on a compliant substrate by stretching and relaxing the substrate in a cyclic manner. Using mesangial cells, Chen, et al. found that stretch induces TβRI transactivation and Smad phosphorylation independently of ligand binding, through a mechanism that involves Rac1/Pak1 [47]. Stretch-induced changes in TGFβ signaling pathway activity were blocked by the TβRI inhibitor SB-431542, but not by a neutralizing TGFβ antibody. However, the authors did not evaluate the roles of other TGFβ superfamily ligands in this mechanism, which is imperative, given the overlapping and often compensatory roles of different TGFβ ligands and receptors.

*Fluid shear stress*

Fluid shear stress (FSS) is an important physical cue experienced in a variety of biological contexts, for example, in mechanically-loaded osteocytes, or in epithelial cells such as those in the renal tubule or cornea. In these contexts, it is known to activate the TGFβ signaling pathway through mechanisms that are cell-type specific [48,49]. In platelet releasates and in synovial fluid, stimulation with FSS increased levels of active TGFβ ligand [50,51], however, these studies did not evaluate the receptor-level requirements for FSS activation of TGFβ signaling. In renal tubular epithelial cells, treatment with the ALK4/5/7 inhibitor LY-364947, but not an activin ligand trap, blocked Smad2/3 activation by FSS, suggesting that this mechanism requires the activity of functional TGFβ ligand [52]. Interestingly, Chang, et al. found that FSS-induced Smad1/5

phosphorylation is mediated by ALK3 and not ALK6 in MG63 osteosarcoma cells, through a mechanism that was found to be BMP ligand-independent, but did not evaluate FSS-induced changes in TGFβ/Smad2/3 signaling in their study [53]. Using OCY454 cells, I found that FSS rapidly induces ALK5/TβRII heteromerization, Smad1 and Smad2/3 phosphorylation, and downstream TGFβ gene expression in a ligand-dependent manner, showing that stimulation with FSS concurrently activates several types of TGFβ type I receptors in a manner that differed from that achieved by treatment with TGFβ or BMP4 ligand alone (*in press,* Monteiro, et al. *The FASEB Journal.* 2020).

**TGFβ receptors in disease**

Dysregulation of TGFβ signaling plays a causal role in many pathologies, many of which arise from mutations in TGFβ receptors or induce changes in TGFβ signaling at the receptor-level that promote a damaging feedback loop. These manifest by either enhancing or suppressing the amount of TGFβ signaling that takes place, which consequently shifts the balance of signaling through parallel arms of the TGFβ superfamily. While these pathologies can occur or originate in a variety of tissue types, a significant number of them present with skeletal abnormalities, some of which are discussed below [54].

*Pathologic suppression of TGFβ signaling*

Hereditary hemorrhagic telangiectasia (HHT) is a disease primarily caused by mutations in endoglin or ALK1 that primarily targets endothelial cells [55]. In these cells, TGFβ can signal through ALK1 or ALK5, the choice of which either induces cell proliferation and migration (via ALK1) or blocks it. In healthy cells, a balance between these two pathways promotes homeostasis, but in HHT cells, the ALK1 pathway is impaired. While this would normally shift these cells away from a proliferative phenotype, an adaptive response leads to a compensatory reduction in ALK5 levels [56]. Interestingly, Goumans et al. showed that ALK5 is important for

TGFβ/ALK1 signaling in the endothelium, such that cells lacking ALK5 are deficient in TGFβ/ALK1 responses [57]. This balance between TGFβ signaling through ALK1 and ALK5 is also important in other tissues such as cartilage, where the ALK1/ALK5 ratio increases with age and in osteoarthritis [58,59]. This shift towards ALK1 leads to enhanced downstream signaling through Smad1/5/8, which complements an increase in the matrix metalloproteinase MMP-13 expression, pushing chondrocytes towards a hypertrophic phenotype.

*Pathologic enhancement of TGFβ signaling*

In fibrodysplasia ossificans progressiva (FOP), a mutation in ALK2 induces heterotopic bone formation in soft tissues. In the absence of BMP ligands, BMP signaling through ALK2 is typically blocked; however, in FOP patients, the mutated ALK2 causes an increase in basal levels of signaling even in the absence of ligand [60,61]. Subsequently, in the presence of BMP ligands, cells with the most common R206H mutation in ALK2 respond in a hypersensitive manner, the result of an aberrant accumulation of ALK2 receptors at the cell membrane.

Loeys-Dietz syndrome (LDS) is a connective tissue disorder similar to Marfan syndrome characterized by aortic aneurysm, of which there are several types that are caused by separate mutations in TβRI or TβRII, in addition to TGFβ ligands and Smads [62]. In Marfan syndrome, a mutation in the glycoprotein fibrillin-1 prevents TGFβ from remaining bound to the ECM in a latent form, which leads to an increase in active TGFβ ligand and downstream signaling [63]. Likewise, TGFβ signaling is increased in aortic tissues from LDS patients, however, the mechanisms by which mutations in TGFβ receptors lead to an LDS phenotype appear paradoxical and are yet to be fully elucidated. The same receptors in LDS that lead to increased TGFβ signaling *in vivo* remain capable of binding to exogenous TGFβ ligand *in vitro* but fail to activate Smad2 [64–66]. One current hypothesis is that these mutant receptors regulate the binding and activities of other functional receptors [67].

**Summary**

The overlapping and often compensatory roles of different TGFβ receptors makes identifying their individual responsibilities challenging. *In vitro* experiments provide a means to probe the participation of individual receptor subtypes in response to individual biochemical or physical stimuli in a way that is challenging to do *in vivo*, given the multitude of cues in the cellular microenvironment. How cells generate unique responses to these combinations of cues, each of which might independently activate or suppress TGFβ superfamily signaling, remains a critical unanswered question. One idea is that cells possess discrete receptor subpopulations capable of being independently targeted by distinct stimuli.

The requirement for several distinct TGFβ pathway members – ligand(s), multiple receptors, and effectors – to simultaneously exist in close proximity for signaling to take place provides an effective cellular defense against unwanted signaling. Likewise, feedback loops upregulate the expression of inhibitory Smads and promote the internalization and degradation of receptors after they have been used for signaling. In disease, this intricate system of redundancy and self-regulation collapses, leading to excess signaling or deficiency. The existence of discrete receptor subpopulations would provide cells with an additional level of control over TGFβ signaling, such that certain populations could be exhausted while others remain latent but ready to respond to future stimuli.

A deeper understanding of the interactions between TGFβ receptor subtypes and their individual roles in responding to distinct biological or physical cues has the potential to uncover more precise targets for therapies beyond pan-TGFβ blocking antibodies or receptor-level inhibitors that completely block signaling through multiple receptor subtypes. Ultimately, the quantity and types of signaling-competent TGFβ receptors and their localization at mechanosensory sites or cell surface microdomains plays a major role in defining the duration, intensity, and quality of the cellular TGFβ response, generating a signaling *fingerprint* in response to a unique combination of concurrent inputs.

**References**

1     McLean, S. and Di Guglielmo, G.M. (2010) TGF beta (transforming growth factor beta) receptor type III directs clathrin-mediated endocytosis of TGF beta receptor types I and II. *Biochem. J.* 429, 137–145

2     Derynck, R. and Zhang, Y.E. (2003) Smad-dependent and Smad-independent pathways in TGF-beta family signalling. *Nature* 425, 577–584

3     Feng, X.-H. and Derynck, R. (2005) Specificity and versatility in tgf-beta signaling through Smads. *Annu. Rev. Cell Dev. Biol.* 21, 659–693

4     Bai, J. and Xi, Q. (2018) Crosstalk between TGF-beta signaling and epigenome. *Acta Biochim. Biophys. Sin. (Shanghai).* 50, 60–67

5     Janakiraman, H. *et al.* (2018) The Long (lncRNA) and Short (miRNA) of It: TGFbeta-Mediated Control of RNA-Binding Proteins and Noncoding RNAs. *Mol. Cancer Res.* 16, 567–579

6     Blahna, M.T. and Hata, A. (2012) Smad-mediated regulation of microRNA biosynthesis. *FEBS Lett.* 586, 1906–1912

7     Shen, J. and Hung, M.-C. (2015) Signaling-mediated regulation of MicroRNA processing. *Cancer Res.* 75, 783–791

8     Wrana, J.L. *et al.* (1992) TGF beta signals through a heteromeric protein kinase receptor complex. *Cell* 71, 1003–1014

9     Wrana, J.L. *et al.* (1994) Mechanism of activation of the TGF-beta receptor. *Nature* 370, 341–347

10    Chen, R.H. and Derynck, R. (1994) Homomeric interactions between type II transforming growth factor-beta receptors. *J. Biol. Chem.* 269, 22868–22874

11    Huang, T. *et al.* (2011) TGF-β signalling is mediated by two autonomously functioning TβRI:TβRII pairs. *EMBO J.* 30, 1263–1276

12    Aykul, S. and Martinez-Hackert, E. (2016) Transforming Growth Factor-beta Family

Ligands Can Function as Antagonists by Competing for Type II Receptor Binding. *J. Biol. Chem.* 291, 10792–10804

13    Khalil, A.M. *et al.* (2016) Differential Binding Activity of TGF-beta Family Proteins to Select TGF-beta Receptors. *J. Pharmacol. Exp. Ther.* 358, 423–430

14    Little, S.C. and Mullins, M.C. (2009) Bone morphogenetic protein heterodimers assemble heteromeric type I receptor complexes to pattern the dorsoventral axis. *Nat. Cell Biol.* 11, 637–643

15    Luo, J. *et al.* (2010) TGFbeta/BMP type I receptors ALK1 and ALK2 are essential for BMP9-induced osteogenic signaling in mesenchymal stem cells. *J. Biol. Chem.* 285, 29588–29598

16    Lee, H.-W. *et al.* (2017) Alk2/ACVR1 and Alk3/BMPR1A Provide Essential Function for Bone Morphogenetic Protein-Induced Retinal Angiogenesis. *Arterioscler. Thromb. Vasc. Biol.* 37, 657–663

17    Traeger, L. *et al.* (2018) ALK3 undergoes ligand-independent homodimerization and BMP-induced heterodimerization with ALK2. *Free Radic. Biol. Med.* 129, 127–137

18    Ramachandran, A. *et al.* (2018) TGF-beta uses a novel mode of receptor activation to phosphorylate SMAD1/5 and induce epithelial-to-mesenchymal transition. *Elife* 7,

19    Wu, L. and Derynck, R. (2009) Essential role of TGF-beta signaling in glucose-induced cell hypertrophy. *Dev. Cell* 17, 35–48

20    Huang, S.S. *et al.* (2016) Ethanol Enhances TGF-β Activity by Recruiting TGF-β Receptors From Intracellular  Vesicles/Lipid Rafts/Caveolae to Non-Lipid Raft Microdomains. *J. Cell. Biochem.* 117, 860–871

21    Huang, S.S. *et al.* (2016) DMSO Enhances TGF-β Activity by Recruiting the Type II TGF-β Receptor From  Intracellular Vesicles to the Plasma Membrane. *J. Cell. Biochem.* 117, 1568–1579

22    Duan, D. and Derynck, R. (2019) Transforming growth factor-beta (TGF-beta)-induced

up-regulation of TGF-beta receptors at the cell surface amplifies the TGF-beta response. *J. Biol. Chem.* 294, 8490–8504

23   Vizan, P. *et al.* (2013) Controlling long-term signaling: receptor dynamics determine attenuation and refractory behavior of the TGF-beta pathway. *Sci. Signal.* 6, ra106

24   Le Roy, C. and Wrana, J.L. (2005) Clathrin- and non-clathrin-mediated endocytic regulation of cell signalling. *Nat. Rev. Mol. Cell Biol.* 6, 112–126

25   Anders, R.A. *et al.* (1998) Differential requirement for type I and type II transforming growth factor beta receptor kinase activity in ligand-mediated receptor endocytosis. *J. Biol. Chem.* 273, 23118–23125

26   Di Guglielmo, G.M. *et al.* (2003) Distinct endocytic pathways regulate TGF-beta receptor signalling and turnover. *Nat. Cell Biol.* 5, 410–421

27   Hwangbo, C. *et al.* (2016) Syntenin regulates TGF-beta1-induced Smad activation and the epithelial-to-mesenchymal transition by inhibiting caveolin-mediated TGF-beta type I receptor internalization. *Oncogene* 35, 389–401

28   He, K. *et al.* (2015) Internalization of the TGF-beta type I receptor into caveolin-1 and EEA1 double-positive early endosomes. *Cell Res.* 25, 738–752

29   Anders, R.A. *et al.* (1997) Distinct endocytic responses of heteromeric and homomeric transforming growth factor beta receptors. *Mol. Biol. Cell* 8, 2133–2143

30   López-Casillas, F. *et al.* (1994) Betaglycan can act as a dual modulator of TGF-beta access to signaling receptors:  mapping of ligand binding and GAG attachment sites. *J. Cell Biol.* 124, 557–568

31   Villarreal, M.M. *et al.* (2016) Binding Properties of the Transforming Growth Factor-β Coreceptor Betaglycan:  Proposed Mechanism for Potentiation of Receptor Complex Assembly and Signaling. *Biochemistry* 55, 6880–6896

32   Lewis, K.A. *et al.* (2000) Betaglycan binds inhibin and can mediate functional antagonism of activin  signalling. *Nature* 404, 411–414

33    Vilchis-Landeros, M.M. *et al.* (2001) Recombinant soluble betaglycan is a potent and isoform-selective transforming growth  factor-beta neutralizing agent. *Biochem. J.* 355, 215–222

34    David, L. *et al.* (2007) Identification of BMP9 and BMP10 as functional activators of the orphan activin  receptor-like kinase 1 (ALK1) in endothelial cells. *Blood* 109, 1953–1961

35    Alt, A. *et al.* (2012) Structural and functional insights into endoglin ligand recognition and binding. *PLoS One* 7, e29948

36    Barbara, N.P. *et al.* (1999) Endoglin is an accessory protein that interacts with the signaling receptor complex  of multiple members of the transforming growth factor-beta superfamily. *J. Biol. Chem.* 274, 584–594

37    Lee, N.Y. *et al.* (2009) The transforming growth factor-beta type III receptor mediates distinct subcellular  trafficking and downstream signaling of activin-like kinase (ALK)3 and ALK6 receptors. *Mol. Biol. Cell* 20, 4362–4370

38    Clement, C.A. *et al.* (2013) TGF-beta signaling is associated with endocytosis at the pocket region of the primary cilium. *Cell Rep.* 3, 1806–1814

39    Spasic, M. and Jacobs, C.R. (2017) Lengthening primary cilia enhances cellular mechanosensitivity. *Eur. Cell. Mater.* 33, 158–168

40    Labour, M.-N. *et al.* (2016) TGFbeta1 - induced recruitment of human bone mesenchymal stem cells is mediated by the primary cilium in a SMAD3-dependent manner. *Sci. Rep.* 6, 35542

41    Vion, A.-C. *et al.* (2018) Primary cilia sensitize endothelial cells to BMP and prevent excessive vascular regression. *J. Cell Biol.* 217, 1651–1665

42    Hinz, B. (2015) The extracellular matrix and transforming growth factor-beta1: Tale of a strained relationship. *Matrix Biol.* 47, 54–65

43    Klingberg, F. *et al.* (2014) Prestress in the extracellular matrix sensitizes latent TGF-beta1 for activation. *J. Cell Biol.* 207, 283–297

44      Rys, J.P. *et al.* (2015) Discrete spatial organization of TGFbeta receptors couples receptor multimerization and signaling to cellular tension. *Elife* 4, e09300

45      Zhang, J. *et al.* (2017) Topography of calcium phosphate ceramics regulates primary cilia length and TGF receptor recruitment associated with osteogenesis. *Acta Biomater.* 57, 487–497

46      Allen, J. *et al.* (2016) Tunable Microfibers Suppress Fibrotic Encapsulation via Inhibition of TGFbeta Signaling. *Tissue Eng. Part A* 22, 142–150

47      Chen, G. *et al.* (2013) TGFβ receptor I transactivation mediates stretch-induced Pak1 activation and CTGF  upregulation in mesangial cells. *J. Cell Sci.* 126, 3697–3712

48      Nguyen, J. *et al.* (2013) Load regulates bone formation and Sclerostin expression through a TGFbeta-dependent mechanism. *PLoS One* 8, e53813

49      Utsunomiya, T. *et al.* (2016) Transforming Growth Factor-beta Signaling Cascade Induced by Mechanical Stimulation of Fluid Shear Stress in Cultured Corneal Epithelial Cells. *Invest. Ophthalmol. Vis. Sci.* 57, 6382–6388

50      Kouzbari, K. *et al.* (2019) Oscillatory shear potentiates latent TGF-beta1 activation more than steady shear  as demonstrated by a novel force generator. *Sci. Rep.* 9, 6065

51      Albro, M.B. *et al.* (2012) Shearing of synovial fluid activates latent TGF-β. *Osteoarthr. Cartil.* 20, 1374–1382

52      Kunnen, S.J. *et al.* (2017) Fluid shear stress-induced TGF-beta/ALK5 signaling in renal epithelial cells is modulated by MEK1/2. *Cell. Mol. Life Sci.* 74, 2283–2298

53      Chang, S.-F. *et al.* (2008) Tumor cell cycle arrest induced by shear stress: Roles of integrins and Smad. *Proc. Natl. Acad. Sci. U. S. A.* 105, 3927–3932

54      MacFarlane, E.G. *et al.* (2017) TGF-β Family Signaling in Connective Tissue and Skeletal Diseases. *Cold Spring Harb. Perspect. Biol.* 9,

55      Fernández-L, A. *et al.* (2006) Hereditary hemorrhagic telangiectasia, a vascular dysplasia affecting the TGF-beta  signaling pathway. *Clin. Med. Res.* 4, 66–78

56      Fernandez-L, A. *et al.* (2005) Blood outgrowth endothelial cells from Hereditary

Haemorrhagic Telangiectasia  patients reveal abnormalities compatible with vascular

lesions. *Cardiovasc. Res.* 68, 235–248

57      Goumans, M.J. *et al.* (2003) Activin receptor-like kinase (ALK)1 is an antagonistic

mediator of lateral  TGFbeta/ALK5 signaling. *Mol. Cell* 12, 817–828

58      Blaney Davidson, E.N. *et al.* (2009) Increase in ALK1/ALK5 ratio as a cause for elevated

MMP-13 expression in osteoarthritis in humans and mice. *J. Immunol.* 182, 7937–7945

59      van der Kraan, P.M. *et al.* (2012) Age-dependent alteration of TGF-β signalling in

osteoarthritis. *Cell Tissue Res.* 347, 257–265

60      Kaplan, F.S. *et al.* (2008) Fibrodysplasia ossificans progressiva. *Best Pract. Res. Clin.
Rheumatol.* 22, 191–205

61      Shen, Q. *et al.* (2009) The fibrodysplasia ossificans progressiva R206H ACVR1 mutation

activates  BMP-independent chondrogenesis and zebrafish embryo ventralization. *J. Clin.
Invest.* 119, 3462–3472

62      Loeys, B.L. *et al.* (2005) A syndrome of altered cardiovascular, craniofacial,

neurocognitive and skeletal  development caused by mutations in TGFBR1 or TGFBR2.

*Nat. Genet.* 37, 275–281

63      Benke, K. *et al.* (2013) The role of transforming growth factor-beta in Marfan syndrome.

*Cardiol. J.* 20, 227–234

64      Hara, H. *et al.* Activation of TGF-β signaling in an aortic aneurysm in a patient with

Loeys-Dietz  syndrome caused by a novel loss-of-function variant of TGFBR1. , *Human
genome variation*, 6. (2019) , 6

65      Gallo, E.M. *et al.* (2014) Angiotensin II-dependent TGF-β signaling contributes to Loeys-

Dietz syndrome  vascular pathogenesis. *J. Clin. Invest.* 124, 448–460

66      Horbelt, D. *et al.* (2010) Quantitative analysis of TGFBR2 mutations in Marfan-syndrome-

related disorders  suggests a correlation between phenotypic severity and Smad

signaling activity. *J. Cell Sci.* 123, 4340–4350

67 Iwata, J. *et al.* (2012) Modulation of noncanonical TGF-β signaling prevents cleft palate in Tgfbr2 mutant  mice. *J. Clin. Invest.* 122, 873–885

68 Budi, E.H. *et al.* (2019) Integration of TGF-β-induced Smad signaling in the insulin-induced transcriptional  response in endothelial cells. *Sci. Rep.* 9, 16992

69 Finnson, K.W. *et al.* (2010) Endoglin differentially regulates TGF-β-induced Smad2/3 and Smad1/5 signalling and  its expression correlates with extracellular matrix production and cellular differentiation state in human chondrocytes. *Osteoarthr. Cartil.* 18, 1518–1527

# Chapter 3

# Materials and Methods

*Cell culture, transfection, and reagents*

Studies were performed using ATDC5 murine chondroprogenitor cells (RCB0565, RIKEN) and human embryonic kidney (HEK) 293 cells (Chapter 4), in addition to osteocyte-like MLO-Y4 cells (gift from Lynda Bonewald) and OCY454 cells (gift from Paola Divieti Pajevic), an osteocyte cell line that can undergo terminal differentiation *in vitro* [1] (Chapters 5-6). All cells were maintained on tissue-culture treated cell culture dishes. For imaging experiments, ATDC5 cells were cultured on collagen II (1 mg/mL in acetic acid at 1% in PBS)-coated glass-bottom imaging wells (Cellvis). For biochemical assays, HEK 293 cells were plated in 10 cm cell culture dishes. MLO-Y4 and OCY454 cells were grown on collagen type I-coated tissue culture treated dishes in α-MEM (12571, Gibco) supplemented with 2.5% fetal bovine serum, 2.5% bovine calf serum, and 1% penicillin/streptomycin (MLO-Y4) or 10% fetal bovine serum and 1% Antibiotic/Antimycotic (Gibco) (OCY454). All cell types were kept at 37ºC - except OCY454 cells which were maintained at 33ºC - with 5% $CO_2$, and passaged every 2-3 days.

For plating in microfluidic devices, OCY454 cells were detached with TrypLE Express (Gibco) and resuspended in media to a concentration of $4 \times 10^6$ cells/mL before seeding. After

filling the microfluidic chambers with the cell suspension (~100k cells/chamber), media was replaced daily, and experiments were performed 2 days after seeding. Cells were serum starved with reduced serum media (α-MEM, 1% fetal bovine serum, 1% Antibiotic/Antimycotic) for 1 hour before treatment which was maintained during experiments.

Cells were transfected following manufacturer's instructions using previously optimized protocols. HEK293 cells were transiently transfected with mEmerald-cofilin, Flag-TβRI, Flag-TβRII, and Myc-TβRI using Effectene (Qiagen). ATDC5 cells were transfected using Nucleofection (Lonza) or Effectene (Qiagen) following manufacturer's instructions prior to plating onto the imaging wells. OCY454 cells were transfected using Fugene6 (Promega). Except where noted in the figures, cells were treated as indicated with TGFβ1 (5 ng/mL), BMP4 (50 ng/mL) (both from Peprotech); 1d11 (TGFβ ligand blocking antibody, 1.25 μg/mL, Clone 1d11.16.8, BioXCell); Noggin (BMP ligand antagonist, 100 ng/mL, SRP3227, Sigma Aldrich); SB-431542 (ALK4/5/7 inhibitor, 10 μM), LDN-193189 (ALK1/2/3/6 inhibitor, 1 μM), LDN-214117 (ALK1/2 inhibitor, 1 μM), SC-79 (AKT agonist, 10 μM) (all from Selleckchem); recombinant mouse ALK1Fc (100 ng/mL, R&D Systems); LY294002 (AKT antagonist, 50 μM, Calbiochem); Y27632 (ROCK inhibitor 10 μM, Sigma); or blebbistatin (Myosin II inhibitor, 10 μM, Cayman Chemical).

*Antibodies*

Primary antibodies used in this study are listed in Table 2.1. For immunofluorescence, primary antibodies were used at 1:200 and secondary antibodies at 1:400 unless otherwise indicated. For Western blotting, anti-mouse and anti-rabbit secondary antibodies conjugated to 680 or 800 IRDye fluorophores (1:15000, LI-COR Biosciences) were used.

**Table 3.1: Antibodies used for imaging and Western blotting**

| Target | Product Information | Conc. | Use | Chapter |
|---|---|---|---|---|
| Cofilin | ACFL02, Cytoskeleton | 1:500 | WB, IP | 4 |
| pSmad3 | gift, Edward Leof, Mayo Clinic | 1:1000 | WB | 4 |
| pSmad2/3 | ab52903, Abcam | 1:2000 | WB | 5-6 |
| Smad2/3 | 610842, BD Biosciences | 1:1000, 1:200 | WB, IF | 5-6 |
| Beta-actin | ab8226, Abcam | 1:2500 | WB | 4-6 |
| TβRI | sc398, Santa Cruz Biotechnology | 1:1000 | WB, IP | 4 |
| TβRI | ab31013, Abcam | 1:200 | PLA | 6 |
| TβRII | sc17799, Santa Cruz Biotechnology | 1:50 | PLA | 6 |
| Flag | F3165, Sigma Aldrich | 1:1000 | WB, IP | 4,6 |
| pAKT | #4060, Cell Signaling | 1:2000 | WB | 6 |
| AKT | #9272, Cell Signaling | 1:1000 | WB | 6 |

**Key:** WB, Western Blotting; IP, Immunoprecipitation; IF, Immunofluorescence; PLA, proximity ligation assay

*Microfluidic device fabrication and shear stress experiments*

The microfluidic devices used for shear stress experiments were fabricated using soft lithography techniques. Briefly, a 3-inch diameter silicon wafer was spin-coated (i.e. for SU-8 3050, 1900rpm) with a 75 µm layer of photoresist (SU-8, Kayaku) and then exposed to UV light through a custom photomask (CAD/Art Services) following a pre-exposure bake (i.e. for SU-8 3050: 2 minutes at 65ºC, 30 seconds at 95ºC, 3 minutes at 65ºC). Following a post-exposure bake (i.e. for SU-8 3050: 2 minutes at 65ºC, 4 minutes at 95ºC, 2 minutes at 65ºC), the unreacted photoresist was removed, followed by a 30-minute hard bake at 150ºC. The chambers (Fig. 1A) had an elongated hexagonal culture area (25 mm long, 10 mm wide, 75 µm tall) with a chamber volume of ~15 µL.

Polydimethylsiloxane (PDMS, Sylgard 184, Dow) was prepared at a 10:1 elastomer/curing agent ratio, degassed for 30 minutes, poured over the silicon wafer mold, and allowed to cure overnight at 60°C. The cured PDMS was cut from the mold (2 chambers per PDMS piece, to fit on one 25 mm x 75 mm glass slide), inlets were cored with a 1 mm biopsy punch, and the PDMS was bonded to a glass slide following exposure of mating surfaces to 40 seconds of air plasma using a plasma cleaner (PDC-32G, Harrick Plasma). PDMS chambers were sterilized with 70% ethanol and glass surfaces were coated with a rat tail collagen type I solution (CB-40236, Corning) prior to cell seeding.

For shear stress experiments, a peristaltic pump (Masterflex L/S, Masterflex) was installed within a sterile incubator and used to circulate media through microfluidic chambers to stimulate the cells precisely with the designated amounts of shear stress ($\tau = 6 \times Q \times \mu / w \times h^2$). The volumetric flow rate of the reduced-serum media ($Q$) was varied to achieve the desired wall shear stress ($\tau$) experienced by the cells. The viscosity of media ($\mu$) pumped through the chambers (with width $w$ and height $h$) was estimated as that of water at 37°C. Chambers were connected to the pump with sterilized polyethylene tubing (1.19 mm ID, Scientific Commodities). Cells grown in non-flow conditions were also grown in microfluidic chambers unless otherwise indicated.

*Western blotting and co-immunoprecipitation*

Whether grown on traditional cell culture plates or in microfluidic chambers, cells were rinsed with 4°C PBS and lysed with 4°C RIPA buffer (50 mM Tris pH 7.4, 1% NP-40, 0.25% sodium deoxycholate, 150 mM NaCl, 1 mM EDTA, supplemented with phosphatase inhibitor (A32957, Pierce), protease inhibitor (cOmplete Mini, Roche), and 1 mM PMSF). Lysates were collected by scraping plates, or by collecting RIPA eluates flowed through the chambers. Lysates were sonicated on ice using a cuphorn sonicator (5 15-second pulses, 45 seconds between pulses) and cleared by centrifugation at 10000 $g$ for 10 minutes at 4°C. For western analysis, protein separation was achieved using 10% polyacrylamide gels with an SDS/PAGE protocol,

prior to transfer to a nitrocellulose membrane, blocking with 5% milk, and probing with antibodies in 1% milk or 5% BSA, all of which were suspended in TBS with 0.1% Tween 20. After probing, band intensities were visualized using an Odyssey infrared imaging system (LI-COR Biosciences) and quantified using Image Studio Lite (v5.2, LI-COR Biosciences). Fold changes were normalized to beta actin, and treatment groups to unstimulated controls as indicated.

For co-immunoprecipitation, cell lysates were harvested as described above with ice-cold IP lysis buffer (50 mM Tris pH 7.5, 150 mM NaCl, 2 mM EDTA, 0.5% IGEPAL CA-630, 0.25% sodium deoxycholate, supplemented with protease and phosphatase inhibitors) and were incubated with Anti-FLAG M2 Magnetic Beads (Sigma Aldrich) overnight at 4ºC, washed three times in TBS (5 minutes each), and eluted by boiling at 90ºC (10 minutes) before western analysis.


*Quantitative RT-PCR and RNAseq*

Cells were rinsed with PBS and lysed with 700 μL QIAzol (Qiagen), collected by scraping or as chamber eluate, and mRNA was purified using the miRNeasy kit (Qiagen) following manufacturer's instructions. The concentration of mRNA was determined using a NanoDrop spectrophotometer and quality for RNAseq was verified using an Agilent Bioanalyzer.

For qRT-PCR, RNA (1 μg) per sample was reverse transcribed to generate cDNA using iScript (Bio-Rad) and analysis was performed in a C1000 Thermal Cycler/CFX96 Real-Time System (Bio-Rad) using TaqMan probes (Table 1, below). 30 ng equivalent of cDNA was used for each gene, and reactions were run in duplicate, followed by quantification using the ΔΔCt method with normalization to the housekeeping gene *Rn18s* [2], which was not regulated in an FSS-dependent manner.

For RNAseq, 250 ng was used as input to library preparation using the QuantSeq 3' mRNA-Seq Library Prep Kit FWD for Illumina (Lexogen). Libraries were multiplexed and 50 bp single-end reads were generated using one lane of an Illumina HiSeq 4000 at the UCSF Center for Advanced Technology (San Francisco, CA). Sequencing adapters were trimmed using

cutadapt [3] and trimmed reads were subjected to quality control analysis using FastQC (www.bioinformatics.babraham.ac.uk/projects/fastqc). Transcript expression was quantified using the quasi-mapping-based mode of Salmon and the reference mouse genome build GRCm38—Ensembl using k-mers of length 25 with otherwise default parameters [4]. The R Statistical Computing Environment was used to obtain read counts and the DESeq2 package [5] was used to find differentially expressed genes (DEGs) with a false discovery rate (FDR) of 0.05, which were input into Enrichr for pathway analysis [6,7]. Pathways were considered significantly regulated with FDR<0.05. Our datasets are publicly available (NCBI BioProject PRJNA673223).

**Table 3.2: TaqMan probe IDs for qRT-PCR**

| Gene | TaqMan probe ID |
|---|---|
| *Rn18s* | Mm03928990_g1 |
| *Ptgs2* | Mm00478374_m1 |
| *Serpine1* | Mm00435858_m1 |
| *Smad7* | Mm00484742_m1 |
| *Cdkn1a* | Mm04207341_m1 |
| *Fos* | Mm00487425_m1 |
| *Jun* | Mm00495062_s1 |

*Imaging and image analysis*

For immunofluorescence, cells were fixed with 4% paraformaldehyde in PBS (10 minutes), permeabilized with 0.5% Triton X-100 in PBS (5 minutes), and blocked with 10% goat serum in PBS (60 minutes). Cells were then incubated overnight at 4ºC with primary antibody (in PBS with 2% goat serum and 3% Triton X-100). Secondary antibodies conjugated to Alexa Fluor 488 or 647 were applied for 60 minutes. For DAPI, a 300 nM solution of DAPI in PBS was applied to the cells for 5 minutes. For F-actin staining, a 1:500 solution of rhodamine phalloidin (ThermoFisher Scientific) in PBS was applied to the cells for 15 minutes. All steps were carried out at room temperature unless otherwise indicated, and three washes with PBS (5 minutes each) were

carried out between all steps. Images were obtained using a DMi8 confocal laser scanning microscope (Leica) using a 40X/1.15NA oil-immersion objective.

Quantification of Smad2/3 nuclear localization was performed on individual cells using ImageJ [8] by determining the average Smad2/3$^{cyto}$ intensity value, for pixels within the cytosol, and the average Smad2/3$^{nuc}$ intensity value, for pixels within the nucleus, following a maximum intensity projection of Z-stacks taken to capture the entirety of the cell. ΔFluorescence values (Smad2/3$^{nuc}$ - Smad2/3$^{cyto}$) were standardized to control cells (setting mean = 0 and SD = 1). The response threshold was set as one standard deviation above the mean ΔFluorescence in control cells. DAPI and rhodamine phalloidin channels were Gaussian blurred (radius=1) and used to create binary masks of nuclear and cytosolic cell regions.

For calcium imaging, cells transiently transfected with G-CaMP3 (gift from Loren Looger, Addgene plasmid #22692; RRID:Addgene_22692) [9] were grown in microfluidic chambers attached to coverslips and placed on the microscope stage before application of 0.1 Pa FSS. Images were collected from one region of interest per flow chamber. Imaging began 2-3 frames prior to FSS stimulation, and baseline G-CaMP3 fluorescence was calculated from these frames and used to normalize cellular fluorescence to account for cell-to-cell differences in intensity. Fluorescence quantification was performed using ImageJ on individual cells.

For proximity ligation assay (PLA) analysis, a Green Duolink In Situ Detection Kit (Sigma Aldrich) was used with anti-mouse MINUS and anti-rabbit PLUS probes following manufacturer's instructions. Cells were processed and treated overnight with primary antibodies following the immunofluorescence protocol above. Images were quantified using IMARIS v9.5.1 (Oxford Instruments). Raw fluorescence channels were background subtracted and puncta were identified using the Spot Detector function. Non-cell localized puncta were removed from analysis by masking using a distance transformed, void filling surface model of actin stress fibers.

*Statistical analysis*

Unless otherwise indicated in the figure legends, we report mean and standard deviation (mean ± SD) from ≥3 biological replicates. Western blots shown are representative of at least 3 biological replicates. For quantification across western blots and qRT-PCR, values were normalized to unstimulated, control cells. For qRT-PCR, each sample was run in duplicate and expression was normalized to the housekeeping gene *Rn18s*. Significance was calculated with ANOVA followed by Holm-Bonferroni *post hoc* correction. In all figures p<0.05 was considered statistically significant.

*Python source code*

Python (v.2.7, source code written in 2015) was used to generate scripts used for visualization and quantification of high-resolution microscopy datasets. The source code for sptPALM visualization/analysis and colocalization quantification are available online as Supplementary data to Rys, DuFort, et al [10].

*sptPALM analysis and quantification*

Each cellular sptPALM dataset contains tens of thousands of protein trajectories (tracks) – a list of ordered pairs of coordinates that represent how each individual protein's location changes from frame-to-frame. Only protein tracks lasting between 0.5 s and 2 s (5 to 20 frames at 10 fps) were kept for analysis, which filtered out tracks that were too short or too long to quantify accurately. For each individual protein trajectory, several parameters were calculated, including mean squared displacement (MSD) and diffusion coefficient (*D*) as per $MSD(\tau = n \cdot \Delta t) = \frac{\sum_{i=1}^{N-n}(x_{i+n}-x_i)^2 + (y_{i+n}-y_i)^2}{N-n}$, where $x_i$ and $y_i$ are the x and y coordinates of the molecule at time $i * \Delta t$ and $N$ is the duration of that individual track [11]. The diffusion coefficient *D* is defined in two-

dimensions as ¼ the slope of the regression line fitted to the first four values of the MSD $(MSD(\tau) = 4D\tau)$.

Trajectories were split into three categories based on the confinement radius ($r_{conf}$), equal to the length of the radius of the smallest circle that encloses all of the points in that track. Immobile molecules were defined as those with $r_{conf}$ < 0.166 μm; confined molecules are non-immobile tracks with $D$ < 0.2 μm$^2$/s and the remaining tracks were characterized as freely diffusive. To compare the diffusive behavior of TβRI and TβRII at focal adhesion-rich regions, an enrichment ratio was calculated by dividing the local track density (tracks/μm$^2$) inside adhesions (vinculin-positive regions) to that outside them.


*TIRF colocalization*

To quantify the extent to which two distributions of proteins are localized, an algorithm that maps two gray scale images – one for each protein – covering the same region of interest to a colocalization index value between 0 and 1 was developed. These images were obtained from TIRF mode imaging, so they represent a thin slice of proteins existing at the cell-substrate interface. As a result, any differences in pixel intensities can be assumed to the be the result of differences in protein distribution in 2-D, and the effect of proteins at different heights of the cell can be ignored. Two proteins are highly colocalized if they have similar spatial distributions, with pixels at the same coordinate in each channel having high intensity values. On the contrary, two proteins are not colocalized if a pixel with a high (or low) intensity value in one channel happens to have a low (or high) intensity value in the other channel – these locations are occupied by only one of the two proteins preferentially. By considering each coordinate across the entire region of interest with a minimum grayscale value of 5 (out of 256) in both image channels, and plotting these ordered pairs of intensity values on a plot, a distribution of points is obtained and the slope of the regression line that best fits those points has a range of 0 to infinity. By reflecting points above the line y=x across it so that all of the points lie between the positive x-axis and y=x, the

range of the slope of the regression line lies between 0 and 1. Points that lie on y=x represent

pixels with the same intensity value in both image channels, and these points shift the slope of

the line of best fit towards a value of 1. On the contrary, coordinates with large mismatches in

intensities between the two channels will lie further from y=x, and these will reduce the magnitude

of the slope of the regression line. The slope of the regression line that goes through (0,0) and

best fits the distribution of points was used as a quantitative metric of protein colocalization.

**References**

1       Spatz, J.M. *et al.* (2015) The Wnt Inhibitor Sclerostin Is Up-regulated by Mechanical Unloading in Osteocytes in Vitro. *J. Biol. Chem.* 290, 16744–16758

2       Schmittgen, T.D. and Livak, K.J. (2008) Analyzing real-time PCR data by the comparative C(T) method. *Nat. Protoc.* 3, 1101–1108

3       Martin, M. (2011) Cutadapt removes adapter sequences from high-throughput sequencing reads. *EMBnet.journal; Vol 17, No 1 Next Gener. Seq. Data Anal.  - 10.14806/ej.17.1.200*  at <http://journal.embnet.org/index.php/embnetjournal/article/view/200>

4       Patro, R. *et al.* (2017) Salmon provides fast and bias-aware quantification of transcript expression. *Nat. Methods* 14, 417–419

5       Love, M.I. *et al.* (2014) Moderated estimation of fold change and dispersion for RNA-seq data with DESeq2. *Genome Biol.* 15, 550

6       Chen, E.Y. *et al.* (2013) Enrichr: interactive and collaborative HTML5 gene list enrichment analysis tool. *BMC Bioinformatics* 14, 128

7       Kuleshov, M. V *et al.* (2016) Enrichr: a comprehensive gene set enrichment analysis web server 2016 update. *Nucleic Acids Res.* 44, W90-7

8       Schneider, C.A. *et al.* (2012) NIH Image to ImageJ: 25 years of image analysis. *Nat. Methods* 9, 671–675

9       Tian, L. *et al.* (2009) Imaging neural activity in worms, flies and mice with improved GCaMP calcium  indicators. *Nat. Methods* 6, 875–881

10     Rys, J.P. *et al.* (2015) Discrete spatial organization of TGFbeta receptors couples receptor multimerization and signaling to cellular tension. *Elife* 4, e09300

11     Rossier, O. *et al.* (2012) Integrins β1 and β3 exhibit distinct dynamic nanoscale organizations inside focal  adhesions. *Nat. Cell Biol.* 14, 1057–1067

# Chapter 4

# Cytoskeletal tension regulates TGFβ receptor localization and heteromerization

This chapter is based on work published in two peer-reviewed articles:

Rys JP, DuFort CC, Monteiro DA, et al. Discrete spatial organization of TGFβ receptors couples receptor multimerization and signaling to cellular tension. *Elife* 4, e09300 (2015).

Rys JP, Monteiro DA, Alliston T. Mechanobiology of TGFβ signaling in the skeleton. *Matrix Biol.* 52-54:413-425 (2016).

**Introduction**

Physical cues are powerful regulators of cellular behavior, and they play fundamental roles in controlling cellular decisions such as proliferation, migration, lineage selection, and differentiation, among others. These cues – both static, such as substrate stiffness or topography, and dynamic, such as mechanical compression, tension, or shear – exert their effects through direct and indirect processes at different length scales. At the locus of several of these mechanisms is the cytoskeleton, which provides a structure for the cytosol and cell membrane

and plays many important roles that allow the cell to accurately probe and adapt to its surroundings. Primarily consisting of actin, microtubules, and intermediate filaments, the cytoskeleton spans from the LINC (linker of nucleoskeleton and cytoskeleton) complex at the interior of the cell through to focal adhesions and integrins at the cell-substrate interface. Through physical deformation of the cell membrane or as a result of interactions between proteins such as fibronectin or collagen and integrins that induce focal adhesion formation, the cytoskeleton participates in both the detection of mechanical cues and the relay of biological signals that affect signaling pathway activation and downstream gene expression.

As one example, cytoskeletal tension is at the center of a feedback loop that links the material properties of the extracellular matrix (ECM) to the TGFβ signaling pathway (Fig. 4.1). Firstly, ECM stiffness directly regulates cytoskeletal tension – cells calibrate their internal tension to the mechanical properties of their local ECM. In turn, cytoskeletal tension regulates the magnitude and quality of TGFβ signaling, for example by affecting the ease with which cells activate latent TGFβ ligand [1] or through control of TGFβ effector phosphorylation and nuclear translocation. These effectors often act as transcription factors which bind to promoters of lineage-specific ECM proteins that control the material properties of the ECM. On the other side, TGFβ regulates the expression levels of lineage-specific ECM proteins and controls ECM synthesis and remodeling [2,3]. Through these mechanisms, cell-ECM interactions coordinate major cell decisions such as mesenchymal stem cell differentiation [4–6]. However, the full extent to which TGFβ receptors are targeted by these mechanobiological mechanisms remains to be elucidated.

Using a combination of high-resolution imaging, particle tracking, and biochemical techniques, we tested the hypothesis that cytoskeletal tension regulates TGFβ receptor-receptor interactions [7]. While cytoskeletal tension initially kept two focal adhesion-localized subpopulations of TGFβ receptors segregated and unable to physically interact, its collapse resulted in receptor colocalization and multimerization, revealing a new role for the cytoskeleton in calibrating TGFβ signaling.
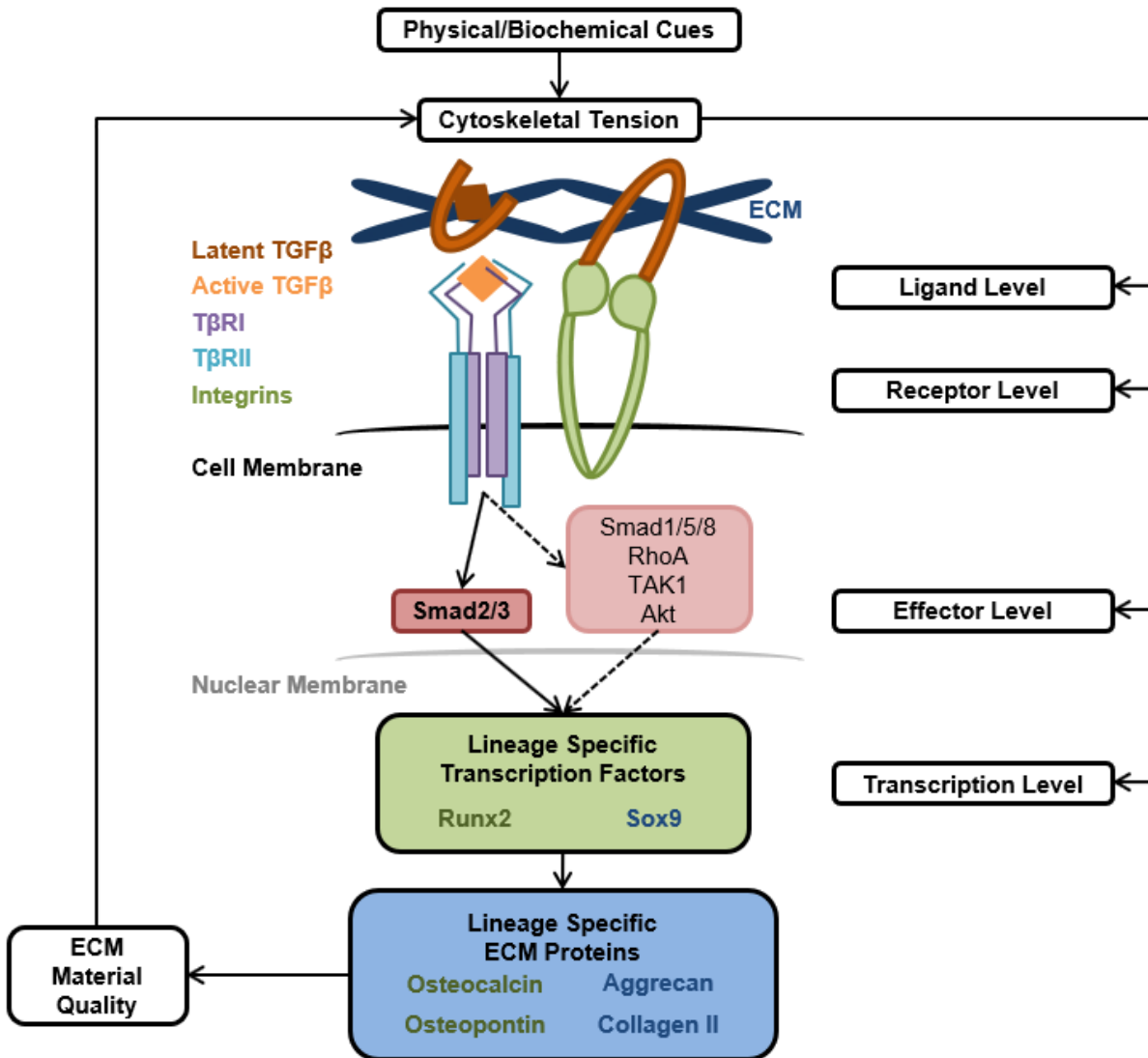
45

**Figure 4.1: A feedback loop links cytoskeletal tension and the TGFβ pathway.** Cells calibrate their cytoskeletal tension to the physical and biochemical cues in their microenvironment, such as the material quality of the ECM. Cytoskeletal tension, in turn, concurrently regulates many levels of the TGFβ signaling pathway, for example, by controlling the spatial organization of TGFβ receptors or in the choice between canonical Smad2/3 and non-canonical effectors. These effectors translocate to the nucleus where they control the expression of transcription factors that bind to promoters of specific ECM proteins and participate in control of ECM material quality.

**Results**

*Distinct localization and diffusive behavior of TβRI and TβRII*

TIRF-mode imaging of ATDC5 cells transiently transfected with fluorescently-tagged TβRI and TβRII revealed a unique spatial organization of these receptors that was not observed when in widefield mode, suggesting that this organization is limited to the subpopulation of receptors in close proximity to the cell-substrate interface (Fig. 4.2A-C). Specifically, hollow rings of TβRII were found surrounding, but generally not overlapping, regions rich in TβRI (Fig. 4.2D-F). Since TβRI-TβRII colocalization and heteromerization are prerequisites for TGFβ effector phosphorylation and nuclear translocation, the mobility and diffusion of these receptors at these sites was assessed and compared to that of receptors away from these sites, to test the hypothesis that these receptors were somehow being restrained or confined to distinct regions of the cell membrane.

Using single particle tracking photoactivated localization microscopy (sptPALM) in ATDC5 cells transfected with photoswitchable mEos2-tagged receptors, the movements of thousands of individual receptors were captured (Fig. 4.3A-B). sptPALM is a technique that tracks the movements of individual molecules via the capture of images with resolutions beyond the diffraction limit enabled by PALM [8]. Normally, image resolution is limited by the inability to accurately distinguish photons emitted from fluorescent molecules in close proximity, making it challenging to study the localization or movements of individual molecules. However, fluorophores such as mEos2 are designed to avoid the presence of too many active fluorophores in the sample, by making it such that molecules in close proximity do not simultaneously emit photons. Use of these photoactivatable markers provided us the ability to examine the dynamics of individual receptor proteins.
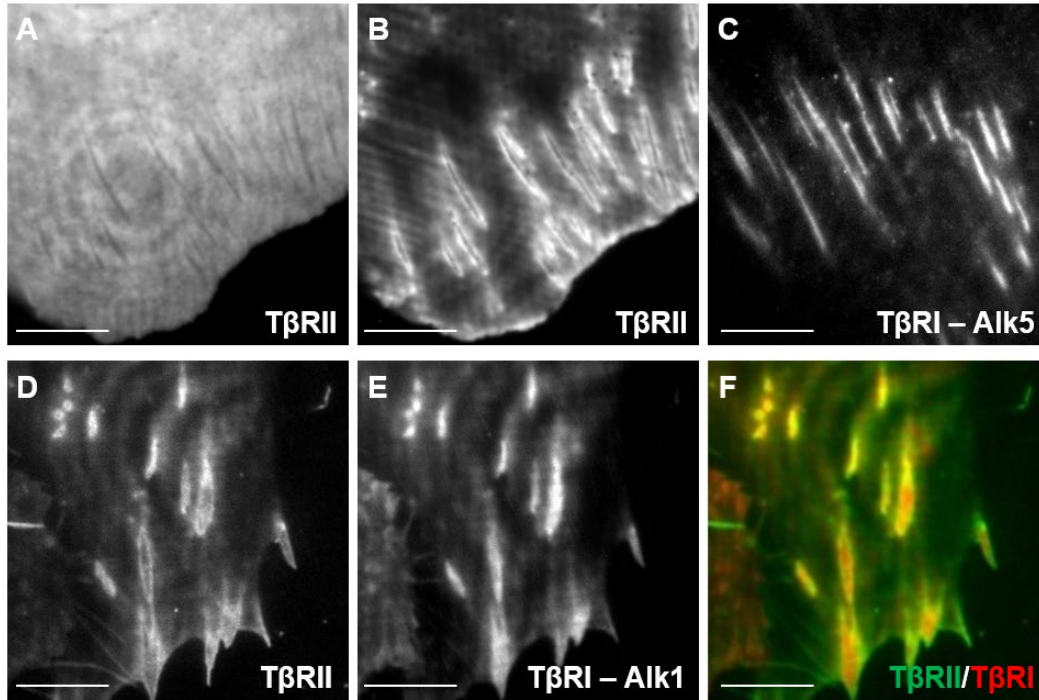
**Figure 4.2: TIRF-mode imaging reveals distinct localization of TβRI and TβRII.** (A, B) Widefield-mode imaging of mEmerald-TβRII transfected ATDC5 cells (A) reveals faint hair-like regions where TβRII appears absent that become significantly more pronounced when imaging in TIRF mode (B). (C) On the contrary, mCherry-TβRI does not form these ring-like structures. (D-F) TIRF-mode imaging of cells expressing both fluorescent constructs reveals the formation of regions of TβRI where TβRII is mostly absent surrounded by rings of TβRII.

While individual receptors of each type exhibited a range of mobilities – either freely diffusive, confined, or immobile (Fig. 4.3C-D) – the mean squared displacement (MSD) values and diffusion coefficients were similar between these two receptor types, albeit slightly lower for TβRII than TβRI, potentially due to its larger molecular weight (TβRII, 65 kDa vs. ALK5/TβRI, 56 kDa). Likewise, the diffusion of TβRII molecules was smaller in regions of the cell away from these areas of segregated receptors. However, the diffusive behavior of both of these molecules was reduced in these regions, suggesting that this receptor subpopulation is more confined and functionally distinct from those elsewhere within the cell (Fig. 4.3E).
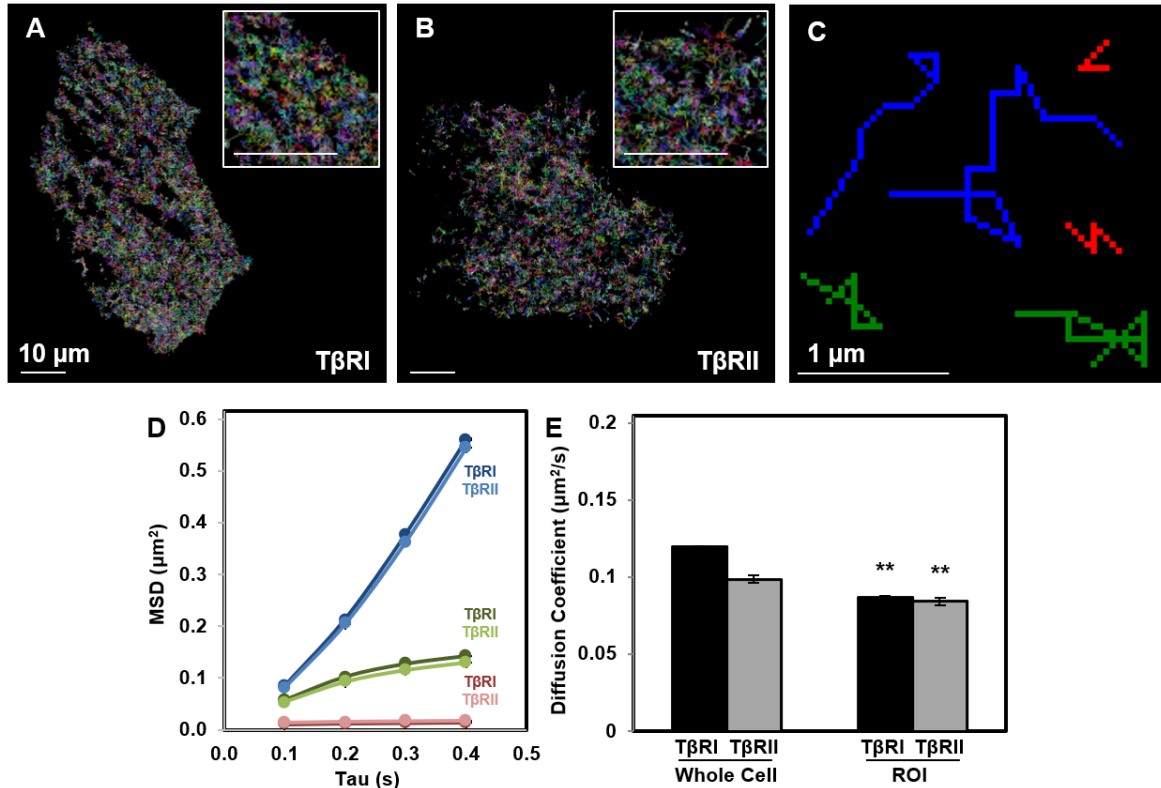
**Figure 4.3: Mobility of mEos2-tagged TβRs – sptPALM visualization and analysis.** (A, B) All mEos2-tagged TβRI and TβRII molecule trajectories with a duration of ≥ 5 frames (500 ms) were plotted, where each color represents a different track. (C) Representative individual TβRI molecule trajectories exhibiting immobile (red), confined (green), or freely diffusive (blue) movement. (D, E) While mean squared displacement plots for each of these three populations of TβRI and TβRII (mean ± SEM) reveal little difference between these two receptor types (E), comparison of diffusion coefficients for TβRI and TβRII (mean ± SEM) in whole cells relative to areas containing segregated TβRI/TβRII identify a significantly less mobile population in these regions of interest (ROI).

*Focal adhesions organize and segregate TβRII from TβRI*

Among other proteins at the cell-substrate interface previously known to interact with the TGFβ pathway are integrins. ATDC5 cells co-labeled with fluorescent integrin α2 and TβRII exhibit a ring-pattern of TβRII around integrin α2 similar to that which was observed in TβRI/TβRII-labeled cells. Cells co-labeled with integrin α2 and TβRI exhibit a high level of overlap between these proteins, suggesting that TβRI/TβRII are precisely segregated at integrin-rich focal adhesion sites. Indeed, using sptPALM to visualize receptor trajectories at integrin-rich focal adhesion sites

revealed that TβRI is preferentially enriched within focal adhesions relative to TβRII (Fig. 4.4A-B). The calculated colocalization index between TβRII and integrin α2, which exhibit clear spatial segregation, was low. On the contrary, this parameter was significantly higher when comparing the spatial distributions of integrin α2 and two different TGFβ type I receptors, ALK1 and ALK5, which show similarities in their distributions at the cell-substrate interface (Fig. 4.4C).
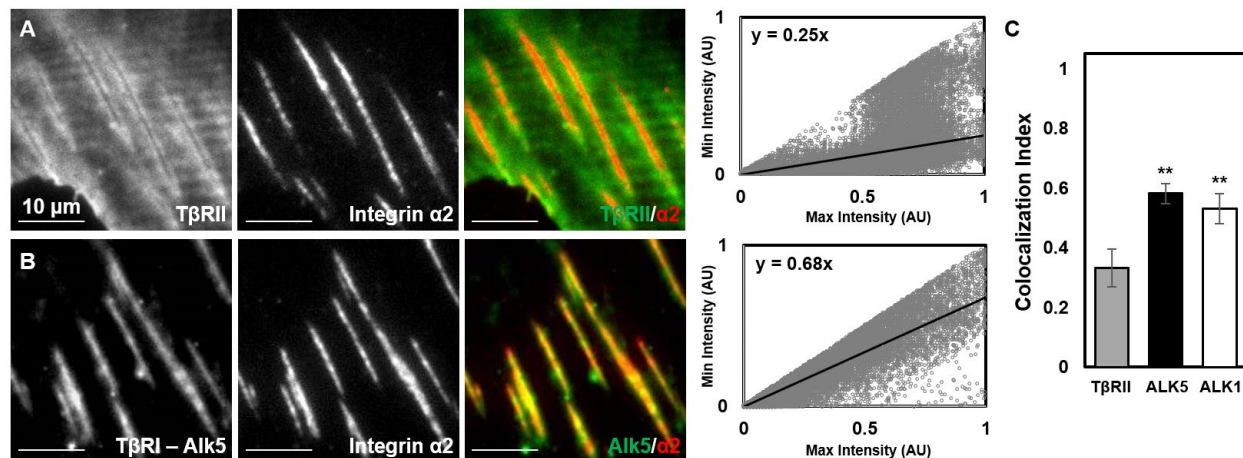


**Figure 4.4: Colocalization of TβRI and TβRII at integrin-rich focal adhesions.** (A-C) TIRF mode imaging and a custom colocalization analysis were used to evaluate the colocalization of TβRII (A), ALK5 (B), and ALK1 (not shown) with integrin α2 at focal adhesion sites. Rings of TβRII surround integrin α2 (A) and these two proteins occupy distinct regions of the cell membrane. Given that bright pixels in one protein's channel tend to be dim in the other protein's channel, the plot of the relative pixel intensities has a low slope, and the corresponding colocalization ratio is low (C). On the contrary, ALK5 and integrin α2 exhibit similar distributions along the cell-substrate interface (B), and the same pixels tend to bright in both protein channels, which leads to a high colocalization index.

*Focal adhesions immobilize ALK5 and preferentially exclude TβRII*

Further investigation into the dynamics of these two receptor types at focal adhesion sites revealed several interesting observations: 1) TβRI appears to diffuse freely into and around focal adhesion sites, whereas TβRII tends to bounce around the perimeter of these sites (Fig. 4.5A-B, D-E), 2) a significantly larger fraction of the total TβRI tracks are localized within these adhesions relative to TβRII (Fig. 4.5C), and 3) a higher fraction of TβRI tracks within focal adhesions are

immobile relative to TβRI and TβRII tracks outside focal adhesions, with a corresponding lower diffusion coefficient (Figure 4.5F-G).
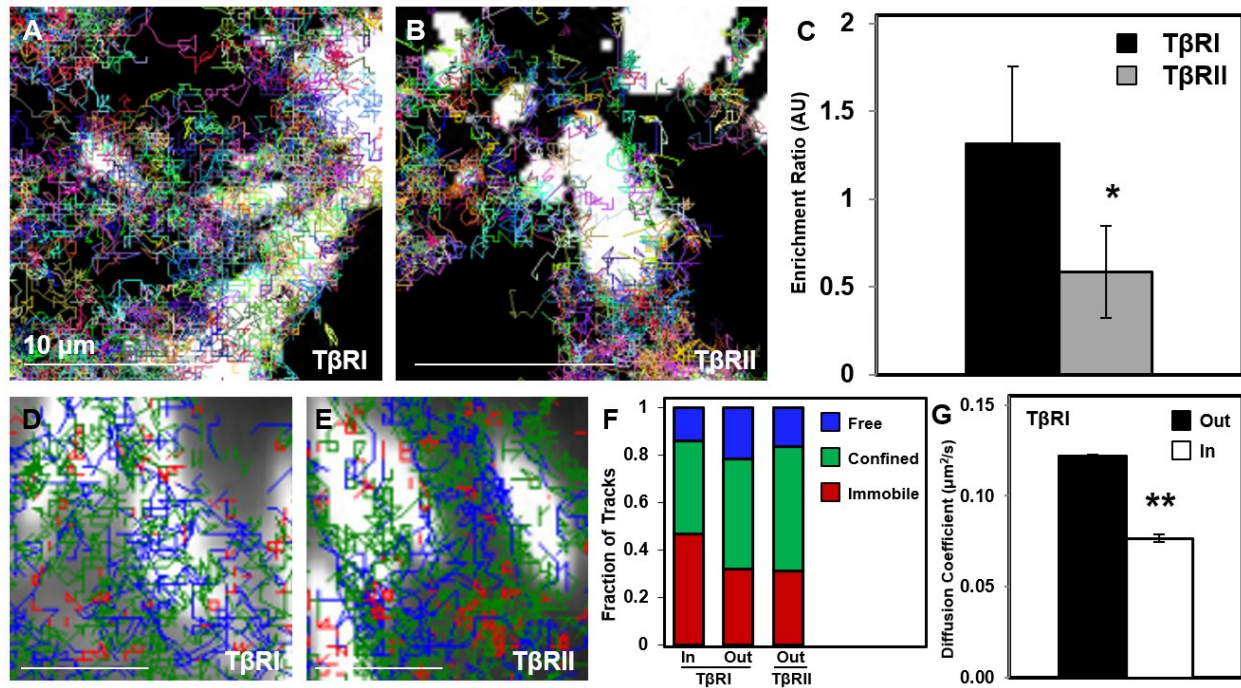


**Figure 4.5: Receptor localization and dynamics at focal adhesion sites.** (A-C) Trajectories (colored paths) of individual ALK5 (A) and TβRII (B) proteins overlaid with the mature focal adhesion marker vinculin reveal preferential exclusion of TβRII but not ALK5 from focal adhesions, which were enriched within them (C). (D-G) Analysis of these individual tracks based on their diffusion coefficients shows both a larger fraction of ALK5 tracks within adhesions (D, E). These ALK5 trajectories within focal adhesions which were more likely to be immobile (F) and had a lower diffusion coefficient on average (mean ± SD, G).

*Cytoskeletal tension regulates the spatial organization of focal adhesion-localized TβRs*

To determine the extent to which this receptor segregation requires maintained levels of high cytoskeletal tension, cells were treated with pharmacological inhibitors that disrupt cytoskeletal tension – the myosin II inhibitor blebbistatin or the ROCK inhibitor Y27632. Treatment with either of these reagents led to a significant increase in fluorescence overlap between TβRII and integrin α2 (Fig. 4.5A-D) and the calculated colocalization index (Fig. 4.5E) – up to values similar to those observed with integrin α2 and either ALK1 or ALK5 (Fig. 4.3C). Interestingly,

despite seemingly different patterns of TβRII localization in the vehicle treated groups in Figure 4.5, the calculated colocalization values remain similar, suggesting this method is robust enough to handle moderate variations in signal intensity and quality across images.
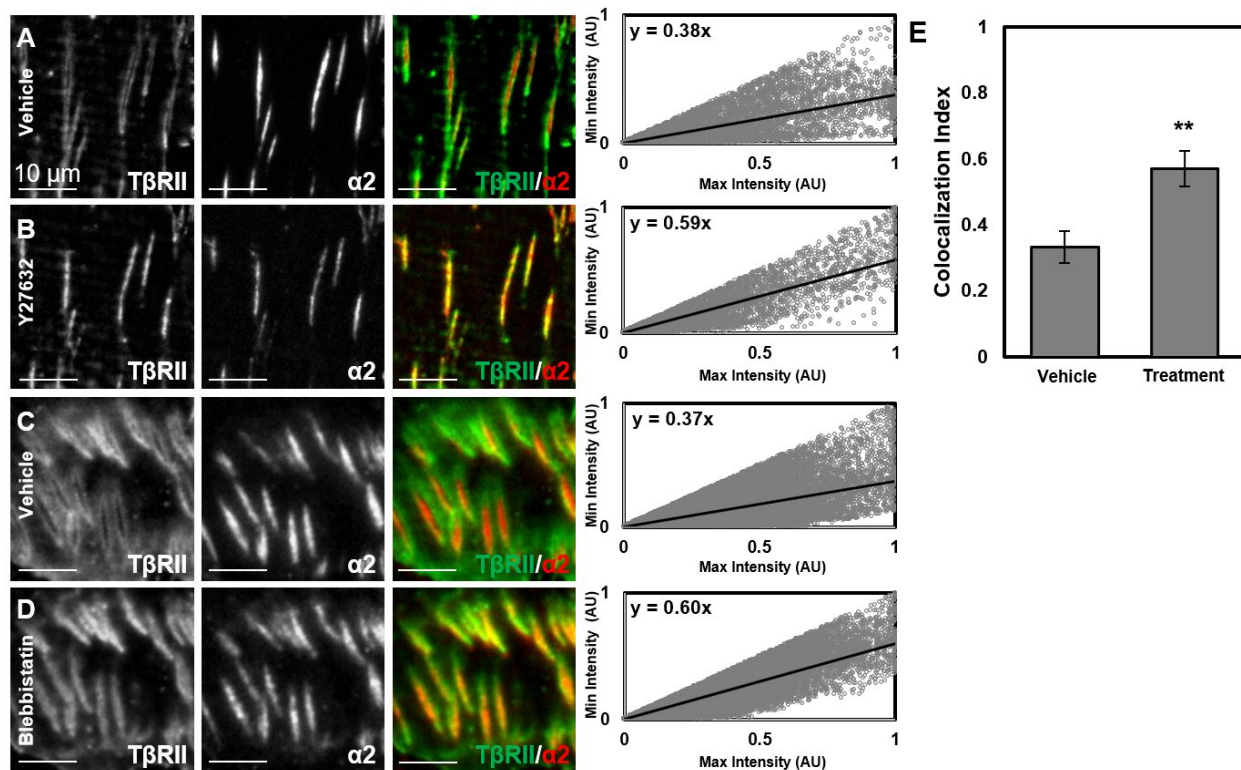


**Figure 4.6: Cytoskeletal tension-sensitive regulation of TβRII localization.** (A-E) Treatment with the ROCK inhibitor Y27632 (A, B) or the myosin II inhibitor blebbistatin (C, D) causes the peripheral ring of TβRII surrounding focal adhesions to collapse, inducing colocalization of TβRII and integrin α2 (E).

*Disruption of TβR segregation increases receptor multimerization and Smad phosphorylation*

Disruption of cytoskeletal tension enables colocalization of TβRI, TβRII, and integrin α2 at focal adhesions. Flag co-IP of lysates from cells expressing myc-TβRI and Flag-TβRII revealed that TβRI/TβRII colocalization is accompanied by receptor heteromerization, providing evidence of cytoskeletal tension-sensitive control of functional TβRI-TβRII interactions in cells treated with Y27632 and those grown on soft 0.5 kPa PDMS substrates (Fig. 4.7A). Consistent with these

results, increased Smad2/3 phosphorylation was also observed in cells grown on PDMS (Fig. 4.7B). While the extent to which the spatial organization of TβRI and TβRII is dependent on physical interactions with integrins or other proteins is unknown, the actin depolymerizing factor cofilin was found to interact with TβRII but not TβRI, suggesting that it might initially restrain TβRII outside of focal adhesions in a manner sensitive to changes in cytoskeletal tension (Fig. 4.7C).
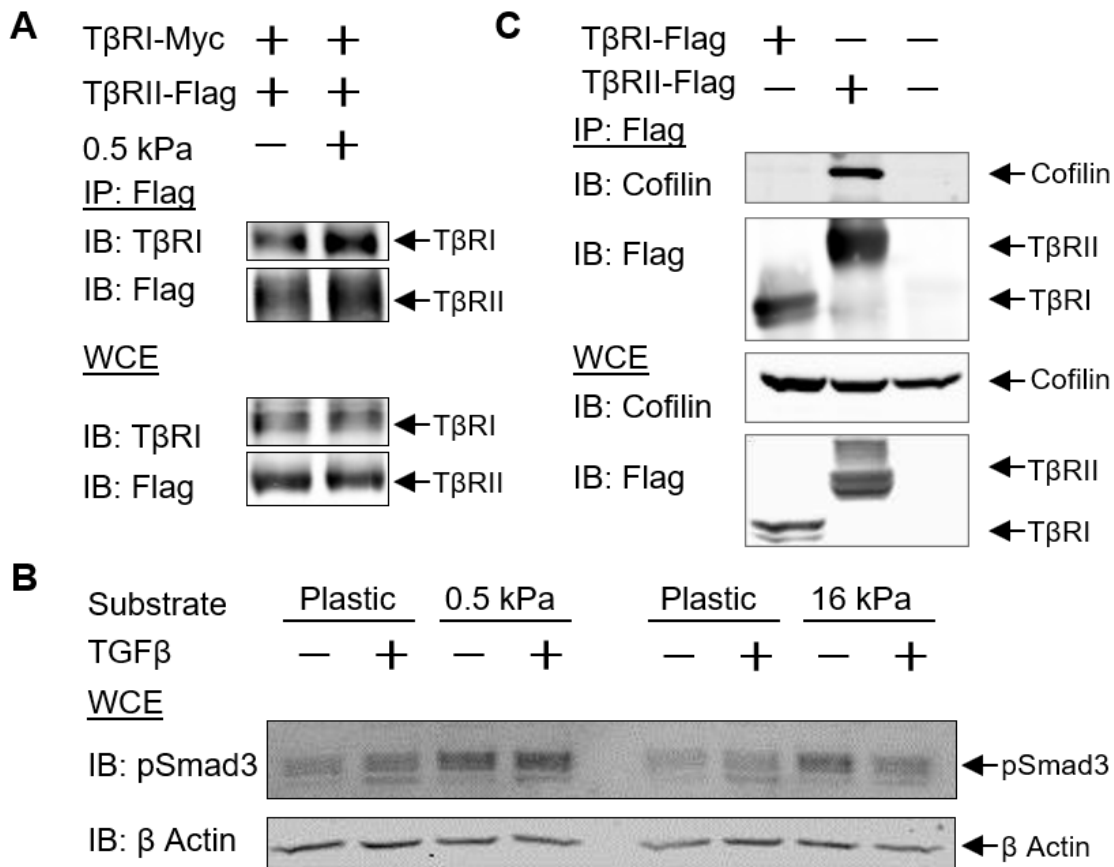


**Figure 4.7: Substrate stiffness modifies cytoskeletal tension to regulate TGFβ signaling.** (A) Cells grown on 0.5 kPa PDMS substrates exhibit higher levels of multimeric ALK5/TβRII complexes shown by Flag co-immunoprecipitation (IP), similar to results obtained in cells grown on glass substrates treated with the ROCK inhibitor Y27632 (not shown). (B) Endogenous Smad3 phosphorylation is increased in cells grown on softer PDMS substrates compared to tissue culture plastic. (C) The actin depolymerization protein cofilin might play a critical role in conferring cytoskeletal tension-sensitivity to TβRII localization, given it preferentially interacts with TβRII but not ALK5.

**Discussion**

This study identifies a novel mechanism underlying mechanoregulation of the TGFβ signaling pathway through cytoskeletal tension-mediated control of TGFβ receptor localization and heteromerization at focal adhesions. Our results reveal the existence of a receptor subpopulation initially charactered by the segregation of TβRII from TβRI at adhesion sites that exhibits reduced mobility relative to receptors away from these sites. While the specific protein-protein interactions responsible for this segregation remain unknown, we have shown that TGFβ receptors physically interact with cytoskeletal proteins such as integrin αv or the actin depolymerization protein cofilin, the latter of which preferentially interacts with TβRII over TβRI. This mechanosensitive control of TGFβ receptor localization and heteromerization, which occurs in the absence of treatment with exogenous TGFβ ligand, highlights the importance of receptor-level regulation in controlling the quantity and quality of downstream signaling.

Cytoskeletal tension not only regulates the TGFβ pathway at the receptor-level, but it also coordinates integrin-mediated activation of TGFβ ligand from its latent form [9–11]. Thus, changes in receptor localization at focal adhesions might be part of a coordinated mechanism that additionally provides them with access to newly-activated TGFβ ligand, for example, following changes in substrate stiffness. Receptor segregation as a default configuration might work to prevent unwanted signaling, suggesting that cells require the correct combination of both physical and biological cues to maximize downstream signaling. In-line with other results [12], we showed that substrate stiffness-sensitive regulation of Smad2/3 phosphorylation in cells grown on soft gels is nonlinear. The extent to which the "optimal" level of stiffness that maximizes Smad phosphorylation varies across cell types remains to be elucidated. Whether similar mechanisms exist in response to other physical cues such as fluid shear stress, for example by targeting receptor subpopulations at other mechanosensory sites such as the primary cilium, is unknown.

**References**

1       Hinz, B. (2015) The extracellular matrix and transforming growth factor-beta1: Tale of a strained relationship. *Matrix Biol.* 47, 54–65

2       Tang, S.Y. and Alliston, T. (2013) Regulation of postnatal bone homeostasis by TGFβ. *Bonekey Rep.* 2, 255

3       Balooch, G. *et al.* (2005) TGF-beta regulates the mechanical properties and composition of bone matrix. *Proc. Natl. Acad. Sci. U. S. A.* 102, 18813–18818

4       Rape, A.D. *et al.* (2015) A synthetic hydrogel for the high-throughput study of cell-ECM interactions. *Nat. Commun.* 6, 8129

5       McBeath, R. *et al.* (2004) Cell shape, cytoskeletal tension, and RhoA regulate stem cell lineage commitment. *Dev. Cell* 6, 483–495

6       Park, J.S. *et al.* (2011) The effect of matrix stiffness on the differentiation of mesenchymal stem cells in  response to TGF-β. *Biomaterials* 32, 3921–3930

7       Rys, J.P. *et al.* (2015) Discrete spatial organization of TGFbeta receptors couples receptor multimerization and signaling to cellular tension. *Elife* 4, e09300

8       Manley, S. *et al.* (2008) High-density mapping of single-molecule trajectories with photoactivated  localization microscopy. *Nat. Methods* 5, 155–157

9       Wipff, P.-J. *et al.* (2007) Myofibroblast contraction activates latent TGF-beta1 from the extracellular matrix. *J. Cell Biol.* 179, 1311–1323

10      Munger, J.S. and Sheppard, D. (2011) Cross talk among TGF-β signaling pathways, integrins, and the extracellular matrix. *Cold Spring Harb. Perspect. Biol.* 3, a005017

11      Giacomini, M.M. *et al.* (2012) Epithelial cells utilize cortical actin/myosin to activate latent TGF-β through  integrin α(v)β(6)-dependent physical force. *Exp. Cell Res.* 318, 716–722

12      Allen, J.L. *et al.* (2012) ECM stiffness primes the TGFbeta pathway to promote chondrocyte differentiation. *Mol. Biol. Cell* 23, 3731–3742

# Chapter 5

# Using microfluidics to study the osteocyte response to fluid shear stress

**Introduction**

Mechanical compression of bone tissue manifests as changes in fluid shear stress (FSS) within the lacunocanalicular network that are sensed by osteocytes. One major goal of *in vitro* FSS experiments carried out using osteocytes, osteocyte-like cell lines, or other bone cells is to recapitulate the mechanical environment found within bone to elucidate the specific mechanisms through which these cells detect and respond to changes in FSS. Many questions about the confined mechanical environment of osteocytes remain unanswered, and thus, significant differences exist across *in vitro* studies that test the effects of stimulation with FSS. These include differences in cell line (e.g. MLO-Y4 vs. OCY454); flow system (chamber width, length, and height; pump choice (syringe pump vs. peristaltic pump); media recirculation or lack thereof); flow magnitude, duration, and profile (steady, pulsatile, or oscillatory); pre- and post-stimulation/recovery durations; and choice of media used during flow, among others. The system and flow parameters used in particular studies often depend on the specific readouts desired by

56

the authors, and are strongly influenced by previous results or those that yielded exciting preliminary data. The sensitivity of osteocytes - or the results of a study performed on them - to changes in any of these parameters is difficult to quantify, in part due to the complexity of the osteocyte response to FSS. In some cases, small changes in certain parameters only enhance or mute a certain downstream response. For example, early work by Jacobs et al. showed that different flow profiles and different frequencies of pulsatile and oscillatory flow control the fraction of responding cells [1], similar to *in vivo* results observed by Lewis et al. [2]. On the contrary, Spatz et al. showed that stimulation with FSS enhances *RANKL* gene expression at one magnitude of shear stress, but represses it at another [3]. Thus, initial experiments should attempt to identify the robustness of obtained results under different conditions.
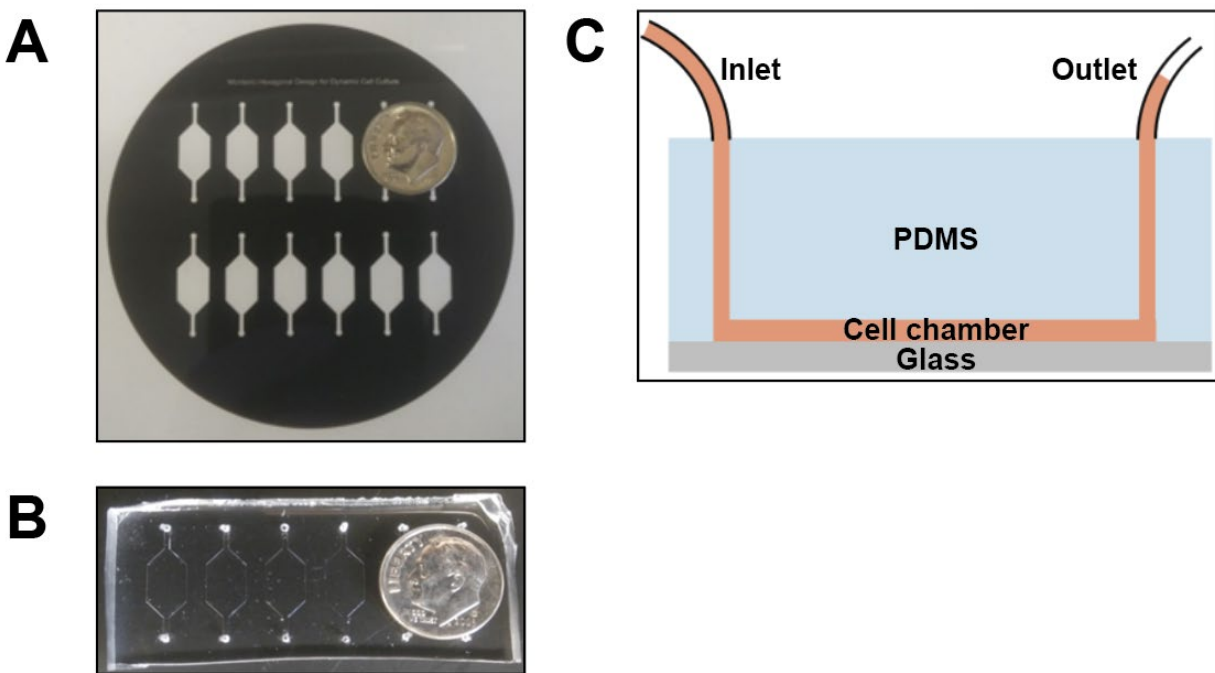


**Figure 5.1: Microfluidic system design and flow diagram.** (A, B) Photomask (A) used in an earlier iteration of the PDMS flow chambers (B), designed so six chambers (width, 6 mm) could be formed in one piece of PDMS and bonded to fit on a glass slide. (C) Side view of the chambers showing positions of the inlet and outlet and direction of fluid flow.

**Microfluidic system design**

The PDMS microfluidic chambers used in this work were designed with several constraints in mind. The first version of chambers were designed such that 6 chambers formed across a single piece of PDMS could be easily bonded to a 75 mm x 25 mm glass slide (Figs. 5.1A, 5.1B). These chambers were themselves quite small, with an initial surface area of ~0.78 cm$^2$ (maximum width = 6 mm) and an initial chamber height of 0.15 mm. The elongated hexagonal chambers were designed to contain 1) a large central chamber of constant width where the majority of cells would exist; 2) a narrow inlet and outlet to match the 1.19 mm polyethylene tubing used to connect the chambers to the peristaltic or syringe pump; and 3) a transition zone between these regions where the chamber gradually widens (Fig. 5.1C). In general, the size of the center of the chambers was limited both by their ability to fit in parallel on a single glass slide, and because large chambers are more prone to collapsing at their centers (where the PDMS ceiling droops and sticks to the glass at the center of the chamber, creating an obstacle for cell growth and significantly affecting the laminar flow of fluid through the chamber).

While this small chamber format remains convenient for sequential imaging of different experimental conditions, collecting enough protein or RNA from cells grown in them proved to challenging, and required pooling several chambers together. To address this challenge, a second, larger chamber was designed, this time with a surface area of ~2 cm$^2$ (maximum width = 10 mm) and a lower chamber height of 0.075 mm that would fit 2-to-a-slide. The lower chamber height made it so that smaller volumes of media could be pumped through the chamber to achieve target shear stresses, which both lowered reagent costs and made it easier to manage the volumes required for experiments. In addition, the reduced chamber height did not appear to affect cell viability or behavior during FSS stimulation, nor did it affect the mechanical integrity of the PDMS chambers. These larger chambers had volumes of approximately 15 μL and were used for all experiments discussed in this work.

58

**Flow through a microfluidic chamber**

In addition to shear stress, cells stimulated with fluid flow also experience changes in hydrostatic pressure, however, the geometry of the microfluidic chambers are such that the relative contribution of this latter cue is minimal. Given the rectangular nature of the flow chamber – with walls that meet at 90º angles – flow through it can be well approximated by equations that govern flow through rectangular pipes. The accuracy of the results of these approximations can be subsequently validated with computational modeling given the exact experimental conditions. The shear stress experienced by the cells ($\tau$) can be estimated as a function of chamber and fluid parameters through $\tau = 6 \times Q \times \mu / w \times h^2$, with volumetric flow rate (Q) of media with viscosity ($\mu$) through chambers (with width w and height h). Then, the desired shear stress can be achieved through manipulation of the volumetric flow rate of media pumped through the chambers. Likewise, the pressure drop across the chambers (of length L) can be estimated by multiplying the volumetric flow by the chamber resistance ($R$), which itself can be estimated using $R = 12 \times L \times \mu / w \times h^3$. Thus, the volumetric flow rate of media needed to achieve a wall fluid shear stress of 1 Pa using the flow chambers described above concurrently yields a pressure drop of 400 Pa (3 mmHg). This represents an approximately 0.4% change in pressure relative to atmospheric pressure (760 mmHg).

**Results**

*Effects of fluid flow profile, magnitude, and duration on TGFβ signaling*

I refer the reader to chapter 6 for more details about the effects of flow profile and magnitude on FSS-induced TGFβ signaling. Briefly, 0.01 Pa FSS was sufficient to induce phosphorylation of Smad1 and Smad2/3, with only a marginal increase at higher levels of FSS up to 1 Pa (Fig. 5.2A). Likewise, pulsatile FSS (1 s on, 1 s off) had an effect on TGFβ signaling pathway activation that mimicked that of steady FSS. Our equipment made it challenging to explore the effect of oscillatory FSS, but future studies should consider the effect of this third type

of flow profile. With regard to flow duration, early experiments showed that stimulation of OCY454 cells with 10 minutes of 0.1 Pa FSS is sufficient to increase levels of phosphorylated Smad2/3. This increase in TGFβ signaling pathway activation seems to plateau after between 30-60 minutes of FSS (Fig. 5.2B). Once FSS is removed after 60 minutes of stimulation, levels of pSmad2/3 decrease until they return to baseline levels after approximately 4 hours (Fig. 5.2C). The mechanisms that govern the dynamics of FSS-induced TGFβ pathway activation remain unclear. After prolonged stimulation with TGFβ ligand, internalization of cell-surface TGFβ receptors can prevent superfluous signaling, but it is unclear whether or not such a shut-off mechanism could be triggered by prolonged FSS stimulation.
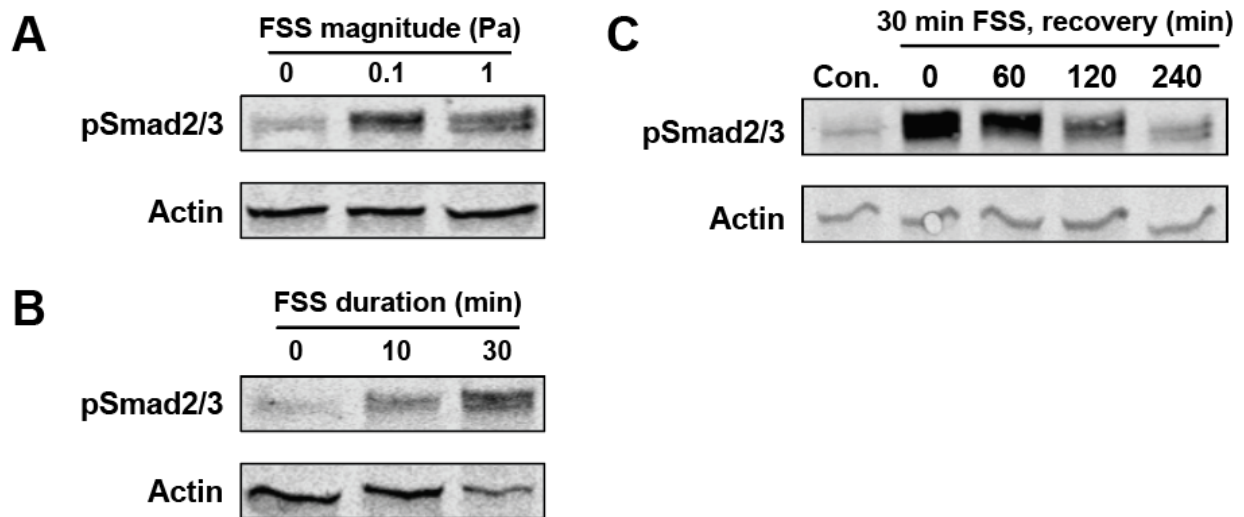


**Figure 5.2: Effects of FSS magnitude, duration, and post-flow recovery on pSmad2/3.** (A) Shear stress of 0.1 Pa is sufficient to maximize pSmad2/3 and increasing shear stress to 1 Pa results in no additional increase in Smad phosphorylation in OCY454 cells. (B) Smad2/3 phosphorylation is already upregulated after only 10 minutes of FSS stimulation, and continues to increase up through 30 minutes of flow. (C) When flow is removed, Smad2/3 phosphorylation begins to decrease, but levels are still elevated 4 h after the end of flow.

*Serum levels, but not media circulation, play a major role in controlling FSS-induced pSmad2/3*

The extent to which fluid flow-mediated increases in TGFβ signaling pathway activity were solely the result of fluid shear stress had to be explicitly addressed. Several alternative hypotheses were generated, including that the volume of flow media used during experiments could boost TGFβ signaling by virtue of the cells being continuously exposed to fresh media, which could contain TGFβ or other ligands present from the added fetal bovine serum (FBS). In fact, FSS stimulation was found to only increase pSmad2/3 levels when it contained a non-zero level of FBS (Fig. 5.3A). In the absence of fetal bovine serum, baseline levels of phosphorylated Smads are reduced, and exhibit only a mild induction upon further stimulation with FSS, potentially due to a shift in signaling equilibrium when the growth factors in FBS are removed.
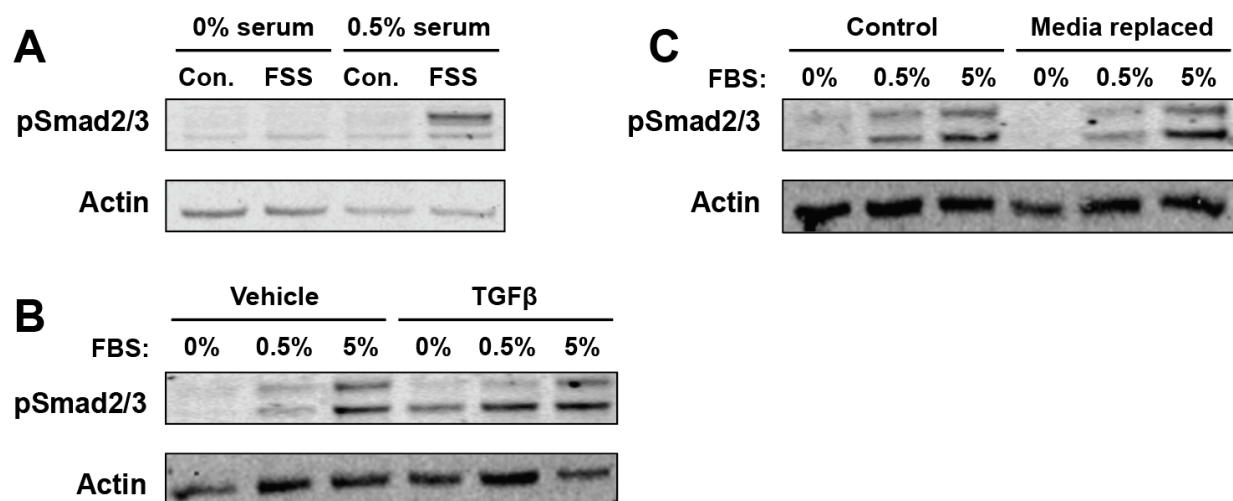


**Figure 5.3: Effects of serum concentration and media circulation on pSmad2/3.** (A) Stimulation of MLO-Y4 cells with 30 minutes of 0.1 Pa FSS increases levels of phosphorylated Smad2/3, but only in the presence of 0.5% FBS (one-tenth of normal serum levels, 5%) in the flow media. (B) Likewise, baseline levels of pSmad2/3 and cellular sensitivity to treatment with TGFβ ligand also depend on FBS concentrations in media. A reduced serum condition, 0.5% FBS, enables the largest observed increase in pSmad2/3 levels following treatment with TGFβ. (C) FSS-mediated increases in pSmad2/3 cannot be the result of cells responding to a continuous supply of fresh media, as media replacement (every five minutes) in cells grown in well plates did not affect levels of pSmad2/3, which were more dramatically regulated by serum concentrations.

A similar result was observed in the ability of FBS concentration to attenuate the cellular response to treatment with TGFβ ligand. A reduced serum concentration (0.5%, relative to the 5% in full serum MLO-Y4 media) proved to be an optimal concentration that did not oversaturate levels of baseline signaling but still allowed for a significant induction following treatment with FSS or TGFβ (Figs. 5.3A, 5.3B). To assess the ability of these cells to pull TGFβ or other ligands out of media they are exposed to, I replaced media on cells growing in well plates with fresh media every 5 minutes over the course of a 30-minute experiment and found no difference between those cells and cells that had the same media during the duration of the experiment (Fig. 5.3C).

Thus, the total amount of ligand that cells are exposed to during an experiment (i.e. increased by continually replacing media) does not affect TGFβ signaling pathway activity. This suggests that media circulation during FSS stimulation is incapable of boosting pathway activity by providing the cells with a replenishing supply of TGFβ ligand. Instead, a more important factor is FBS concentration in the flow media.

*Fluid flow washes out reagents used for pretreatments*

In preliminary experiments and those that led to results shown in Chapter 6, FSS stimulation was often accompanied by treatment with a reagent (e.g. with TGFβ or BMP4) or pretreatment with an inhibitor (e.g. SB-431542). Initial results in OCY454 cells pretreated with SB-431542 and then stimulated with FSS showed potent induction of pSmad2/3 signaling (Fig. 5.4A), while treatment of cells with exogenous TGFβ ligand after SB-431542 pretreatment has a minimal effect on Smad phosphorylation. This was an interesting result suggesting FSS-induced TGFβ signaling was TβRI-independent. However, subsequent experiments that included SB-431542 in the media used during the flow experiment showed results similar to those obtained with TGFβ treatment in well plates. Thus, I considered the hypothesis that fluid flow could "wash out" SB-431542 that would otherwise inhibit FSS-induced TGFβ signaling.
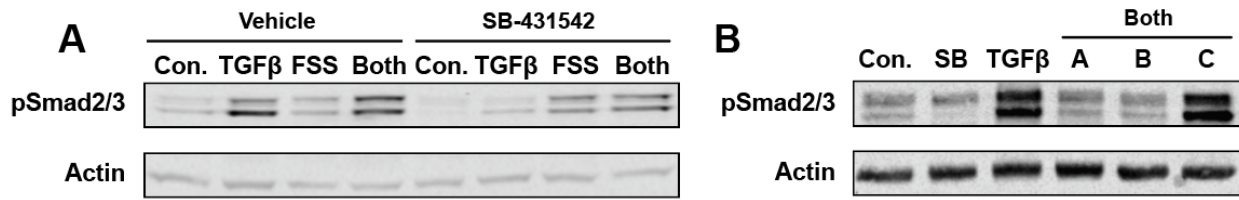
**Figure 5.4: Interactions between SB-431542 and treatment with TGFβ or FSS.** (A) pSmad2/3 induced by treatment with TGFβ is blocked by SB-431542, but FSS appears to induce Smad phosphorylation even after pretreatment with SB-431542. However, as SB-431542 was not included in flow media, its effects could have been disrupted. (B) Treatment of OCY454 cells with SB-431542 reduces levels of baseline phosphorylated Smad2/3, which are enhanced upon treatment with 5 ng/mL TGFβ ligand. In cells treated with both reagents, the resulting effect on pSmad2/3 is dependent on the process by which they are added. In lane A, concurrent treatment with SB-431542 and TGFβ has little effect on pSmad2/3, similar to that observed in lane B, where TGFβ is added after 1 h pretreatment with SB-431542. However, in lane C, rinsing cells with PBS in-between treatments with SB-431542 and TGFβ results in a potent induction in levels of pSmad2/3, showing that the inhibitory effect of SB-431542 can be neutralized by removing the media in contact with the cells.

To test this, I evaluated the interactions of treatment with TGFβ and SB-431542 in well plates (Fig. 5.4B). OCY454 cells treated with TGFβ ligand have increased levels of pSmad2/3, an effect which is blocked in cells pretreated with SB-431542. Concurrent treatment with both reagents results in no visible change in pSmad2/3 levels. However, if cells are rinsed with PBS between treatments, the effect of SB-431542 is nullified, and subsequent treatment with TGFβ remains capable of inducing Smad phosphorylation. As a result, any reagent used during FSS experiments should be maintained during the course of the experiment, unless results show that its effects are not attenuated when the media in the chamber is perfused during fluid flow.

**Summary**

In OCY454 cells plated within a microfluidic chamber, fluid shear stress is a rapid, potent agonist of the TGFβ signaling pathway, but the specific mechanisms remain to be fully elucidated. The requirement for FBS in the media used during flow experiments indicates that this mechanism
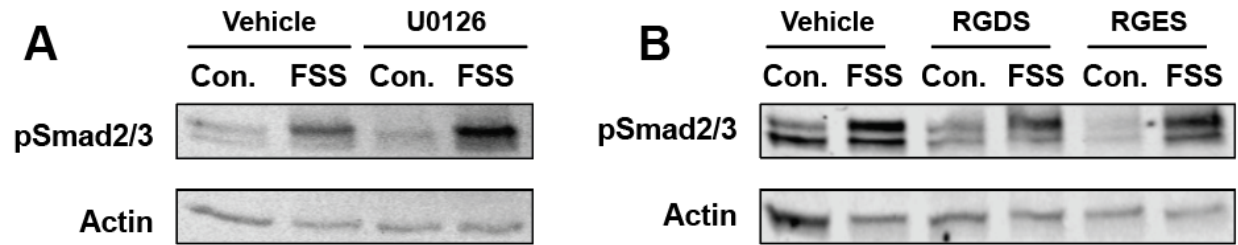
**Figure 5.5: Mechanisms of TGFβ signaling pathway activation by FSS.** (A) FSS-induced upregulation of pSmad2/3 in OCY454 cells is further enhanced in the presence of the MEK1/2 inhibitor U0126 (n=1 biological replicate) (B) Disruption of integrin-substrate interactions with the RGDS blocking peptide only partially attenuates FSS-induced increases in pSmad2/3 when compared to a control peptide RGES (n=4 biological replicates).

requires the presence of TGFβ ligand, however the speed with which levels of phosphorylated Smads increase after FSS is applied suggests that no additional TGFβ ligand is being produced or secreted by the cells. The transduction of FSS into changes in TGFβ signaling pathway activation may involve multiple cell surface mechanosensors and appears to be regulated by other signaling pathways. Inhibition of MEK1/2 using U0126 further enhanced FSS-induced Smad phosphorylation (Fig. 5.5A), in-line with results described by Kunnen et al. using renal tubular epithelial cells [4]. While an RGDS peptide that interferes with integrin-ECM interactions blocked FSS-induced phosphorylation of Smad1/5/8 in osteosarcoma cells [5], it failed to fully block FSS-induced Smad phosphorylation in our studies (Fig. 5.5B).

**References**

1      Jacobs, C.R. *et al.* (1998) Differential effect of steady versus oscillating flow on bone cells. *J. Biomech.* 31, 969–976

2      Lewis, K.J. *et al.* (2017) Osteocyte calcium signals encode strain magnitude and loading frequency in vivo. *Proc. Natl. Acad. Sci. U. S. A.* 114, 11775–11780

3      Spatz, J.M. *et al.* (2015) The Wnt Inhibitor Sclerostin Is Up-regulated by Mechanical Unloading in Osteocytes in Vitro. *J. Biol. Chem.* 290, 16744–16758

4      Kunnen, S.J. *et al.* (2017) Fluid shear stress-induced TGF-beta/ALK5 signaling in renal epithelial cells is modulated by MEK1/2. *Cell. Mol. Life Sci.* 74, 2283–2298

5      Chang, S.-F. *et al.* (2008) Tumor cell cycle arrest induced by shear stress: Roles of integrins and Smad. *Proc. Natl. Acad. Sci. U. S. A.* 105, 3927–3932

# Chapter 6

# Fluid shear stress generates a unique signaling response by activating multiple TGFβ family type I receptors in osteocytes

This chapter is based on work published in the peer-reviewed article Monteiro DA, et al. Fluid shear stress generates a unique signaling response by activating multiple TGFβ family type I receptors in osteocytes. *The FASEB Journal* (2020, in press).

**Introduction**

 Cells experience concurrent biochemical and physical cues that coordinate cellular behavior through regulation of critical signaling pathways. These physical cues – substrate stiffness or topography, compression, stretch, or fluid shear stress, among others – can be transduced by cell surface mechanosensors to influence cellular decisions such as migration or differentiation [1,2]. Physical cues act in part by modulating the level or quality of biochemical signaling pathways, including the famously "context-dependent" transforming growth factor beta

(TGFβ) pathway. Three different TGFβ ligands activate this pathway by binding to a pair of TGFβ type II receptors (TβRII), which then recruits a pair of TGFβ type I receptors (also called ALKs) [3]. This heterotetrameric complex then phosphorylates several downstream effectors, including the canonical TGFβ effectors Smad2 and Smad3 [4,5]. Other TGFβ family ligands, such as BMPs and activins, signal through their corresponding receptors and effectors. The specific mechanisms by which distinct biochemical and physical cues target the TGFβ pathway to determine its intensity, downstream targets, or duration remain to be fully elucidated. This is in part because these stimuli can exert multi-level control of the TGFβ signaling pathway, for example, by regulating ligand synthesis and activation; receptor trafficking and multimerization; and Smad phosphorylation and nuclear translocation [6].

Skeletal cell types utilize several of these mechanisms to calibrate the activity of the TGFβ signaling pathway based on the physical features of the extracellular matrix (ECM). To adapt to ECM stiffness or topography, cells generate cytoskeletal tension, which is required for maximal activation of Smad1 by BMPs in human mesenchymal stem cells (hMSCs) [7]. At an optimum level of cytoskeletal tension, chondrocytes exhibit increased Smad2/3 phosphorylation, a potent synergistic response to exogenous TGFβ, and maximal induction of chondrocyte gene expression [8]. Further investigation into the mechanoregulation of TGFβ signaling in chondrocytes implicated a focal adhesion-localized subpopulation of TGFβ receptors, whose spatial organization was sensitive to changes in cytoskeletal tension [9]. More specifically, subpopulations of type I and type II receptors were segregated from each other in cells with high cytoskeletal tension. Disruption of tension enabled receptor colocalization and heteromerization, suggesting a mechanism through which changes in a cell's internal mechanical environment can enhance or suppress TGFβ signaling.

Likewise, fluid shear stress (FSS) has been shown to interact with TGFβ family signaling pathways in several biological contexts [10–15], though its effects on skeletal cells remain to be explored. For example, in proximal tubular epithelial cells, exposure to FSS significantly

upregulated Smad2/3 phosphorylation and nuclear translocation and transcription of TGFβ target genes [16]. Nonetheless, the mechanisms by which FSS modulates TGFβ family signaling appear to differ from one cell type to the next. Kunnen et al. report that FSS-mediated activation of TGFβ signaling is blocked in cells treated with the ALK4/5/7 inhibitor LY-364947, but also observed mild decreases of active and total TGFβ1 levels in flow media following application of FSS [16]. On the other hand, Kouzbari et al. and Albro et al. showed that levels of active TGFβ1 in platelet releasates and synovial fluid, respectively, increase after stimulation with FSS [17,18]. As a result, the extent to which this mechanism depends primarily on ligand-level, receptor-level, or downstream regulation in a cell type-specific manner remains unclear.

In bone, mechanoregulation of the TGFβ signaling pathway in response to compression is required for bone anabolism, in part because of its role in coordinating the mechanoregulation of sclerostin expression [19]. Indeed, mice expressing a dominant negative TGFβ receptor type II under control of the osteocalcin promoter exhibit minimal changes in cortical bone thickness and mineral apposition rate following a hindlimb loading regimen relative to wildtype controls. Mechanical compression of bone tissue is known to induce fluid flow within the perilacunar/canalicular network that leads to changes in fluid shear stress and hydrostatic pressure sensed by osteocytes [20,21]. However, the extent to which FSS directly regulates TGFβ signaling in these cells remains unknown. A deeper understanding of how and when FSS stimulation affects the TGFβ pathway in osteocytes is essential because careful regulation of TGFβ signaling is necessary for bone homeostasis and dysregulation can drive disease progression [22,23].

While others have evaluated the effects of FSS on cellular function and cytokine expression using osteocyte-like MLO-Y4 cells, these efforts have focused mainly on FSS inhibition of *DKK1* and *Sost* expression, induction of Wnt/β-catenin signaling, and activation of HIF-1α and AMPK inflammatory pathways, with no analysis of its role in regulating TGFβ/Smad signaling [24–26]. Likewise, in the more recently developed osteocyte-like cell line, OCY454,

stimulation of fully differentiated cells with FSS significantly lowered extracellular sclerostin levels and *Sost* mRNA expression [27,28], but its link to TGFβ signaling remains to be elucidated. Thus, using a microfluidic platform to stimulate cells with FSS, we investigated the dynamics and effects of FSS on TGFβ signaling in OCY454 cells. Our results show that FSS rapidly enhances Smad signaling by stimulating heteromerization and activating several distinct subsets of TGFβ type I receptors, in a manner different than that which could be achieved by treatment with ligand alone.

**Results**

*FSS rapidly induces nuclear translocation of Smad2/3 in OCY454 cells*

To identify mechanisms by which fluid shear stress (FSS) regulates TGFβ signaling, we developed and validated a PDMS microfluidic culture system (Fig. 6.1A). The ability to precisely stimulate cells is supported by COMSOL computational modeling, which predicts laminar flow and uniform FSS conditions across the cell chamber (Fig. 6.1B). Accordingly, 0.1 Pa FSS activates a green fluorescent protein (GFP) $Ca^{2+}$ reporter construct (G-CaMP3) in transfected osteocyte-like OCY454 cells. Consistent with prior reports [37], fluorescence intensity measurements revealed a synchronized increase in cytosolic $Ca^{2+}$ levels within seconds after shear stress was applied, with no change in unstimulated control cells grown in identical conditions (Figs. 6.1C, 6.1D). Likewise, FSS activates two well-established mechanoresponsive outcomes, AKT phosphorylation (Fig. 6.1E) and *Ptgs2* mRNA expression (Fig. 6.1F).

Though FSS stimulation activates TGFβ signaling in endothelial and kidney epithelial cells [10,16], the response of TGFβ signaling to FSS in osteocytes has not yet been examined. Within 30 minutes of 0.1 Pa FSS, Smad2/3 translocates to the nucleus, just as it does in response to treatment with 5 ng/mL TGFβ (Fig. 6.1G). Interestingly, while stimulation with FSS and treatment with TGFβ both induce increases in nuclear-localized Smads in a majority of cells quantified, the percentage of responding cells and average difference in fluorescence were greater in TGFβ-treated cells (Fig. 6.1H).
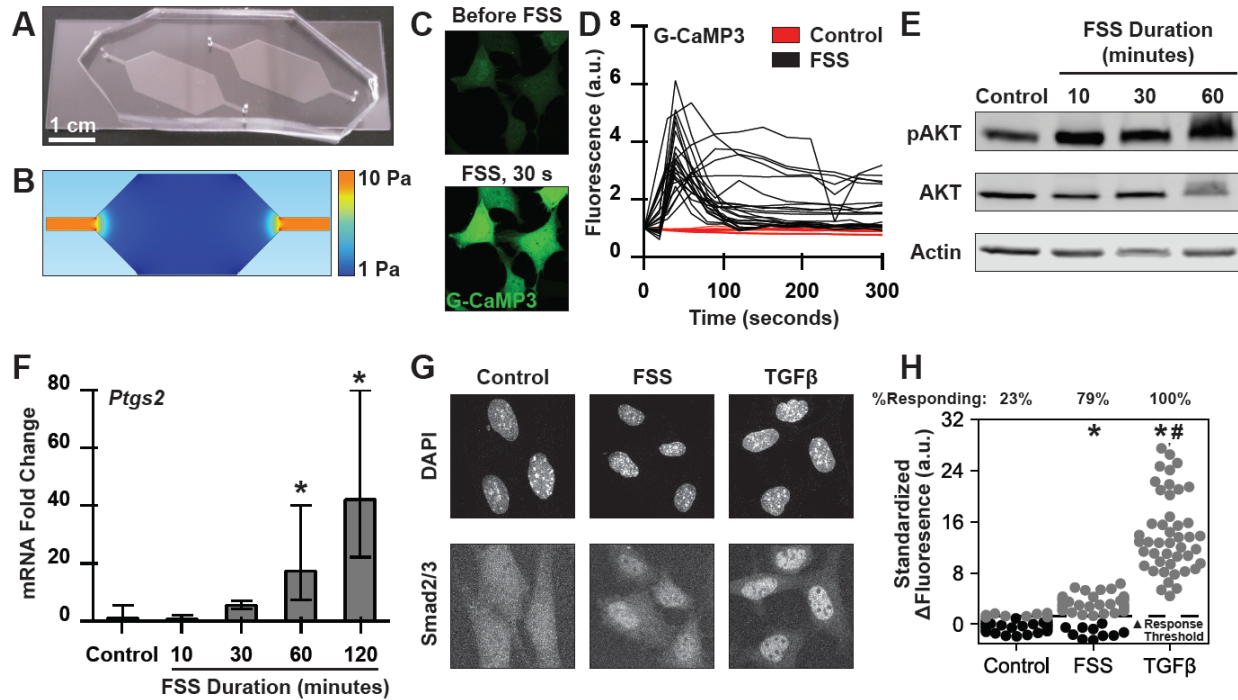
**Figure 6.1: FSS rapidly induces nuclear translocation of Smad2/3 in OCY454 cells.** (A, B) Fluid flow through the elongated hexagonal polydimethylsiloxane (PDMS) microfluidic chambers designed and used in FSS experiments was modeled using COMSOL. (C, D) Images and fluorescence intensity quantification of individual OCY454 cells transfected with the calcium reporter G-CaMP3 prior to and following stimulation with 0.1 Pa FSS, normalized to initial cellular intensity (n=3-6 biological replicates). (E) Western analysis of AKT phosphorylation following stimulation with 0.1 Pa FSS. (F) qRT-PCR analysis of mechanoresponsive gene Ptgs2 following stimulation with 1 Pa FSS, normalized to control cells. (G) Representative images of Smad2/3 nuclear localization in control cells or following 30-minute treatments with FSS (0.1 Pa) or TGFβ (5 ng/mL). (H) Fluorescence quantification on individual OCY454 cells showing differences in (nuclear – cytosolic) Smad2/3 intensity and %responding cells per condition (standardized to controls, n=3 biological replicates). *p<0.05 compared to unstimulated cells and #p<0.05 compared to FSS-stimulated cells.

*TGFβ and FSS exhibit overlapping, but distinct, responses in OCY454 cells*

Other studies that have evaluated FSS regulation of osteocyte-like cells have used shear stress magnitudes ranging from 0.2-0.5 Pa through 1.6-5 Pa in steady, pulsatile, and oscillatory profiles [28,38–40]. To determine the sensitivity of TGFβ signaling to these FSS parameters, levels of pSmad2/3 were assessed after stimulating cells with 0.01, 0.1, and 1.0 Pa FSS for 30
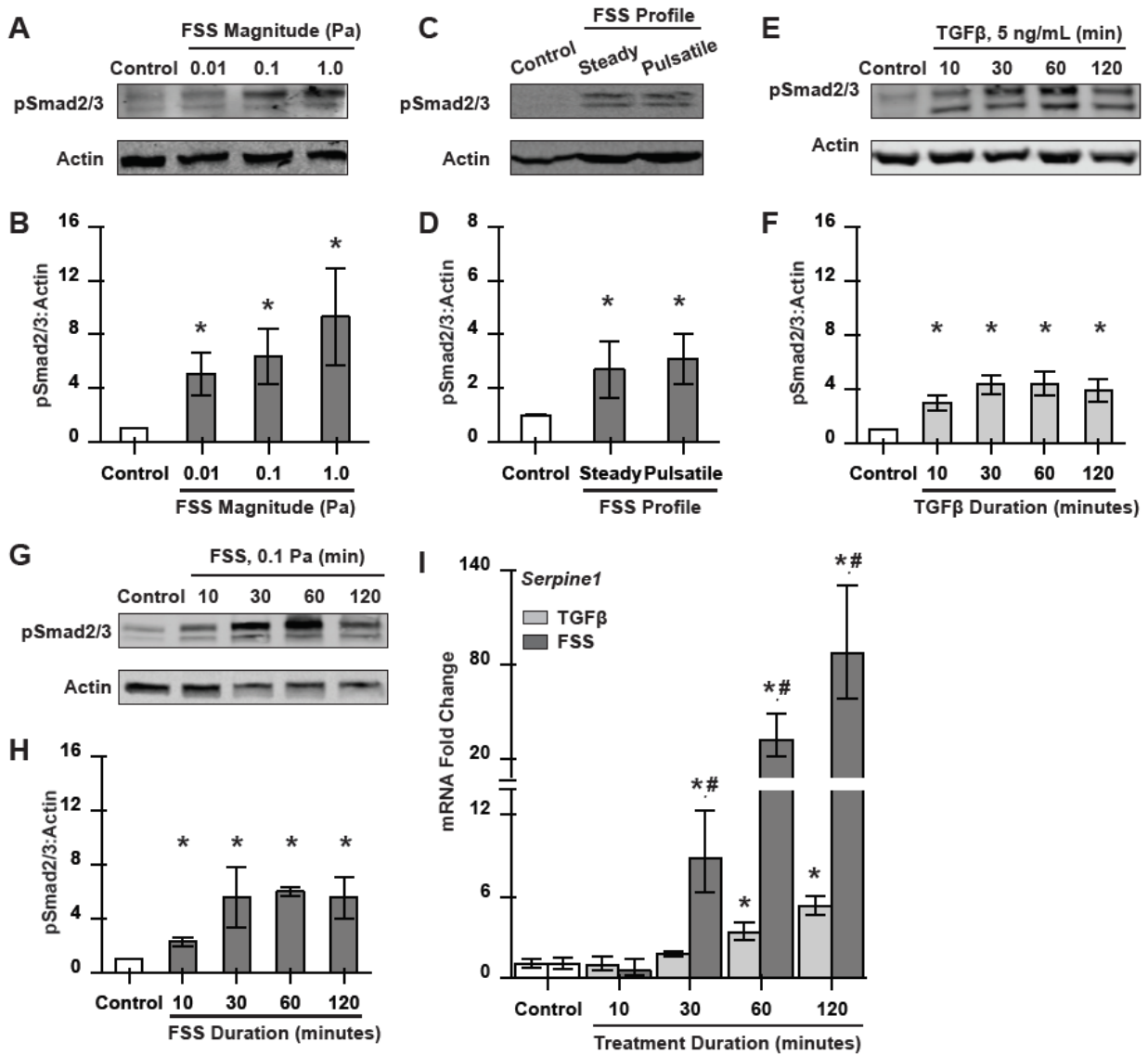
70

**Figure 6.2: TGFβ and FSS exhibit overlapping, but distinct, responses in OCY454 cells.** (A – H) Western analysis and quantification of Smad phosphorylation in OCY454 cells grown in control conditions or following stimulation with steady or pulsatile (1 s on, 1 s off) FSS for 30 minutes as labeled (A - D), or a time-course of TGFβ treatment (E, F) or FSS stimulation (G, H). FSS profile is steady unless otherwise indicated. (I) qRT-PCR analysis of TGFβ pathway target gene Serpine1 in control, TGFβ-treated, or FSS-stimulated cells. All values normalized to control cells. *p<0.05 compared to unstimulated cells and #p<0.05 compared to TGFβ-treated cells.

minutes (Figs. 6.2A, 6.2B) or pulsatile and steady FSS profiles (Figs. 6.2C, 6.2D). pSmad2/3 levels were increased in all cells exposed to FSS compared to static controls even at the lowest level, with only a modest increase in pathway activation above 0.01 Pa. Likewise, no differences were observed when comparing the effects of pulsatile FSS (1 s on, 1 s off) and steady FSS. The rapid, FSS-induced phosphorylation and nuclear translocation of these TGFβ-activated Smads suggest that FSS is sufficient to activate TGFβ signaling even in the absence of added TGFβ.

To compare the dynamics of TGFβ signaling following activation by TGFβ ligand or by FSS, we evaluated a time course of Smad2/3 phosphorylation and TGFβ-responsive gene expression in each condition. TGFβ induces Smad2/3 phosphorylation in OCY454 cells in as little as 10 minutes, with a plateau from 30-120 minutes (Figs. 6.2E, 6.2F). These dynamics matched what was observed after stimulation with 0.1 Pa FSS (Figs. 6.2G, 6.2H). In addition, both TGFβ and FSS induce the expression of the TGFβ target gene *Serpine1* within 30 minutes (Fig. 6.2I). Although the kinetics by which TGFβ and FSS activate TGFβ signaling outcomes are comparable, their effects differ considerably. Relative to TGFβ, FSS causes a 1.5-fold larger induction in the level of phosphorylated Smad2/3, and stimulates an approximately 10-fold greater increase in *Serpine1* mRNA levels.

*Concurrent stimulation with FSS and TGFβ results in higher levels of phosphorylated Smads than either treatment alone*

Since other physical cues can stimulate TGFβ signaling through mechanoactivation of latent stores of TGFβ, we tested the effect of FSS on Smad phosphorylation in the presence of saturating levels of active TGFβ. We first determined that 1 ng/mL of exogenously added active TGFβ is sufficient to maximally induce Smad phosphorylation in OCY454 cells within 30 minutes (Figs. 6.3A, 6.3B). To determine if FSS could further stimulate Smad phosphorylation, even in the presence of saturating levels of active TGFβ ligand, cells were stimulated with 0.1 Pa FSS and 5 ng/mL TGFβ. Concurrent treatment with both stimuli resulted in levels of pSmad2/3 greater than

those achieved by either treatment alone. This result suggests that an FSS-dependent increase in the activation of latent TGFβ ligand alone is insufficient to explain this enhancement (Figs. 6.3C, 6.3D).

Furthermore, we observed a differential effect of TGFβ and FSS on the phosphorylation of Smads. FSS preferentially induces phosphorylation of the upper band that migrates at the position of Smad2, whereas TGFβ induces phosphorylation of both Smad bands relatively equally. These qualitative and quantitative differences in Smad phosphorylation suggest that TGFβ ligand and FSS employ distinct mechanisms to activate downstream targets of TGFβ signaling in osteocytes.
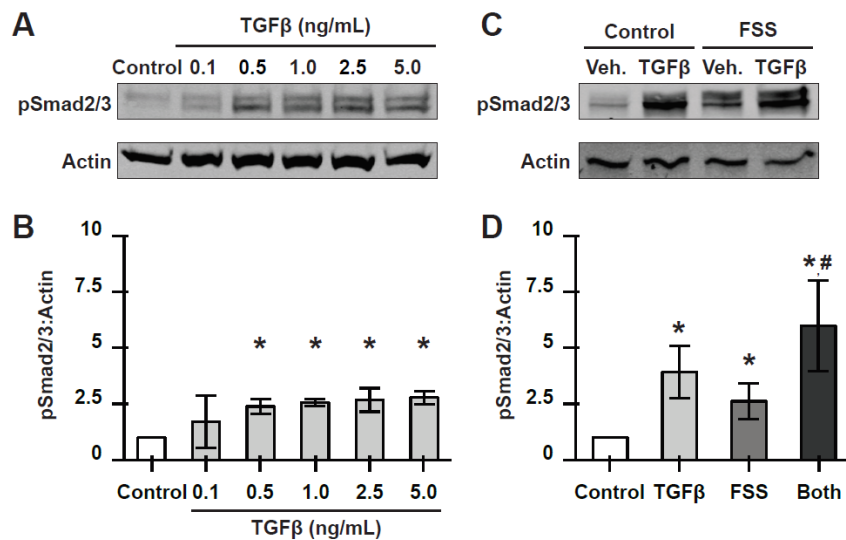


**Figure 6.3: Concurrent stimulation with FSS and TGFβ results in higher levels of phosphorylated Smads than either treatment alone.** (A, B) Western analysis and quantification of control or TGFβ-treated OCY454 cells grown in cell culture dishes for 30 minutes, normalized to control cells. (C, D) Western analysis and quantification of OCY454 cells grown in microfluidic devices in the absence of stimulation or following 30-minute treatment with TGFβ (5 ng/mL) and/or FSS (0.1 Pa). All values normalized to control cells. *$p<0.05$ compared to unstimulated cells and #$p<0.05$ compared to FSS-stimulated group.

*FSS-mediated activation of TGFβ and BMP R-Smads require their corresponding ligand*

The differential phosphorylation of Smads by FSS and TGFβ opened the possibility that Smad2 and Smad3 respond selectively to physical or biochemical cues. We also considered the possibility that the pSmad2/3 antibody cross-reacted with pSmad1/5, since FSS induces the phosphorylation of BMP-activated Smad1 and Smad5 in osteosarcoma cells [41]. The molecular weight of Smads 1 and 5 are similar to Smad2 (~52 kDa), all of which are larger than Smad3 (~49 kDa). While the pSmad2/3 antibody detected 2 bands following TGFβ treatment, it also detected the upper band in BMP4-treated OCY454 cells (Fig. 6.4A). Stimulation of these cells with Activin A did not result in observable changes in levels of phosphorylated Smads (data not shown). Furthermore, pSmad2/3 western analysis of Flag-immunoprecipitated lysates from OCY454 cells expressing Flag-tagged Smad1, Smad2, and Smad3 verified that the lower band is pSmad3, whereas the upper band is likely a composite of pSmad1 and pSmad2 (Fig. 6.4B).
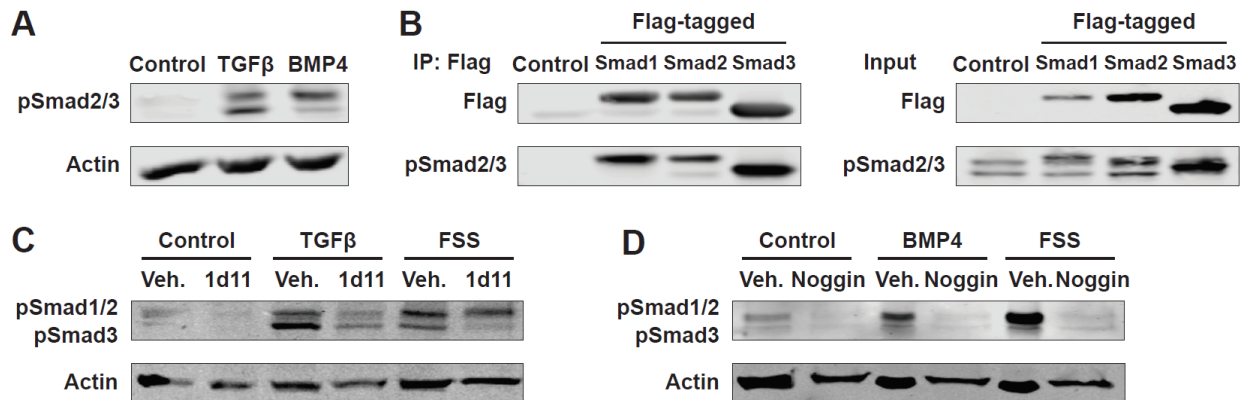


**Figure 6.4: FSS-mediated activation of TGFβ and BMP R-Smads require their corresponding ligand.** (A) Representative western analysis of control or ligand-treated cells grown in culture dishes revealing independent regulation of pSmad bands. (B) Anti-Flag co-immunoprecipitation (left panels) or western (Input, right panels) of lysates from control or Flag-Smad transfected OCY454 cells, followed by corresponding western analysis with antibodies against Flag or pSmad2/3. (C, D) Representative western analysis of cells pretreated (60 minutes) with vehicle, 1d11 TGFβ-blocking antibody (C), or the BMP ligand antagonist Noggin (D) followed by stimulation (30 minutes) with TGFβ (5 ng/mL), BMP4 (50 ng/mL), or FSS (0.1 Pa) with Smads labeled as identified in B.

Using specific ligand antagonists, we evaluated the extent to which the effects of FSS on TGFβ and BMP-responsive Smads are ligand-dependent. As expected, the TGFβ blocking antibody 1d11 significantly attenuated the TGFβ-inducible phosphorylation of both bands. However, 1d11 only partially blocked the effect of FSS (Fig. 6.4C). While 1d11 abrogated the FSS-inducible phosphorylation of Smad3, it had little effect on the upper band. On the other hand, treatment of cells with the BMP ligand antagonist Noggin was sufficient to selectively reduce phosphorylation of the upper molecular weight Smads induced by either BMP4 or FSS (Fig. 6.4D). These experiments indicate that FSS concurrently activates signaling through multiple arms of the TGFβ family signaling pathway, such that Smads canonically phosphorylated by both the TGFβ and BMP signaling pathways are activated by FSS. Furthermore, FSS activation of signaling through either Smad2/3 or Smad1 requires the corresponding TGFβ or BMP ligand.

*FSS stimulation activates multiple distinct TGFβ family type I receptors*

Consistent with the results in Figure 6.2I, FSS induces upregulation of *Serpine1* mRNA independently of added TGFβ. Like the additive effect of TGFβ and FSS on Smad phosphorylation (Figs. 6.3C, 6.3D), levels of *Serpine1* were further increased in cells that were treated concurrently with TGFβ during stimulation with FSS (Fig. 6.5A). To probe the role of the TGFβ type I receptor in the FSS-regulation of *Serpine1*, we pretreated cells with the ALK4/5/7 inhibitor SB-431542. SB-431542 not only attenuated the effect of FSS, but also blocked the additive contribution of TGFβ in cells treated with both stimuli concurrently, demonstrating the requirement for one or more of these receptors for the effect of FSS on *Serpine1*.

However, part of the FSS-mediated effect on *Serpine1* resists ALK4/5/7 inhibition, leading us to hypothesize that other TGFβ and BMP type I receptors also respond to FSS in osteocytes. To determine which type I receptors participate in FSS activation of Smad signaling, we stimulated cells with FSS in the presence of pharmacologic inhibitors that specifically block distinct subsets of TGFβ superfamily type I receptors [3] (Fig. 6.5B).
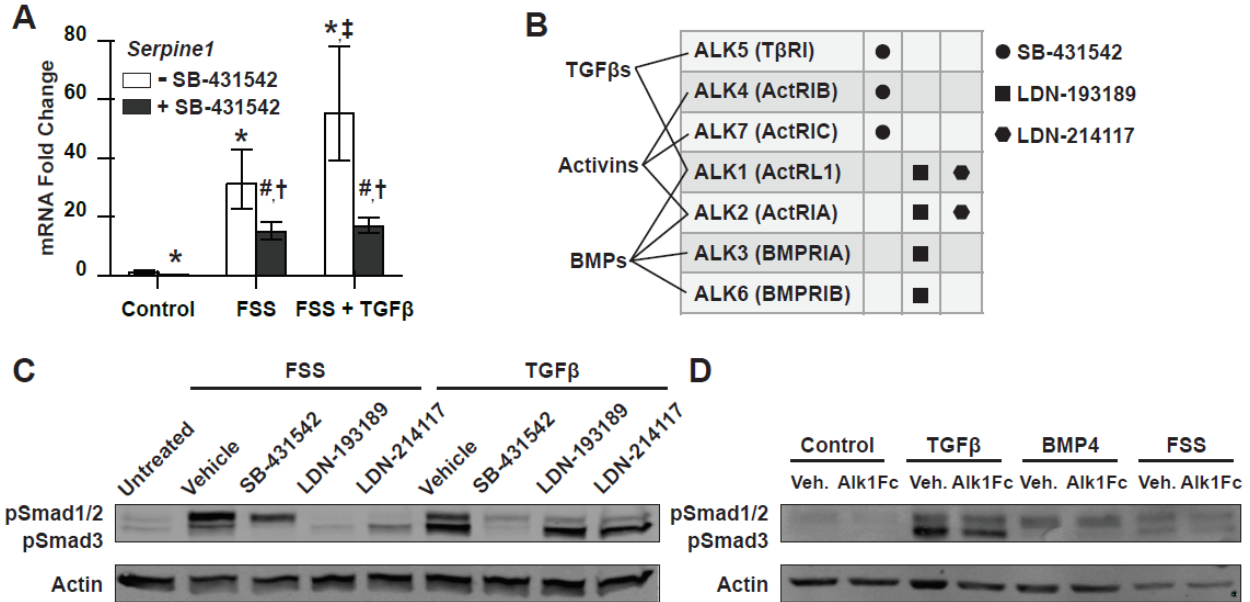
**Figure 6.5: FSS stimulation activates multiple distinct TGFβ family type I receptors.** (A) qRT-PCR analysis of TGFβ target gene Serpine1 after 60-minute treatment with vehicle or SB-431542 followed by 120-minute treatment with TGFβ or FSS stimulation as indicated (n=4 biological replicates). All values normalized to control cells. *p<0.05 compared to unstimulated cells and #p<0.05 compared to SB-treated controls; †p<0.05 compared to corresponding treatment group without SB-431542, ‡p<0.05 compared to FSS-stimulated cells. (B, C) Representative western analysis of Smad phosphorylation in control cells and cells pretreated (60 minutes) with vehicle or an inhibitor of a subset of TGFβ type I receptors (SB-431542, ALK4/5/7 inhibitor; LDN-193189, ALK1/2/3/6 inhibitor; LDN-214117, ALK1/2 inhibitor, as shown in B), followed by treatment (30 minutes) with TGFβ or FSS (C) (n=3 biological replicates). (D) Representative western analysis of cells pretreated (60 minutes) with ALK1Fc followed by treatment (30 minutes) with TGFβ, BMP4, or FSS (n=2 biological replicates, non-flow conditions were collected from cells grown in well plates).

While Smad phosphorylation following treatment with TGFβ was almost entirely blocked in OCY454 cells pretreated with the ALK4/5/7 inhibitor SB-431542, only a portion of the shear stress response was attenuated by that inhibitor (Fig. 6.5C). Indeed, the upper Smad1/2 band persisted. On the contrary, treatment with inhibitors against BMP type I receptors, specifically those against ALK1/2/3/6 (LDN-193189) or ALK1/2 (LDN-214117) had moderate effects on Smad1/2 phosphorylation induced by TGFβ but only minimal effects on its phosphorylation of Smad3. However, inhibition of these receptors completely ablated FSS-induced phosphorylation

of the upper Smad1/2 band. The ALK1/2/3/6 inhibitor was the most effective antagonist of FSS-induced, but not TGFβ-induced, phosphorylation of both Smad bands, whereas the more selective ALK1/2 inhibitor allowed FSS-induced phosphorylation of the lower Smad3 band.

Because ALK1 has been implicated in chondrocyte function and chondrogenic differentiation [42], as well as in FSS-sensitive control of BMP signaling in endothelial cells [14], we further tested its role in OCY454 osteocytes using ALK1Fc, which specifically blocks signaling through ALK1 [43]. Pretreatment of these cells with recombinant murine ALK1Fc partially blocked FSS-induced Smad phosphorylation but had little effect on Smad phosphorylation following stimulation with TGFβ or BMP4 (Fig. 6.5D). Collectively, these data suggest that FSS induces phosphorylation of multiple Smads by activating a combination of TGFβ and BMP type I receptors, different than that which could be achieved by treatment with either ligand alone.

### *RNAseq analysis supports potent FSS regulation of TGFβ superfamily signaling*

To further explore the biological pathways targeted by FSS stimulation, we performed RNA sequencing analysis on unstimulated control OCY454 cells or those stimulated with 1 Pa FSS for 2 hours in the presence or absence of the ALK4/5/7 inhibitor SB-431542. To assess the similarity between biological replicates within and across samples, principal component analysis (PCA) was used to visualize relationships between groups (Fig. 6.6A). Interestingly, the top two principal components show that the effects of FSS (along PC1) and treatment with SB-431542 (along PC2) on OCY454 cells are mostly independent of each other.

The effect of FSS in the absence of SB-431542 yielded 1392 upregulated and 1122 downregulated differentially expressed genes (DEGs) (total = 2514 genes, FDR<0.05) (Fig. 6.6B). In the presence of SB-431542, stimulation with FSS yielded 1974 DEGs (1205 upregulated and 769 downregulated, Figure 6.7). In-line with other studies that have evaluated changes in the osteocyte transcriptome in response to FSS [26], pathway analysis of our DEGs identified pro-inflammatory pathways such as TNFα and IL6 in addition to MAPK and TGFβ (Fig. 6.6C).
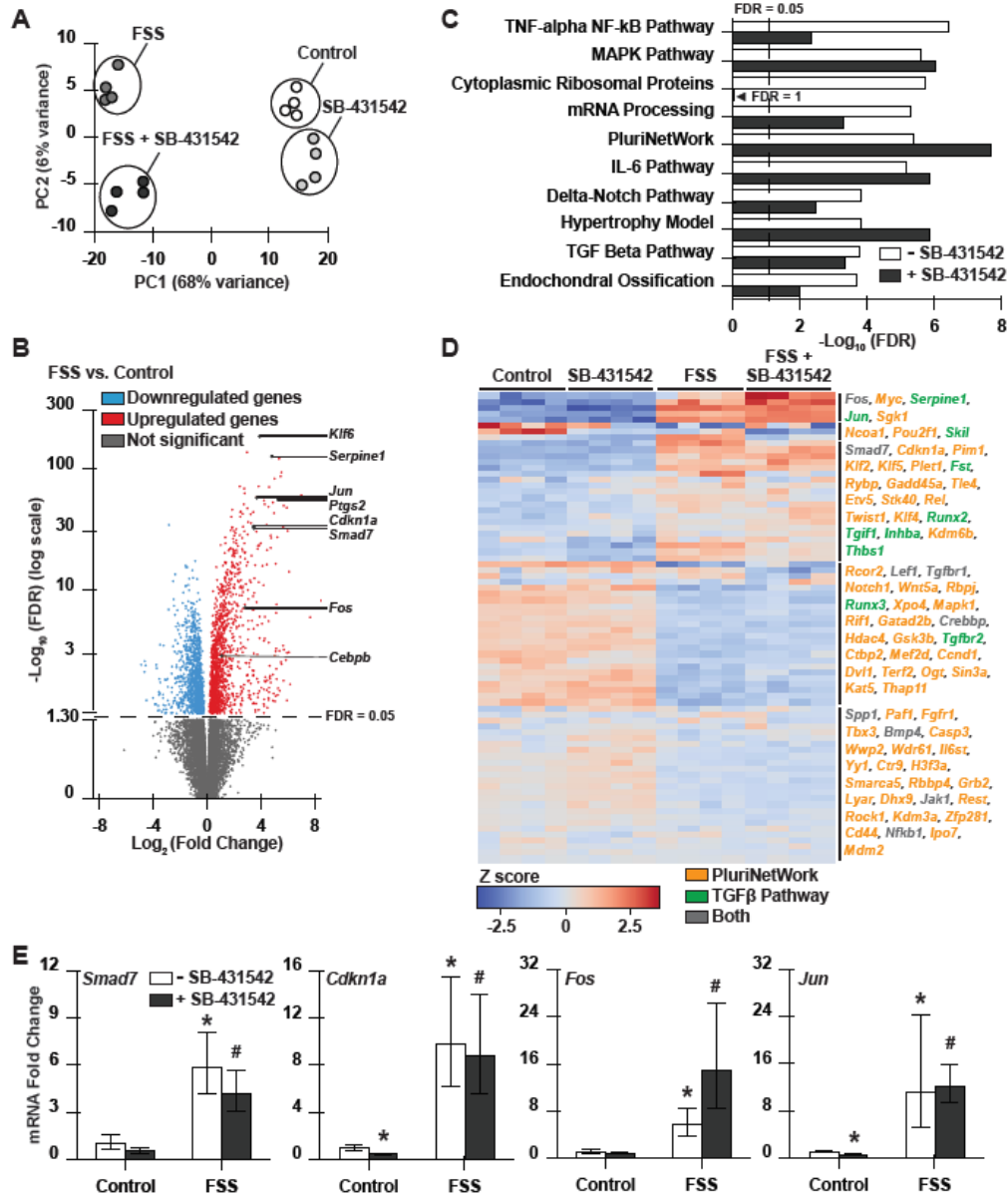
77

**Figure 6.6: RNAseq analysis supports potent FSS regulation of TGFβ superfamily signaling.** (A) Principal component analysis of sample variation considering the 500 genes with greatest variance. (B) Volcano plot showing the distribution of differential gene expression in FSS-stimulated and unstimulated cells, and identifying induced (red) and repressed (blue) differentially expressed genes (DEGs). (C) Enrichr pathway analysis using the WikiPathways database reveals the top ten most significantly regulated pathways, including TGFβ, that remain significantly regulated even in the presence of SB-431542. (D) Genes related to the TGFβ and PluriNetWork pathways were clustered in a heatmap, and genes in each cluster are grouped. (E) qRT-PCR analysis of established TGFβ-inducible genes Smad7, Cdkn1a, Fos, and Jun following FSS stimulation in the presence or absence of SB-431542. Vehicle is 1% DMSO. Dotted lines on graphs indicate threshold for statistical significance (FDR<0.05). *p<0.05 compared to unstimulated cells and #p<0.05 compared to SB-treated controls.

Of the 88 genes significantly FSS-regulated genes (FDR<0.1) identified by Govey et al., 13 met the significance threshold in this study and were regulated in the same direction: *Areg, Bcl9l, Cxcl1, Dnajb9, Ell2, Ereg, Klf16, March9, Nfkbiz, Pik3r1, Ptgs2, Rxrb,* and *Tpp2*. Among the top 10 FSS-regulated pathways, SB-431542 inhibition of ALK4/5/7 had surprisingly modest effects on FSS regulation of the TGFβ pathway. Though the Cytoplasmic Ribosomal Proteins pathway was no longer significantly regulated by FSS in the presence of SB-431542, others were more significantly regulated, including the PluriNetWork pathway which contains genes associated with pluripotency in mice. This and other FSS-sensitive pathways include many genes implicated in TGFβ and BMP signaling (Figure 6.8).
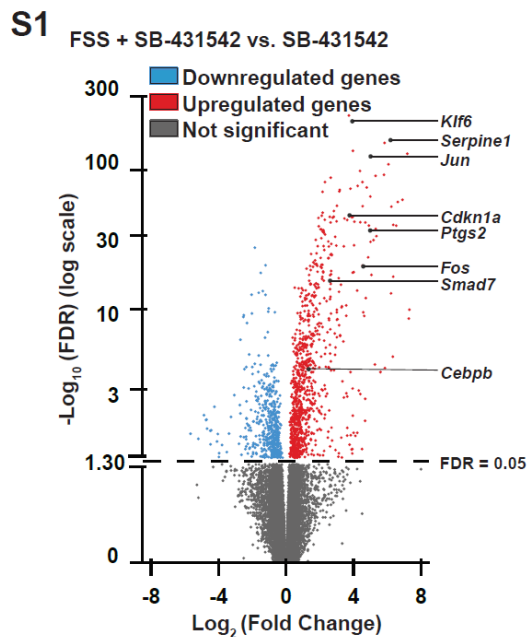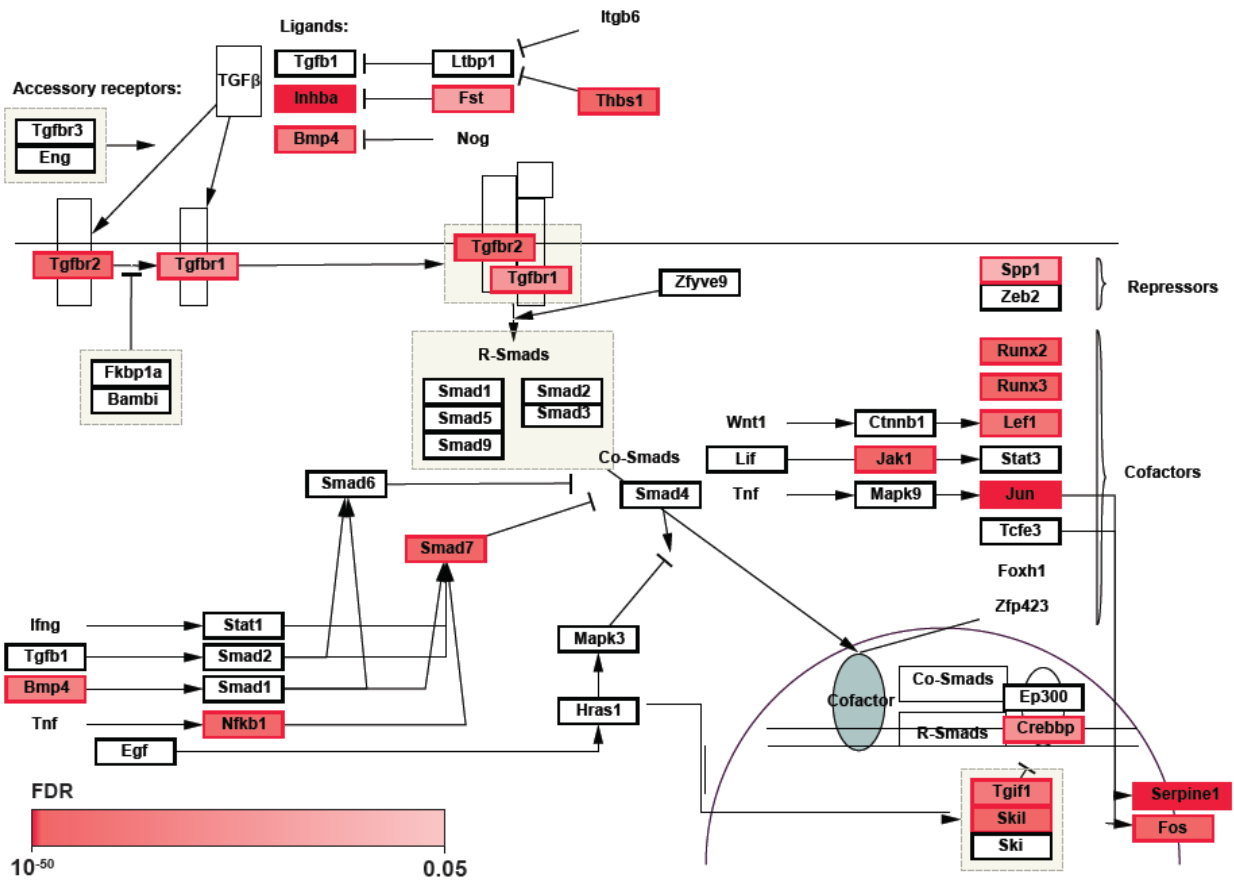


**Figure 6.7: Volcano plot from FSS + SB-431542 vs. SB-431542.** Volcano plot showing the distribution of differential gene expression in FSS-stimulated and unstimulated cells pretreated with the ALK4/5/7 inhibitor SB-431542, and identifying induced (red) and repressed (blue) differentially expressed genes (DEGs).

# S2

## A FSS vs. Control
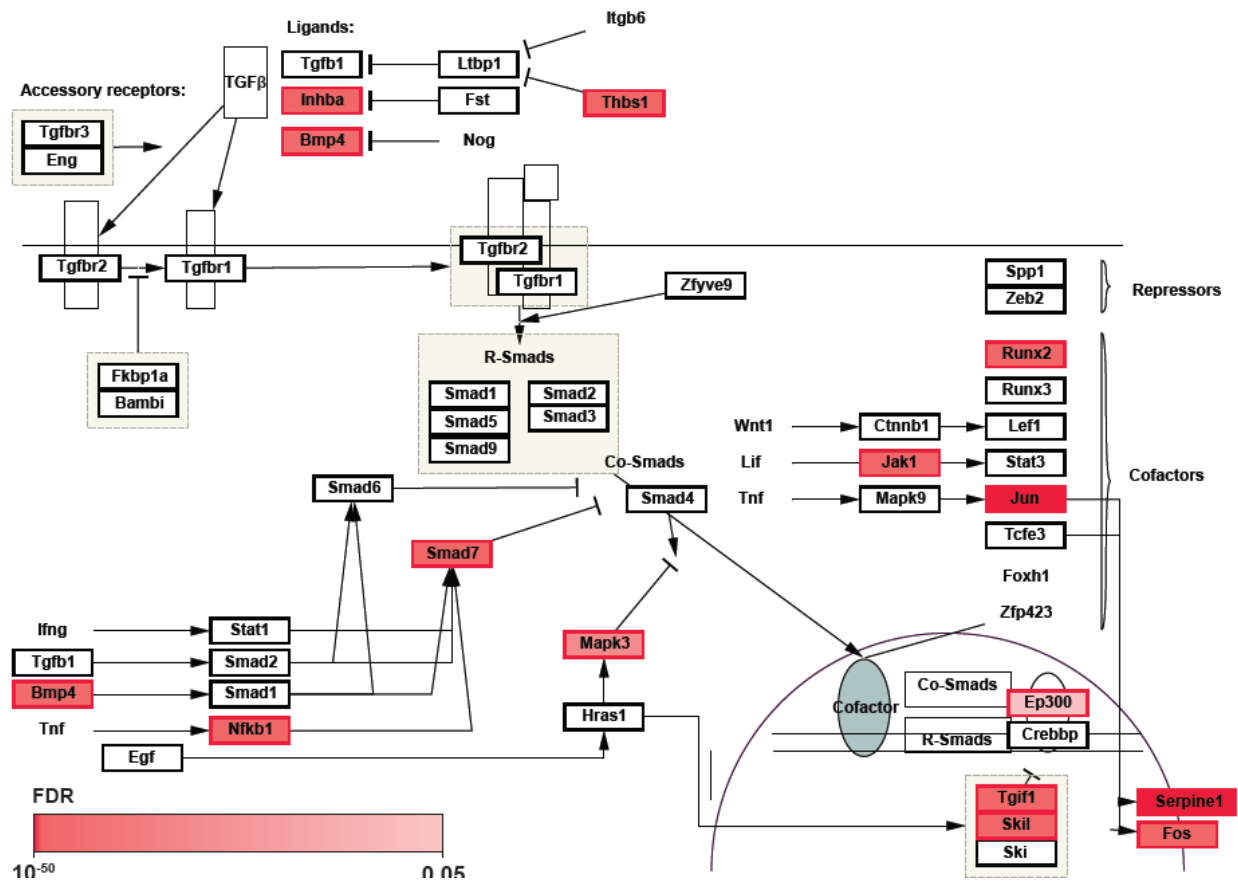
**Figure 6.8: Cytoscape visualization of FSS-regulated TGFβ pathway differentially expressed genes (DEGs).** Cytoscape (v3.8.0) [66] along with the WikiPathways app for Cytoscape [67] was used to visualize FSS regulated TGFβ signaling pathway DEGs (FDR<0.05), both in the presence (A) or absence (B) of the ALK4/5/7 inhibitor SB-431542. DESeq2 results (FDR values) were imported into the WikiPathways app for Cytoscape, and DEGs from the TGFβ signaling pathway have a red border and are color-coded according to their FDR values. Non-DE genes have a thick black border.

To further examine the effect of SB-431542 on FSS-inducible genes, we generated a heatmap of all DEGs from the TGFβ and PluriNetWork pathways across all samples. While no significant differences in the expression levels of many TGFβ superfamily ligands, receptors, or effectors were observed, many TGFβ and BMP target genes were upregulated by FSS, even in the presence of SB-431542, supporting the notion that FSS-regulation of TGFβ signaling occurs through TβRI-dependent and independent mechanisms (Fig. 6.6D). Interestingly, some of the most upregulated genes by FSS in each of these conditions were the transcription factors *Myc*, *Fos,* and *Jun*, as well as *Serpine1*. Indeed, qRT-PCR validation of established TGFβ-inducible genes revealed significant FSS-mediated increases of *Smad7*, *Cdkn1a*, *Fos*, and *Jun*, even in the presence of SB-431542 (Fig. 6.6E).

## *FSS-dependent regulation of TGFβ receptor heteromerization*

Our data indicate that unlike biochemical ligands, which can activate discrete subsets of the TGFβ signaling pathways, the physical cue FSS activates a unique combination of these pathways concurrently, resulting in a pattern of gene expression that is distinct from that which could be achieved by either ligand alone. At least part of this effect results from FSS-mediated activation of multiple TGFβ and BMP type I receptors. The mechanisms involved in FSS activation of TGFβ family signaling in OCY454 cells seem to differ somewhat from those observations reported in other cell types [10–15], therefore, we evaluated mechanisms by which FSS might alter TGFβ family receptor function in osteocytes.

To examine the effect of FSS on TGFβ type I and type II receptor heteromerization, we utilized a proximity ligation assay (PLA). Relative to the negative control, in which only TβRI (ALK5) is labelled, fluorescent PLA signal identifies multimeric TβRI/TβRII complexes in baseline control conditions when both TβRI (ALK5) and TβRII are labelled (Fig. 6.9A). Exposure to FSS rapidly and transiently induces formation of TβRI/TβRII complexes within 10 minutes and PLA
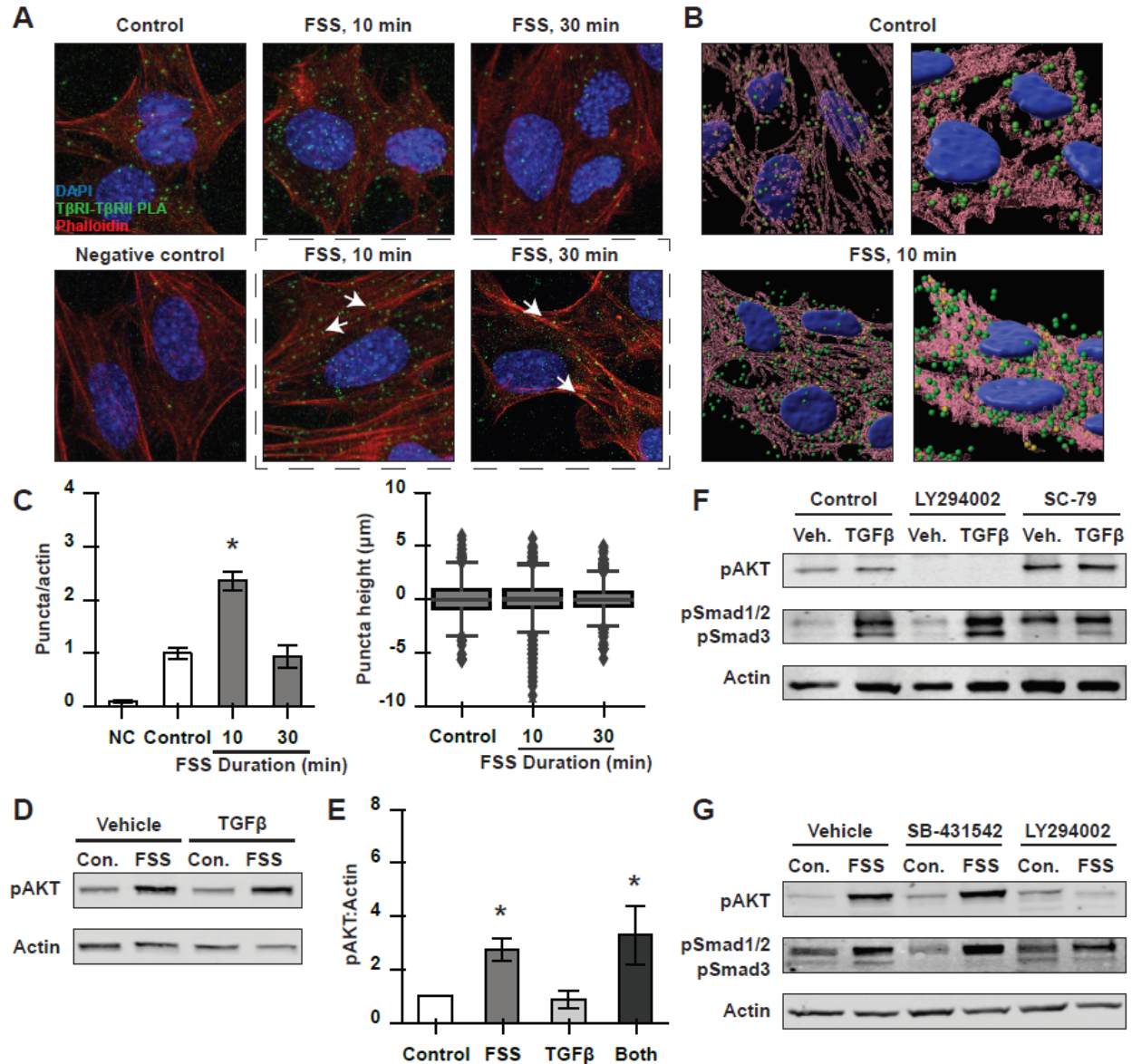
**Figure 6.9: FSS-dependent regulation of TGFβ receptor heteromerization.** (A) Images of proximity ligation assay (PLA) between TβRI and TβRII (n=5 regions of interest). Dashed lines show puncta localization relative to Actin fibers. (B, C) IMARIS analysis of images (B) allows quantitative analysis of puncta frequency and spatial distribution in the presence or absence of FSS (C). (D, E) Western analysis and quantification of control cells and cells treated with TGFβ or stimulated with FSS (30 minutes). (F) Representative western analysis from cells pretreated (60 minutes) with vehicle or a PI3K/AKT inhibitor (LY294002) or agonist (SC-79) followed by treatment with TGFβ (30 minutes). (G) Representative western analysis from cells pretreated (60 minutes) with vehicle or a TβRI or PI3K/AKT inhibitor followed by treatment (30 minutes) with 0.1 Pa FSS. All values normalized to control cells. *$p < 0.05$ compared to unstimulated cells.

signal returns to baseline levels by 30 minutes (Fig. 6.9A). FSS also appears to elicit a change in puncta localization, particularly along actin stress fibers (Fig. 6.7A, within dashed border). Although quantitative IMARIS analysis confirmed a 2-3 fold increase in unique puncta following 10 minutes of FSS stimulation, no significant increase in the fraction of puncta in close proximity to actin fibers was observed (gold puncta, Fig. 6.9B; green puncta are further from actin fibers) (Fig. 6.9C). Further, no differences were observed in the distribution of puncta along cellular depth, thus receptor heteromerization induced by FSS stimulation does not seem to be preferentially localized to the top or bottom of the cells, but mimics the original distribution of receptor complexes (Fig. 6.9C).

Several established mechanisms enable precise cellular control of TGFβ receptor colocalization and heteromerization, including at specific mechanosensory sites such as the primary cilium [44] or focal adhesions [9], or through pAKT-induced shuttling of intracellular receptors to the cell membrane [45]. Among other mechanisms we explored, we perturbed AKT activity to test the hypothesis that FSS induces Smad phosphorylation by stimulating AKT-dependent membrane presentation of vesicular TGFβ receptors. Within 30 minutes of treatment, FSS but not TGFβ increased AKT phosphorylation in osteocytes (Figs. 6.9D, 6.9E). To determine the extent to which AKT activation regulates the osteocytic response to TGFβ, cells were pretreated with a PI3K/AKT inhibitor (LY294002) or agonist (SC-79) and levels of Smad phosphorylation were evaluated in the presence or absence of TGFβ (Fig. 6.9F). While AKT inhibition had little effect on baseline pSmad2/3 levels, it mildly enhanced the cellular response to TGFβ. On the contrary, AKT activation increased baseline Smad phosphorylation in a manner similar to FSS stimulation, and enabled an incremental increase in Smad phosphorylation upon cotreatment with TGFβ. However, FSS activation of AKT is insufficient to fully explain the effects of FSS on Smad phosphorylation, as AKT inhibition did not block FSS-mediated Smad phosphorylation (Fig. 6.9G). Collectively, our data show that FSS acts through a number of

mechanisms, including regulated receptor multimerization and selective activation of multiple type I receptors, to induce a unique pattern of downstream signaling.

**Discussion**

We find that fluid shear stress activates TGFβ family signaling in a manner that differs qualitatively and quantitatively from signaling activated by either TGFβ or BMP ligands. In the osteocyte-like cell line OCY454, FSS rapidly induces Smad phosphorylation, Smad nuclear translocation, and expression of TGFβ target genes, the dynamics of which mimic that of treatment with TGFβ ligand. However, relative to TGFβ, FSS induces a larger increase in levels of pSmad2/3 and *Serpine1*. Combined stimulation with TGFβ ligand and FSS resulted in even higher levels of Smad phosphorylation and *Serpine1* gene expression than that induced by either treatment alone. The additive response to FSS and TGFβ may result from FSS-inducible TGFβ type I and type II receptor multimerization, effectively priming cells to respond to available ligand. Furthermore, FSS generates responses distinct from those achieved by either TGFβ or BMP by concurrently activating multiple TGFβ family type I receptors, providing new insight into mechanisms by which cells integrate signaling through biochemical and physical cues to generate a unique response.

In this way, discrete physical cues add diversity and specificity to the signaling outcomes produced by the molecular machinery of the TGFβ family signaling pathway. For example, the effects of TGFβ and BMP ligands are highly sensitive to the physical properties of the ECM, such that the ability of TGFβ or BMP to promote chondrogenic or osteogenic differentiation, respectively, requires an optimal level of cytoskeletal tension [7,8,46–48]. Mechanoregulation of the cellular response to TGFβ family ligands amplifies their effects at the time and site of skeletal development, but can also exacerbate pathological mineralization, such as in fibrodysplasia ossificans progressiva [49]. Among the mechanosensitive mechanisms controlling TGFβ family signaling is integrin-dependent activation of latent TGFβ ligand [50]. While FSS has been shown

to activate latent TGFβ through a mechanism sensitive to FSS magnitude and flow profile (steady vs. oscillatory [17]), we find that FSS stimulates Smad phosphorylation even with saturating levels of active TGFβ ligand. This suggests that mechanoactivation of latent TGFβ is not the sole mechanism through which FSS targets this pathway in osteocytes. Further, although physical cues can also regulate mRNA levels for TGFβ ligands [51], our transcriptomic analysis revealed no significant regulation of TGFβ1 mRNA, and only a significant 1.46-fold increase in the levels of TGFβ2 along with a 2.64-fold reduction in TGFβ3 after 2 h of stimulation with 1 Pa FSS.

The TGFβ family has seven type I, five type II, and two type III receptors. Multimeric receptor complexes regulate the activity of canonical (Smad) or non-canonical (i.e. TAK1, AKT) effectors in response to diverse ligands, including TGFβs, BMPs, GDFs, activins, and inhibins [5,52]. Thus, receptor-level regulation enables cells to precisely couple activation of specific downstream effectors to distinct TGFβ family ligands. For example, the TGFβ type I receptor ALK5 responds to TGFβ by activating Smad2/3. However, in chondrocytes, ALK5 also plays an essential role in antagonizing BMP9 signaling through another type I receptor, ALK1 [53]. In osteocytes, we observe a complementary effect of ALK5 and ALK1/ALK2 activation by FSS, such that phosphorylation of canonical TGFβ and BMP R-Smads is induced, suggesting that the effect of crosstalk between these type I receptors could depend on the cellular or mechanical context.

The mechanisms by which FSS concurrently activates multiple TGFβ receptors in osteocytes, and the physiological significance of these mechanisms in bone, remain to be determined. Nonetheless, we and others have identified mechanisms responsible for mechanoregulation of TGFβ family receptor function. Physical cues influence the heteromerization and spatial localization of TGFβ family receptors at the cell surface and within specific cellular domains. At high cytoskeletal tension, integrin-rich focal adhesions confine a population of TGFβ and BMP type I receptors (ALK5 and ALK1) and preferentially exclude TβRII. Changes in the physical microenvironment that reduce cytoskeletal tension enable colocalization and heteromerization of these type I and type II receptors and the subsequent activation of

downstream Smad2/3 [9]. Chang et al. showed that αvβ3 and β1 integrins were required to observe FSS-mediated increases in Smad1/5 phosphorylation in MG63 osteosarcoma cells, but did not report their effects on TGFβ/Smad2/3 signaling [41]. A role for integrins in the FSS-mediated control of TGFβ receptor heteromerization would be exciting, especially since integrin-rich mechanosomes are thought to sense FSS in canalicular networks [54]. Indeed, we also observed a rapid, transient increase in TβRI-TβRII interactions following the onset of FSS stimulation, but technical constraints of the microfluidic chambers currently limit our ability to monitor these changes locally at focal adhesions.

In addition to integrins, FSS may exert its effects on TGFβ receptors in osteocytes through other potential mechanosensors, such as transient receptor potential subfamily V member 4 (TRPV4) ion channels and the primary cilium. FSS-induced activation of NADPH oxidase 2 (NOX2) in osteocytes generates reactive oxygen species that drive $Ca^{2+}$ influx through TRPV4 [55]. In MLO-Y4 osteocyte-like cells, intact primary cilia were implicated in the FSS-dependent induction of *Ptgs2* mRNA [56]. Given the regulated localization of TGFβ and BMP receptors in the primary cilium and at the ciliary base [44,57,58], an attractive model posits that FSS regulates TGFβ family signaling in a cilia-dependent manner. However, studies by Kunnen et al. of FSS-inducible TGFβ family signaling in renal epithelial cells found that cilia ablation failed to block FSS-induced Smad2/3 phosphorylation or FSS-dependent EMT [16]. Likewise, we observed preservation of FSS-inducible Smad2/3 phosphorylation even upon ablation of the primary cilia in MLO-Y4 osteocyte-like cells and after ciliation in IMCD3 kidney epithelial cells (Figure 6.10). We further examined the possibility that FSS-dependent activation of AKT promotes the translocation of sequestered intracellular TGFβ receptors to the cell surface where they gain access to TGFβ ligand [45,59]. Though we observed rapid AKT activation upon stimulation with FSS, AKT inhibition did not completely block FSS-induced Smad phosphorylation in the current study.
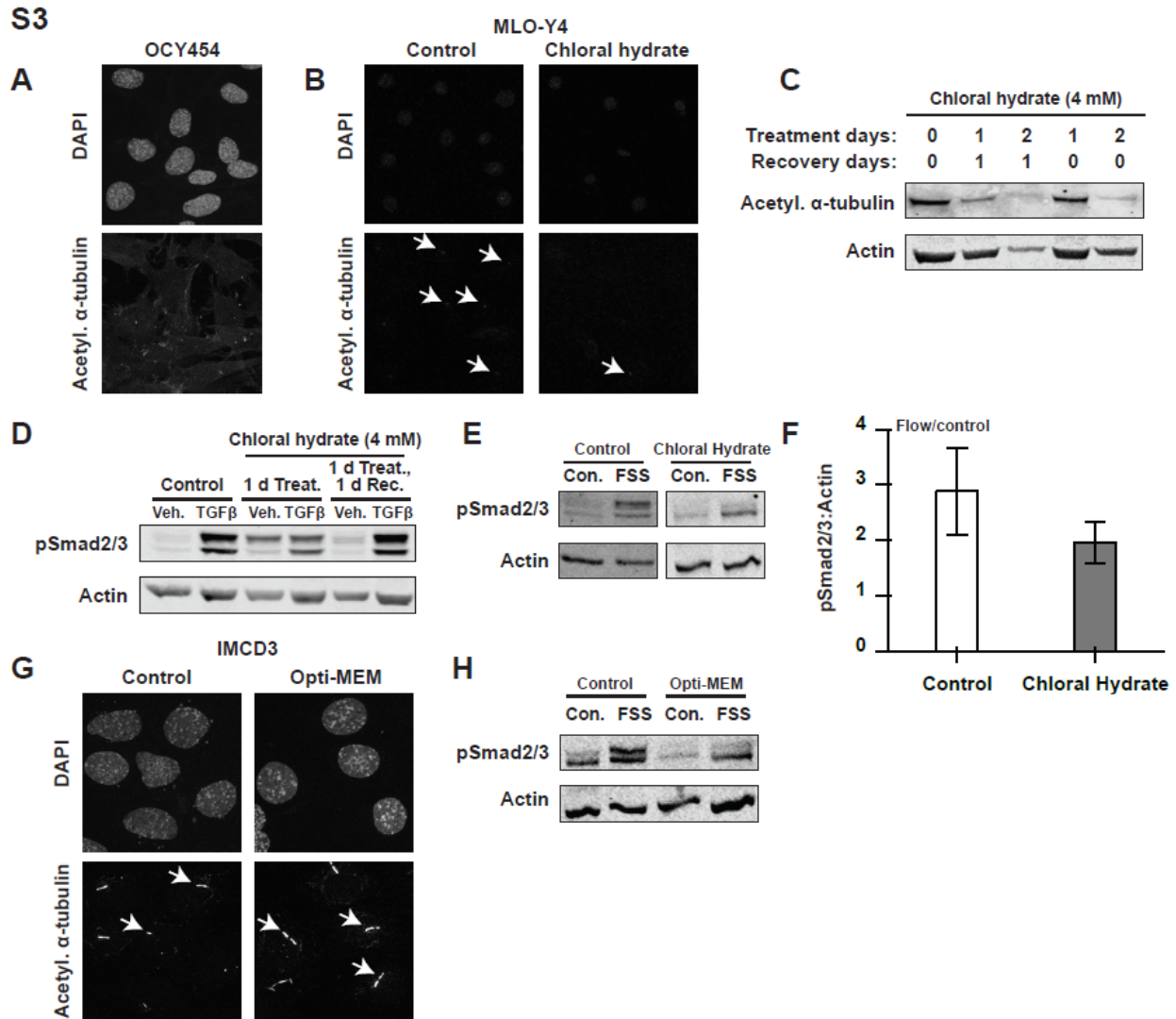
**Figure 6.10: Role of primary cilium length in regulating FSS activation of TGFβ signaling.**
(A) OCY454 cells appear to not possess clear primary cilia that are positive for acetylated-α-tubulin. (B) Most MLO-Y4 cells treated with 4 mM chloral hydrate for 24 h followed by 24 h recovery lose their primary cilia, shown using immunofluorescence for acetylated α-tubulin. (C) Treatment of MLO-Y4 with chloral hydrate for longer than 24 h has detrimental effects on cell viability, and lack of a recovery period after treatment reduces deciliation effectiveness. (D) A 24 h treatment, 24 h recovery regimen of chloral hydrate does not affect baseline TGFβ signaling nor TGFβ sensitivity in MLO-Y4 cells. (E, F) Stimulation of chloral hydrate-treated MLO-Y4 cells with FSS (0.1 Pa, 30 minutes) still induces Smad2/3 phosphorylation. Although FSS-induction of pSmad2/3 levels appears lower in chloral hydrate treated cells than in control cells, these differences are not statistically significant. (G) IMCD3 kidney epithelial cells natively possess long primary cilia that increase in length following treatment with Opti-MEM reduced serum media (24 h). (H) IMCD3 cells with lengthened primary cilia still show FSS-inducible Smad2/3 phosphorylation, but may be less responsive to FSS stimulation than control cells.

Future studies can derive mechanistic insight and clinical relevance from prior work on FSS regulation of BMP signaling in endothelial cells. FSS sensitizes endothelial cells to BMP9 signaling by stimulating association between type I (ALK1) and type III (endoglin) receptors [13]. Human loss-of-function mutations in either ALK1 or endoglin prevent the FSS-dependent control of BMP signaling in endothelial cells, resulting in arteriovenous malformations in hereditary hemorrhagic telangiectasia (HHT) [13]. ALK1 is also an attractive candidate receptor for FSS-inducible activation of Smad phosphorylation in osteocytes. ALK1 responds to both TGFβ and BMP ligands [3,42,60] and all three of the ALK1 inhibitors tested in the current study antagonize FSS-inducible Smad phosphorylation. Though endoglin is highly expressed in endothelial cells [61], other mesenchymal lineage cell types also express endoglin and the other TGFβ family type III receptor, betaglycan [62,63]. Additional research will be needed to identify the specific receptors and mechanisms by which FSS alters the type and magnitude of TGFβ family signaling in osteocytes, as well as to examine these mechanisms in differentiated osteocytes and *in vivo*.

The complex roles of these intersecting TGFβ family pathways in the context of the skeleton have yet to be fully understood; however, both TGFβ and BMP signaling are fundamental in skeletal development and in the anabolic response of bone to applied loads [19,64,65]. Receptor-level regulation of TGFβ family signaling appears to be essential to maintaining skeletal homeostasis. For example, mice with an osteocyte-intrinsic knockout of TβRII exhibit disrupted perilacunar/canalicular remodeling and poor bone quality [22]. Likewise, fibrodysplasia ossificans progressiva is the result of a gain-of-function mutation in the BMP type I receptor ALK2 [49]. Future studies using osteocyte-specific mutations in different TGFβ family type I, II, and III receptors could clarify the precise role of these proteins in coordinating the osteocyte response to mechanical load. In conclusion, we find that fluid shear stress rapidly and concurrently activates TGFβ and BMP signaling through distinct subsets of TGFβ family type I receptors, revealing a novel mechanism by which physical cues calibrate TGFβ family signaling.

**References**

1       Rape, A.D. *et al.* (2015) A synthetic hydrogel for the high-throughput study of cell-ECM interactions. *Nat. Commun.* 6, 8129

2       Guilak, F. *et al.* (2009) Control of stem cell fate by physical interactions with the extracellular matrix. *Cell Stem Cell* 5, 17–26

3       Heldin, C.-H. and Moustakas, A. (2016) Signaling Receptors for TGF-β Family Members. *Cold Spring Harb. Perspect. Biol.* 8,

4       Massagué, J. (1998) TGF-beta signal transduction. *Annu. Rev. Biochem.* 67, 753–791

5       Feng, X.-H. and Derynck, R. (2005) Specificity and versatility in tgf-beta signaling through Smads. *Annu. Rev. Cell Dev. Biol.* 21, 659–693

6       Hinz, B. (2015) The extracellular matrix and transforming growth factor-beta1: Tale of a strained relationship. *Matrix Biol.* 47, 54–65

7       Wang, Y.-K. *et al.* (2012) Bone morphogenetic protein-2-induced signaling and osteogenesis is regulated by cell shape, RhoA/ROCK, and cytoskeletal tension. *Stem Cells Dev.* 21, 1176–1186

8       Allen, J.L. *et al.* (2012) ECM stiffness primes the TGFbeta pathway to promote chondrocyte differentiation. *Mol. Biol. Cell* 23, 3731–3742

9       Rys, J.P. *et al.* (2015) Discrete spatial organization of TGFbeta receptors couples receptor multimerization and signaling to cellular tension. *Elife* 4, e09300

10      Walshe, T.E. *et al.* (2013) The role of shear-induced transforming growth factor-beta signaling in the endothelium. *Arterioscler. Thromb. Vasc. Biol.* 33, 2608–2617

11      Zhou, J. *et al.* (2012) Force-specific activation of Smad1/5 regulates vascular endothelial cell cycle progression in response to disturbed flow. *Proc. Natl. Acad. Sci. U. S. A.* 109, 7770–7775

12      Baeyens, N. *et al.* (2015) Vascular remodeling is governed by a VEGFR3-dependent fluid shear stress set point. *Elife* 4,

13    Baeyens, N. *et al.* (2016) Defective fluid shear stress mechanotransduction mediates hereditary hemorrhagic telangiectasia. *J. Cell Biol.* 214, 807–816

14    Laux, D.W. *et al.* (2013) Circulating Bmp10 acts through endothelial Alk1 to mediate flow-dependent arterial quiescence. *Development* 140, 3403–3412

15    Utsunomiya, T. *et al.* (2016) Transforming Growth Factor-beta Signaling Cascade Induced by Mechanical Stimulation of Fluid Shear Stress in Cultured Corneal Epithelial Cells. *Invest. Ophthalmol. Vis. Sci.* 57, 6382–6388

16    Kunnen, S.J. *et al.* (2017) Fluid shear stress-induced TGF-beta/ALK5 signaling in renal epithelial cells is modulated by MEK1/2. *Cell. Mol. Life Sci.* 74, 2283–2298

17    Kouzbari, K. *et al.* (2019) Oscillatory shear potentiates latent TGF-beta1 activation more than steady shear as demonstrated by a novel force generator. *Sci. Rep.* 9, 6065

18    Albro, M.B. *et al.* (2012) Shearing of synovial fluid activates latent TGF-β. *Osteoarthr. Cartil.* 20, 1374–1382

19    Nguyen, J. *et al.* (2013) Load regulates bone formation and Sclerostin expression through a TGFbeta-dependent mechanism. *PLoS One* 8, e53813

20    Morrell, A.E. *et al.* (2018) Mechanically induced Ca(2+) oscillations in osteocytes release extracellular vesicles and enhance bone formation. *Bone Res.* 6, 6

21    Moore, E.R. *et al.* (2018) Adenylyl cyclases and TRPV4 mediate Ca(2+)/cAMP dynamics to enhance fluid flow-induced osteogenesis in osteocytes. *J. Mol. Biochem.* 7, 48–59

22    Dole, N.S. *et al.* (2017) Osteocyte-Intrinsic TGF-beta Signaling Regulates Bone Quality through Perilacunar/Canalicular Remodeling. *Cell Rep.* 21, 2585–2596

23    Blaney Davidson, E.N. *et al.* (2009) Increase in ALK1/ALK5 ratio as a cause for elevated MMP-13 expression in osteoarthritis in humans and mice. *J. Immunol.* 182, 7937–7945

24    Yan, Z. *et al.* (2018) Fluid shear stress improves morphology, cytoskeleton architecture, viability, and regulates cytokine expression in a time-dependent manner in MLO-Y4 cells. *Cell Biol. Int.* 42, 1410–1422

25    Govey, P.M. *et al.* (2014) Integrative transcriptomic and proteomic analysis of osteocytic cells exposed to fluid flow reveals novel mechano-sensitive signaling pathways. *J. Biomech.* 47, 1838–1845

26    Govey, P.M. *et al.* (2015) Mapping the osteocytic cell response to fluid flow using RNA-Seq. *J. Biomech.* 48, 4327–4332

27    Xu, L.H. *et al.* (2019) OCY454 Osteocytes as an in Vitro Cell Model for Bone Remodeling Under Mechanical Loading. *J. Orthop. Res. Off. Publ. Orthop. Res. Soc.* 37, 1681–1689

28    Spatz, J.M. *et al.* (2015) The Wnt Inhibitor Sclerostin Is Up-regulated by Mechanical Unloading in Osteocytes in Vitro. *J. Biol. Chem.* 290, 16744–16758

29    Schmittgen, T.D. and Livak, K.J. (2008) Analyzing real-time PCR data by the comparative C(T) method. *Nat. Protoc.* 3, 1101–1108

30    Martin, M. (2011) Cutadapt removes adapter sequences from high-throughput sequencing reads. *EMBnet.journal; Vol 17, No 1 Next Gener. Seq. Data Anal. - 10.14806/ej.17.1.200* at <http://journal.embnet.org/index.php/embnetjournal/article/view/200>

31    Patro, R. *et al.* (2017) Salmon provides fast and bias-aware quantification of transcript expression. *Nat. Methods* 14, 417–419

32    Love, M.I. *et al.* (2014) Moderated estimation of fold change and dispersion for RNA-seq data with DESeq2. *Genome Biol.* 15, 550

33    Chen, E.Y. *et al.* (2013) Enrichr: interactive and collaborative HTML5 gene list enrichment analysis tool. *BMC Bioinformatics* 14, 128

34    Kuleshov, M. V *et al.* (2016) Enrichr: a comprehensive gene set enrichment analysis web server 2016 update. *Nucleic Acids Res.* 44, W90-7

35    Schneider, C.A. *et al.* (2012) NIH Image to ImageJ: 25 years of image analysis. *Nat. Methods* 9, 671–675

36    Tian, L. *et al.* (2009) Imaging neural activity in worms, flies and mice with improved

GCaMP calcium indicators. *Nat. Methods* 6, 875–881

37    Jin, X. *et al.* (2014) Cilioplasm is a cellular compartment for calcium signaling in response to mechanical and chemical stimuli. *Cell. Mol. Life Sci.* 71, 2165–2178

38    Wittkowske, C. *et al.* (2016) In Vitro Bone Cell Models: Impact of Fluid Shear Stress on Bone Formation. *Front. Bioeng. Biotechnol.* 4, 87

39    Kamel, M.A. *et al.* (2010) Activation of β-catenin signaling in MLO-Y4 osteocytic cells versus 2T3 osteoblastic cells by fluid flow shear stress and PGE2: Implications for the study of mechanosensation in bone. *Bone* 47, 872–881

40    Li, J. *et al.* (2012) Effect of oscillating fluid flow stimulation on osteocyte mRNA expression. *J. Biomech.* 45, 247–251

41    Chang, S.-F. *et al.* (2008) Tumor cell cycle arrest induced by shear stress: Roles of integrins and Smad. *Proc. Natl. Acad. Sci. U. S. A.* 105, 3927–3932

42    de Kroon, L.M.G. *et al.* (2015) Activin Receptor-Like Kinase Receptors ALK5 and ALK1 Are Both Required for TGFβ-Induced Chondrogenic Differentiation of Human Bone Marrow-Derived Mesenchymal Stem Cells. *PLoS One* 10, e0146124

43    Mitchell, D. *et al.* (2010) ALK1-Fc inhibits multiple mediators of angiogenesis and suppresses tumor growth. *Mol. Cancer Ther.* 9, 379–388

44    Labour, M.-N. *et al.* (2016) TGFbeta1 - induced recruitment of human bone mesenchymal stem cells is mediated by the primary cilium in a SMAD3-dependent manner. *Sci. Rep.* 6, 35542

45    Budi, E.H. *et al.* (2019) Integration of TGF-β-induced Smad signaling in the insulin-induced transcriptional response in endothelial cells. *Sci. Rep.* 9, 16992

46    McBeath, R. *et al.* (2004) Cell shape, cytoskeletal tension, and RhoA regulate stem cell lineage commitment. *Dev. Cell* 6, 483–495

47    Park, J.S. *et al.* (2011) The effect of matrix stiffness on the differentiation of mesenchymal stem cells in response to TGF-β. *Biomaterials* 32, 3921–3930

48    Kwon, S.-H. *et al.* (2013) Modulation of BMP-2-induced chondrogenic versus osteogenic differentiation of human mesenchymal stem cells by cell-specific extracellular matrices. *Tissue Eng. Part A* 19, 49–58

49    Stanley, A. *et al.* (2019) Elevated BMP and Mechanical Signaling Through YAP1/RhoA Poises FOP Mesenchymal Progenitors for Osteogenesis. *J. bone Miner. Res. Off. J. Am. Soc. Bone Miner. Res.* 34, 1894–1909

50    Klingberg, F. *et al.* (2014) Prestress in the extracellular matrix sensitizes latent TGF-beta1 for activation. *J. Cell Biol.* 207, 283–297

51    Rys, J.P. *et al.* (2016) Mechanobiology of TGFbeta signaling in the skeleton. *Matrix Biol.* 52–54, 413–425

52    Derynck, R. and Zhang, Y.E. (2003) Smad-dependent and Smad-independent pathways in TGF-beta family signalling. *Nature* 425, 577–584

53    Wang, W. *et al.* (2019) The TGFβ type I receptor TGFβRI functions as an inhibitor of BMP signaling in cartilage. *Proc. Natl. Acad. Sci. U. S. A.* 116, 15570–15579

54    Cabahug-Zuckerman, P. *et al.* (2018) Potential role for a specialized β(3) integrin-based structure on osteocyte processes in bone mechanosensation. *J. Orthop. Res. Off. Publ. Orthop. Res. Soc.* 36, 642–652

55    Lyons, J.S. *et al.* (2017) Microtubules tune mechanotransduction through NOX2 and TRPV4 to decrease sclerostin abundance in osteocytes. *Sci. Signal.* 10,

56    Malone, A.M.D. *et al.* (2007) Primary cilia mediate mechanosensing in bone cells by a calcium-independent mechanism. *Proc. Natl. Acad. Sci. U. S. A.* 104, 13325–13330

57    Clement, C.A. *et al.* (2013) TGF-beta signaling is associated with endocytosis at the pocket region of the primary cilium. *Cell Rep.* 3, 1806–1814

58    Xie, Y.-F. *et al.* (2016) Pulsed electromagnetic fields stimulate osteogenic differentiation and maturation of osteoblasts by upregulating the expression of BMPRII localized at the base of primary cilium. *Bone* 93, 22–32

59    Duan, D. and Derynck, R. (2019) Transforming growth factor-beta (TGF-beta)-induced up-regulation of TGF-beta receptors at the cell surface amplifies the TGF-beta response. *J. Biol. Chem.* 294, 8490–8504

60    Goumans, M.J. *et al.* (2003) Activin receptor-like kinase (ALK)1 is an antagonistic mediator of lateral TGFbeta/ALK5 signaling. *Mol. Cell* 12, 817–828

61    Lebrin, F. *et al.* (2004) Endoglin promotes endothelial cell proliferation and TGF-beta/ALK1 signal transduction. *EMBO J.* 23, 4018–4028

62    Finnson, K.W. *et al.* (2010) Endoglin differentially regulates TGF-β-induced Smad2/3 and Smad1/5 signalling and its expression correlates with extracellular matrix production and cellular differentiation state in human chondrocytes. *Osteoarthr. Cartil.* 18, 1518–1527

63    Cook, L.M. *et al.* (2019) Betaglycan drives the mesenchymal stromal cell osteogenic program and prostate cancer-induced osteogenesis. *Oncogene* 38, 6959–6969

64    Wu, M. *et al.* (2016) TGF-β and BMP signaling in osteoblast, skeletal development, and bone formation, homeostasis and disease. *Bone Res.* 4, 16009

65    Nguyen, J. *et al.* (2020) CYLD, a mechanosensitive deubiquitinase, regulates TGFβ signaling in load-induced bone formation. *Bone* 131, 115148

66    Shannon, P. *et al.* (2003) Cytoscape: a software environment for integrated models of biomolecular interaction networks. *Genome Res.* 13, 2498–2504

67    Kutmon, M. *et al.* (2014) WikiPathways App for Cytoscape: Making biological pathways amenable to network analysis and visualization. *F1000Research* 3, 152

# Chapter 7

# Discussion and future directions

In the skeleton, the TGFβ signaling pathway plays diverse roles in development and maintenance of homeostasis, and its dysregulation is implicated in several skeletal pathologies. The amount, duration, and quality of TGFβ signaling in these tissues is tightly controlled by factors such as extracellular levels of active ligand, receptor localization, and effector availability, each of which are themselves regulated by the multitude of physical and biochemical cues that cells concurrently experience in their microenvironment. However, the mechanisms by which cells distinguish among these cues, especially as they regulate the activity of signaling pathways such as TGFβ, remain unknown. In particular, the ability of these cues to coordinate the activities of TGFβ receptors is of particular interest. For example, treatment of cells with TGFβ induces trafficking of intracellular receptors to the cell membrane [1], as well as reorganization of primary cilium-localized receptors from the ciliary tip to the ciliary base [2]. In this work, I evaluated how two distinct physical cues, substrate stiffness [3] and fluid shear stress (*in press,* Monteiro, et al. *The FASEB Journal.* 2020), regulate the TGFβ pathway by controlling the localization and activation of TGFβ receptors (Fig. 7.1A).
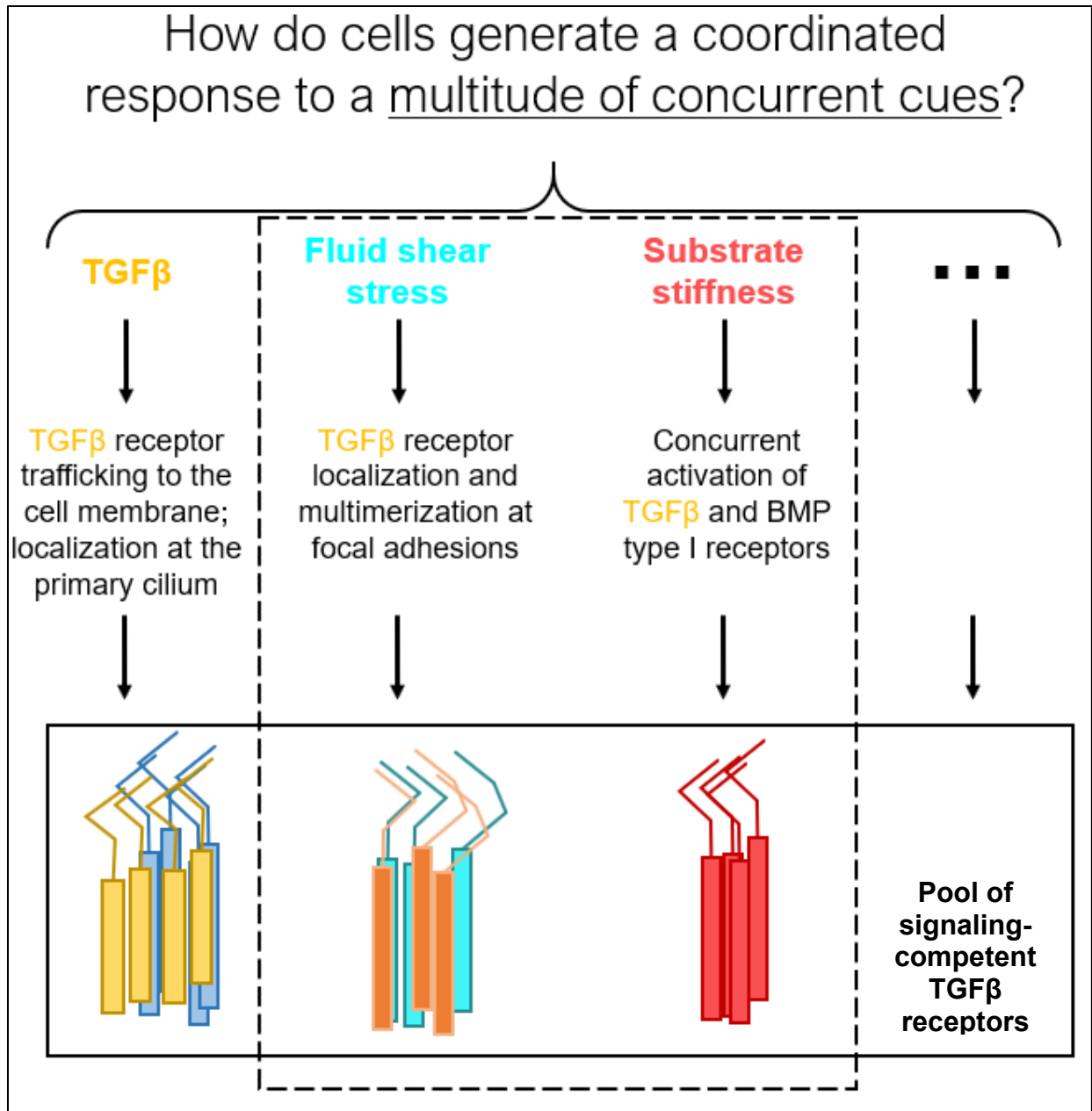
**Figure 7.1: Physical cues regulate the localization and activation of TGFβ receptors.** Through overlapping mechanisms that remain to be fully elucidated, distinct biological and physical cues regulate the makeup of a cell's active pool of signaling-competent TGFβ receptors. Through control of receptor localization at mechanosensory sites or by enabling multimerization of specific receptor isoforms, these cues prime the cellular response to certain TGFβ, BMP, or other TGFβ superfamily ligands. The quantity, types, and locations of these active receptors generates a unique signaling *fingerprint* in response to a combination of concurrent cues.

In Chapter 4, my results revealed the existence of a subpopulation of TGFβ receptors confined to regions near integrin-rich focal adhesions that exhibited unique localization and diffusive behaviors relative to receptors away from these sites. Using TIRF microscopy, we found that these focal adhesions preferentially included ALK1 and ALK5 and excluded TβRII in ATDC5 cells grown on stiff substrates. Using single particle tracking, we were able to quantify changes in the localization and diffusion of individual receptor molecules. We found that receptors within focal adhesions tended to be trapped within these sites, and that TβRII proteins were more likely than TβRI to bounce around the outside of these focal adhesion sites. Treating these cells with blebbistatin or a ROCK inhibitor Y27632, which disrupted cellular tension, led to entry of TβRII and promoted receptor colocalization and TβRI (ALK5)/TβRII heteromerization. However, we did not consider whether other TGFβ type I or type II receptors were spatially regulated in a similar manner, or if BMP signaling was also upregulated upon disruption of cytoskeletal tension. A deeper understanding of how the balance of these parallel signaling pathways shifts with changes in physical cues has important implications in understanding pathologies such as osteoarthritis. Further, using mass spectrometry we assessed the preferential interactions of ALK5 and TβRII with other cytoskeletal proteins. Our results revealed that both receptors complex with integrin αv, while TβRII preferentially interacts with the actin depolymerizing factor cofilin and the dynein light chain component DYNLT1. How these protein-protein interactions vary as a function of substrate stiffness or cytoskeletal tension remain to be fully elucidated, however, these results highlight the overlapping roles of the mechanotransduction and TGFβ pathways.

Based on these early findings, I became interested in studying the extent to which TGFβ receptors are regulated in a similar manner by other physical cues. Literature highlighting a role for DYNLT1 in controlling the length of the primary cilium guided me to fluid shear stress, given the role of the primary cilium as both a fluid flow mechanosensor and a locus for TGFβ signaling. In Chapter 6, I evaluated the ligand- and receptor-level requirements for fluid shear stress activation of TGFβ/Smad signaling in the osteocyte-like cell line OCY454. My results showed that

FSS concurrently activates signaling through TGFβ and BMP type I receptors, in a manner that requires the activity of the corresponding ligand. Specifically, I showed that FSS induces TβRI/TβRII heteromerization, Smad1 and Smad2/3 phosphorylation, Smad2/3 nuclear translocation, and upregulation of known TGFβ-inducible genes, including *Serpine1*, *Smad7*, *Cdkn1a*, *Fos*, *and Jun*, which were upregulated even in the presence of the ALK4/5/7 inhibitor SB-431542.

Many questions remain about the relationships between TGFβ superfamily ligands, receptors, and effectors and how they organize to generate unique downstream responses. In Chapter 3, I highlighted the complexity of signaling at the receptor-level, particularly in response to different physical cues, but the extent to which physical or biochemical cues such as FSS independently regulate the heteromerization of different TGFβ receptor subtypes remains unknown. One interesting observation was the difference in rates of upregulation of known TGFβ and BMP-inducible genes, *Serpine1* and *Id1*, respectively (Fig. 7.2A). Whereas *Serpine1* mRNA levels continued to increase through 2 hours of FSS, *Id1* levels appear to plateau sooner. This result, along with the ability of FSS to upregulate known TGFβ-inducible genes even in the presence of a TβRI inhibitor, suggests that multiple receptors might be activated at different rates after FSS is applied. Future studies could leverage individual receptor siRNAs or transient transfection with dominant negative receptor constructs to help elucidate the roles for each of the several type I, type II, and type III TGFβ receptors in the mechanoactivation of the TGFβ signaling pathway by FSS or other physical cues. Another approach would be to use a series of Smad/non-Smad luciferase assays to assess differences in the activities of individual canonical and non-canonical TGFβ effectors.

Using a microfluidic platform made from PDMS and glass provided an optically-clear system that was compatible with imaging of live- and fixed-cells. In this work, I used this system to show FSS-induced changes in 1) calcium influx using a GCaMP3 plasmid, 2) Smad nuclear translocation both by using antibodies against Smad2/3 and using an MS2 SBE4 plasmid, and 3) TGFβ receptor heteromerization using a proximity ligation assay. While technical limitations

prevented the use of this platform to study FSS-regulation of TGFβ receptors at focal adhesions using TIRF microscopy, future work could consider evaluating FSS-mediated changes in the localization of TGFβ receptors at distinct cell membrane sites such as at the primary cilium, Cx43 hemichannels, or clathrin/caveolae-rich microdomains using proximity ligation assays.
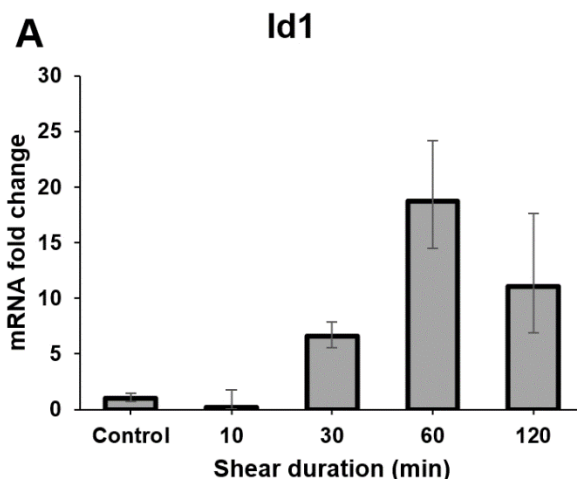


**Figure 7.2: FSS regulation of BMP-inducible gene *Id1*.** (A) In OCY454 cells, FSS rapidly upregulates known BMP-inducible gene, *Id1*, which seems to reach a maximum after only 1 hour of 1 Pa FSS (n=2 biological replicates). On the contrary, *Serpine1* levels continue to increase through 2 hours of FSS stimulation (Fig. 6.2I).

The extent to which the mechanisms described in this work translate to *in vivo* environments remains to be fully elucidated. The experiments in Chapters 5 and 6 used non-terminally differentiated OCY454 cells. Results from additional experiments using fully differentiated OCY454 cells, primary osteocytes, or differentiated primary bone marrow stromal cells would be of particular interest. These approaches are suspected to be quite challenging, given 1) the small volume of the microfluidic chambers which require an initial large concentration of cells suspended in media and 2) the difficulty in delivering fresh media/maintaining cell viability over days/weeks. Of these, two-week long differentiation of OCY454 cells within the chambers is likely to be the strategy with the highest chance of success, however, the sensitivity of a

mineralized, differentiated OCY454 monolayer to FSS and its compatibility with the protein, RNA, and imaging approaches described in this work would have to be evaluated.

While the results in this work evaluated changes in the cellular TGFβ response to individual physical stimuli, understanding the ability of cells to sense and accurately respond to the multitude of concurrent cues they experience *in vivo* remains a long-term objective. One interesting direction for future work would be to study synergies between substate stiffness and fluid shear stress, for example, by growing cells on compliant substrates within microfluidic chambers and subsequently stimulating them with FSS. Given the critical roles that the TGFβ signaling pathway plays in maintaining homeostasis in bone and in cartilage, a more complete understanding of its regulation by substrate stiffness or fluid shear stress may reveal new mechanisms used by cells to detect and differentiate among concurrent physical and biological cues, in addition to helping elucidate how TGFβ receptors are uniquely targeted by these cues to prime the cellular response to TGFβ or BMP ligands.

**References**

1       Duan, D. and Derynck, R. (2019) Transforming growth factor-beta (TGF-beta)-induced

        up-regulation of TGF-beta receptors at the cell surface amplifies the TGF-beta response.

        *J. Biol. Chem.* 294, 8490–8504

2       Clement, C.A. *et al.* (2013) TGF-beta signaling is associated with endocytosis at the

        pocket region of the primary cilium. *Cell Rep.* 3, 1806–1814

3       Rys, J.P. *et al.* (2015) Discrete spatial organization of TGFbeta receptors couples

        receptor multimerization and signaling to cellular tension. *Elife* 4, e09300

**Publishing Agreement**

It is the policy of the University to encourage open access and broad distribution of all theses, dissertations, and manuscripts. The Graduate Division will facilitate the distribution of UCSF theses, dissertations, and manuscripts to the UCSF Library for open access and distribution. UCSF will make such theses, dissertations, and manuscripts accessible to the public and will take reasonable steps to preserve these works in perpetuity.

I hereby grant the non-exclusive, perpetual right to The Regents of the University of California to reproduce, publicly display, distribute, preserve, and publish copies of my thesis, dissertation, or manuscript in any form or media, now existing or later derived, including access online for teaching, research, and public service purposes.

Author Signature

12/14/2020

Date